Master's thesis

NTNU
Norwegian University of Science and Technology
Faculty of Information Technology and Electrical Engineering
Department of Electric Power Engineering

Solveig Samseth Strand

Electromagnetic Design of Modular Generators for Offshore Wind Power Applications

Master's thesis in Energy and Environmental Engineering
Supervisor: Pål Keim Olsen
June 2020

NTNU
Norwegian University of Science and Technology

Solveig Samseth Strand

Electromagnetic Design of Modular Generators for Offshore Wind Power Applications

Master's thesis in Energy and Environmental Engineering
Supervisor: Pål Keim Olsen
June 2020

Norwegian University of Science and Technology
Faculty of Information Technology and Electrical Engineering
Department of Electric Power Engineering

NTNU
Norwegian University of
Science and Technology

Sammendrag

Vindkraftproduksjonen har blitt mer konkurransedyktig sammenlignet med tradisjonelle energikilder. Likevel er det fortsatt mange områder av vindkraftproduksjon som kan dra nytte av økt effektivitet og andre foredringer. En modulær PM-maskin kan være et viktig skritt for å forbedre det generelle vindkraftproduksjonssystemet. Modulære maskiner skiller seg fra tradisjonelle PM-maskiner grunnet segmentering av statoren, rotoren eller begge deler. Denne masteroppgaven er begrenset til en segmentert statorstruktur. En modulær statorstruktur gjør det mulig å oppnå en høyere nominell spenning uten at det fører til en lav fyllfaktor ved å fordele spenningen over statorsegmentene. Den modulære strukturen er for denne masteroppgaven såkalt, symmetrisk modulær. Dette innebærer en modulær struktur hvor hver modul har samme faserepresentasjon. Modulstrukturen kan knyttes opp mot baseviklingene for maskinene.

To maskiner ble designet og testet, ved hjelp av FEM simuleringsprogramvaren COMSOL, en direkte drevet og giret maskin. Begge disse maskinene må oppfylle de samme kravene, og den eneste forskjellen i utgangspunktet for maskindesignet var hastigheten. Designvalgene foretatt var de samme for begge maskinene, og de må også oppfylle de samme generelle maskinbegrensningene. Maskindesign ble utforsket, og dette inkluderer tradisjonelle aspekter og modulære struktureffekter på designet. De modulære aspektene ble inkludert i designprosessen. De modulære maskinene ble sammenlignet med umodulære maskiner som var like med unntak av den fysiske segmenteringen for å observere ytelsesendringer. Maskinoppførselen studert er relatert til magnetiske- og elektriske aspekter, i tillegg til tap. Noen maskin resultater som er spesielt påvirket av fysisk modularitet, ble studert videre med tre forskjellige luftspaltebredder. Disse inkluderer back-EMF, dreiemoment og kjernetap.

Generell symmetrisk modulær struktur for PM-maskiner ble studert i forhold til effekten av antall segmenter for å kategorier fordelene og ulempend ved å konstruere maskiner med en modulær struktur. Disse aspektene inkluderer maskinenes isolasjons krav, poler og stator slot kombinasjoner, viklingsfaktor og frekvens. Det ble observert at isolasjonsreduksjonen grunnet modularitet konvergerer når antall segmenter øker. Det minimale antall slots for en mulig grad av segmentering dobles kontinuerlig når antall moduler øker. Den mulige frekvensen som oppnås for en høy grad av segmentering er begrenset grunnet krav til kombinasjonen av stator slot og poler. En høyere hastighet begrenser ytterligere frekvensen.

Maskinenes prestasjon ble påvirket av å inkludere en modulære struktur grunnet luftspaltene, i tillegg til å påvirke design prosessen. Luftspalten mellom maskin modulene hadde en negativ effekt på maskindriften og ytelse. Effekten av luftspalter mellom statorsegmenter resulterte i størst avvik fra ikke-modulær maskinatferd for den girede maskinen. Årsaken til dette knyttes til maskindimensjonene og antall stator slots sammenlignet med størrelsen på luftspaletene. Likevel ble maskinytelsen minimalt endret på grunn av den modulære strukturen for begge maskinene. De negative aspektene ved luftspalte implementasjon økte med en økning i luftspaltebredden.

Abstract

Wind power production have become more and more competitive compared to traditional energy sources. Nevertheless, there are still many areas of wind power production that could benefit from an increased efficiency and other improvements. A modular PM machine could be an important step for improving the overall wind power production system. Radial modular machines differ from traditional PM machines due to the segmentation of the stator, rotor or both. This thesis is limited to a segmented stator structure. A modular stator structure facilitate a higher nominal voltage without an unsuitably low fill factor by distributing the voltage across the stator segments. The modular structure is for this thesis so called symmetric modularity. This entail a modular structure where each module have the same phase representation in each module and can be closely linked to the base windings expression.

Two machines were designed and tested, utilising FEM simulation software, a direct drive and geared machine. Both of these machines must meet the same requirements and the only difference in the machine design premise was the speed. Design choices included were the same for both machines and they had to adhere to the same general machine limitations. Machine design and construction theory were explored, which included traditional aspects and modular structure effects on the design. The modular aspects were incorporated in the design process. The machines designed were benchmarked against the same machine excluding modularity in order to observe the performance alterations. The machine aspects studied related to magnetic, electrical and loss. Some behavioural aspects especially affected by physical modularity were studied further. These include back-EMF, torque and core losses.

General symmetric modular structures for PM machines were studied in relation to the effect of the number of segments in order to categories the benefits and drawback of constructing a machine with a modular structure. Some of the findings related to the machine insulation requirements, pole and slot combinations, winding factor and frequency. It was observed that the insulation reduction due to modularity converge when the number of segments increase. The minimal number of slots are continuously doubled as the number of modules increase. The possible frequency obtained for increased modularity is limited by an increase in the number of modules, and a higher speed further limits the possible frequencies.

The machine design were affected by implementing modular structures due to flux gaps between the stator modules. The flux gaps between the modules had a deteriorating effect on the machine performance. The effect of air gaps between stator segments resulted in the greatest deviation from non-modular machine behaviour for the geared machine. The cause of this was linked to the machine dimensions and slot number compared to the flux gap width. Nevertheless, the machine performance were minimally altered due to the modular structure for both machines. The negative aspects of the flux gaps implemented increased with an increase in the flux gap width.

Preface

The following Master's Thesis has been written as part of the course TET4900 - Master's Thesis at the Department of Electric Power Engineering at the Norwegian University of Science and Technology. The work has been done during the the spring of 2020, as a continuation of the Specialisation Project *(Electromechanical Design for a Modular HVDC Generator)*.

I would like to acknowledge and thank my supervisor Pål Keim Olsen as well as Professor Robert Nilssen for providing valuable guidance and academic support throughout the semester. Hopefully, this Master's Thesis can help shed light upon some of the parameters found in a modular machine, and be a small contribution to the work done to enhance wind turbine performance.

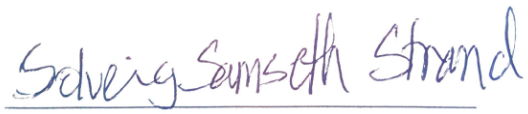

Trondheim, June 19, 2020

List of Figures

List of Tables

Nomenclature

α_m	Relative magnet length
α_u	Slot angle
α_{ph}	Voltage phasor angle
β_0	Flux gap width
ϵ	Coil pitch angle
γ_s	Coil pitch factor
μ_0	Magnet zero permeability
μ_r	Magnet relative permeability
ω_m	Rotational speed [rad/s]
ϕ_1	Fundamental flux per pole
ϕ_p	Flux per pole pairs
$\phi_{p,1}$	Fundamental flux per pole
ϕ_{ry}	Rotor yoke flux
ϕ_{sy}	Stator yoke flux
ϕ_{total}	Total flux produced by magnets
σ	Phase spread angle
τ_p	Pole pitch
τ_r	Nominal torque
τ_s	Slot pitch
τ_c	Coil pitch angle
θ_d	d-axis current angle
θ_q	q-axis current angle
a	Number of flux gaps
A_s	Stator slot area
A_{cu}	Copper area in stator slot
B	Flux density
B_g	Air gap flux density
B_r	Remanence flux
B_{g1}	Fundamental space component of the airgap flux density
B_{ry}	Rotor yoke flux density
B_{sy}	Stator yoke flux density
d_1	Stator slot opening width
d_2	Stator slot opening height
D_{ag}	Air gap diameter
E_0	No-load phase back-EMF
E_{AC}	AC electric stress limit
E_{DC}	DC electric stress maximum
f_e	Electric frequency

h_s	Stator slot height
h_{yr}	Rotor thickness
h_{ys}	Stator slot height
I_r	Rated current
I_s	Rated current
I_{ph}	Phase current
J_{max}	Maximum current density
K_s	Linear current density
k_{dn}	Distribution factor for the nth harmonic
k_{en}	Coil pitch factor of the nth harmonic
K_e	Eddy current constant
k_{fill}	Copper fill factor
K_h	Hysteresis constant
k_{w1}	Fundamental winding factor
k_{wn}	Winding factor of the nth harmonic
L	Length
L_e	End winding inductance
L_g	Air gap inductance
L_m	Mutual inductance
L_s	Slot leakage inductance
L_{ph}	Phase inductance
N_m	Number of magnets
N_m^*	Number of poles per base winding
n_s	Rotational speed [rpm]
N_s^*	Number of stator slots per base winding
n_{coil}	Number of conductors
N_{ph}	Number of phases
N_{segm}	Number of machine modules
N_{sp}	Number of stator slots per phase
P	Power
P_m	Nominal power
p_p	Number of pole pairs
P_a	Anomalous loss
P_{copper}	Copper loss
P_e	Eddy current loss
P_h	Hysteresis loss
q	Stator slot per pole per phase
q_{avg}	Average stator slot per pole per phase
R_e	End winding resistance
R_s	Slot resistance
R_s	Slot winding resistance
R_{ph}	Phase resistance for a PM machine
R_{si}	Inner stator diameter
T	Temperature
t	Number of base winding
T_{cog}	Cogging torque
T_{segm}	Insulation thickness between segments
T_{slot}	Stator slot wall insulation thickness

U_{DC} DC voltage
U_{ph-ph} Phase to phase voltage
U_{ph-scr} Phase to screen voltage
U_{scr-e} Screen to earth voltage
$U_{scr-scr}$ Screen to screen voltage
V_r Rated voltage
$V_{ph,s}$ Peak phase voltage per segment
w_m Circumferential magnet length
w_{st} Stator slot width
w_{tt} Stator tooth width
X_s Reactance

Contents

Chapter 1

Introduction

1.1 Modular HVDC Wind Generator

This thesis include designing two modular PM generators, which can be a part of a machine topology with a higher efficiency. The reason behind constructing modular wind turbine generators are a better integration of wind power production. A modular PM machine can be decomposed into several stator modules. A modular machine have several benefits and disadvantages explored in this thesis. The machine benefits include higher fill factor and higher fault tolerance. Furthermore, a modular PM machine can contribute to a better integration and wind power topology. Modular machines support a higher total nominal voltage for the machine due to the voltage being distributed across the stator modules without a deteriorating fill factor. A lower fill factor would be expected for a non-modular machine. The implementation of a modular structure has the goal of reducing cost, increasing efficiency and integrate the wind power generation.

Modular machine structure can be divided into two categories; functional and physical [32]. Functional modularity denote that a machine have segments, which can operate separately. Physical modularity denote that the machine segments are physically separated which an be constructed and assembled independently. Physical modularity also promote an air gap between the stator segments. The modular structure can be implemented by different methods, either between stator slot pair with a flux gap in the stator teeth or symmetrically according to the winding layout. This thesis have symmetrical modular structure, where each stator module correspond to symmetric phase layout ad thus each module have the same phase representation. The modular structure is explored in the design of a direct drive and geared machine.

A modular PM machine simplifies the AC/DC converter topology connected to the PM machine. The machine modules can be connected to a converter separately when the segments are symmetrical. Thus, the converter topology is simplified and improved by only requiring one converter per segment, which are connected in series. A modular machine also decompose the machine insulation, which further reduce the insulation in the coils. The DC stress are moved to the screen surrounding the stator segments allowing for a more compact machine. Furthermore, if a fault occur in a machine module the converter topology could allow for a continued operation of the other segments, which would be beneficial for operations were maintenance can be difficult to conduct. Therefore, the basis for studying a modular symmetrical PM machine is to create a machine suitable

for the proposed topology with a higher total voltage level. Thus, making the need for transformers redundant and increasing the efficiency in the converter topology further. Another benefit of the modular structure is a more compact machine [24].

1.2 Motivation

The motivation of behind constructing the modular direct drive and geared machine is to increase the converter topology efficiency by designing a machine capable of supporting a higher nominal voltage. Thus, the modular structure facilitate a high fill factor for high voltage levels. By increasing the efficiency of the converter topology and machine system, renewable energy such as wind power can become more competitive due to the higher efficiency and the compact machine structure. Renewable energy production has in later years become increasingly outspread. Nevertheless, further improvements and increased efficiency for wind turbine generators increase the gain of renewable energy production, which is an important step toward green energy production.

An exploration of symmetrical modular structure is also studied since the number of segments implemented in the machine structure greatly influence the machine design. An increased degree of modularity both benefits and impair feasible machine design and behaviour. These benefits and drawbacks are studied in order to determine the machine aspects behaviour in relation to the degree of modularity. Thus, how these benefits and drawback, caused by a modular structure, alter with the degree of modularity.

1.3 Aim

The aim of this thesis is divided into several sub-categories. The fundamental aim is to design a modular direct drive and geared Permanent Magnet machines. The machines must fulfil a given set of specifications that relates to the machine performance and design. The machine modular structure is implemented in the design process and the machine behaviour is studied using FEM simulation software. The machine design and performance include electrical, magnetic and winding design, in addition to geometric dimensions and loss. The behaviour of the machine is simulation utilising the FEM software, COMSOL, in order to observe the behaviour of modular machines compared to their non-modular counterparts. Furthermore, the performance of the direct drive and geared machine are compared. A loss analysis is also included in order to study the efficiency of modular machines compared to non-modular machines. The geared and direct drive machine are designed with the same specifications given with the exception of the machine speed and the same machine selections are also included within the given constraints. Mechanical forces and thermal models are outside the scope of this thesis, but should be conducted. This thesis also includes a study of symmetrical modular PM machine structure. The modular structure is studied in order to determine the alteration a certain modular structure impose on machine design and behaviour. The number of modular segments alter machine requirements and design features. The effect of the number of stator segments are studied in relation to the machine design, aspects considered include winding layout and insulation for different degrees of modularity. Different air gaps widths between the stator segments are also studied for the designed machines to quantify the effect in relation to symmetrical modular structures.

1.4 Content of Thesis

The content of this thesis is divided into several chapters. The theory and modelling process is presented in addition to results obtained from FEM-simulations. It is important to note that some aspects are included in the appendices. These include material properties, FEM-simulation results and theoretical calculations and Matlab scripts. Additionally, some content from the specialisation project *Electromechanical Design for a Modular HVDC Generator* done during the autumn of 2019 have been utilised.

- Chapter 2: Theory related to PM machines in general are presented The machine design aspects considered include magnetic, electrical, winding design and losses. Modularity is incorporated in the design process and seen in relation to traditional machine design.
- Chapter 3: The procedure for designing the direct drive and geared modular machines are explored and presented. The modular aspect is incorporated in the design process, which affect the machine design procedure and limitations. The non-modular machine performance are also presented and validated.
- Chapter 4: Symmetrical modularity in general is studied on the basis of the machine designed and further segmentation in relation to machine design. The results of the FEM-simulations for the modular machines are presented based on the model constructed utilising FEM-software, COMSOL.
- Chapter 5: The result obtained from the FEM simulations are further elaborated and discussed related to the modular structures and machine design. Symmetrical modularity in general is also discussed according to a parameter study in relation to the degree of modularity.
- Chapter 6: Conclusions are drawn based on the results obtained from the FEM-software and discussion. Possible further work is also suggested.

Chapter 2

Theory

The theory in the following sections reflects the fundamental aspects and parameters that are found in a Permanent Magnet Machine. The theory forms the basis for the machine design and modelling found in Chapter 3 relevant for a radial PM machine. In addition, specific theory related to modular PM machines are elaborated.

2.1 Modular Converter Topology

The modular structure for this thesis is limited to symmetric segmentation of the stator, which is both physically and functionally separated. Symmetric modularity denote an equal phase layout for each module, with the same number of phases. A modular structure have several advantages including higher fill factor and efficient AC/DC converter topology. A modular PM generator is especially beneficial in order to induce a high voltage due to the converter topology and the altered isolation requirements. Nevertheless, a modular structure impose new restrictions on the machine design such as air gaps between segment and winding structure limitations.

A segmented PM machine can allow for an altered converter topology compared to traditional PM machines. When each segment is defined as an independent unit it can be designated a converter, and the converters are connected in series. In a traditional PM generator several converters are connected in a parallel structure for one machine, while a modular machine can have one converter per module, which are connected in series. However, this is applicable with a suitable voltage level per module, which correspond to the voltage limit of the converters. The voltage level can generally be lower for converters given a modular structure, compared to a traditional converter topology. This is due to the voltage distribution across the modules. The power electronic topology for symmetric modular machines are presented in Figure 2.1.1.

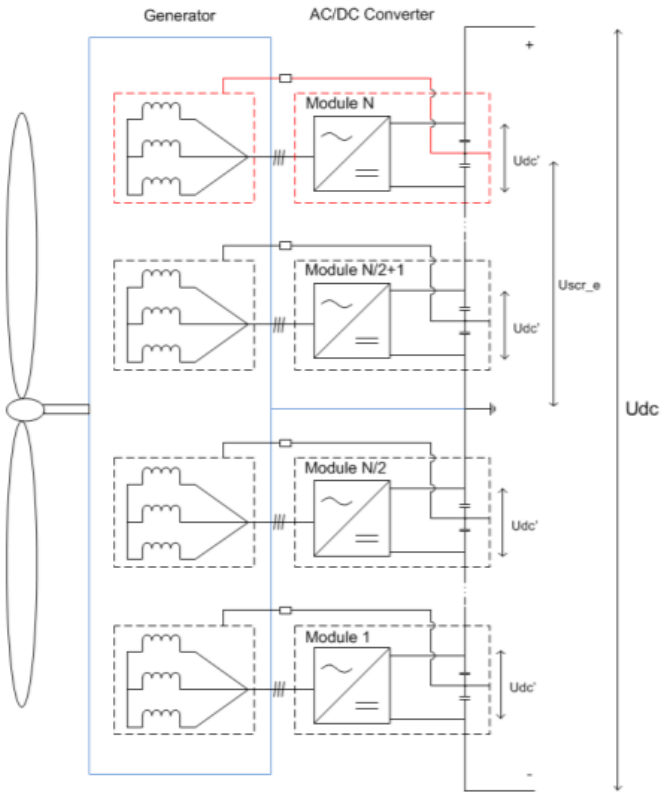

Figure 2.1.1: Modular Converter Topology [24]

Figure 2.1.1 demonstrates that each machine module have a designated individual AC/DC converter. The protective screen around each segment is also connected to the DC potential and contribute to a deconstruction of the machine insulation.

2.2 Torque

Electrical generators are designed in order to produce a given power level. Torque is the rotational force in an electrical machine, which is the product of force and the machine radius. The torque present in a machine is generally measured in the air gap between the rotor and stator. The torque required in order to satisfy power output demands is given by Equation 2.2.1. The power output depends on the relationship between the torque and speed for a given machine. Thus, if the power required is given, the torque and speed must correlate in order to produce the given power [9].

$$\tau = \frac{P_m}{\omega_m}. \tag{2.2.1}$$

A machine with a low speed require a larger torque compared to a machine with a higher speed. Equation 2.2.1 is viable for situations when only the rotational motions are considered [9]. Thus, torque is an important aspect of machine design. Equation 2.2.2 yields an analytical expression of the torque produced in the machine [16].

$$\tau_r = kD_{ag}^2 L, \tag{2.2.2}$$

where k denote the electrical and magnetic contribution. The torque produced in the PM machine can be further derived and given by Equation 2.2.3.

$$\tau_r = \frac{\sqrt{2}\pi}{4} B_{g1} K_s D_{ag}^2 L, \tag{2.2.3}$$

where B_{g1} is the fundamental space component of the air gap flux density and K_s is the linear current density. The torque is closely dependent on the machines diameter and length as observed in Equation 2.2.2 and 2.2.3, in addition to the magnetic flux and linear current density. Thus, magnetic and electrical loading dependencies are apparent by Equation 2.2.3 [33]. The shear stress in the air gap is the product of electric and magnetic loading and can be observed in relation to k in Equation 2.2.2, linear current density and fundamental air gap flux density in Equation 2.2.3 [16]. The required torque given by Equation 2.2.1 is implemented in Equation 2.2.3 and the parameters must correlate to induce the necessary torque level.

The machine diameter and length are varied according to the size of the torque. Furthermore, the electric loading, given as linear current density, is often the parameter altered to reach the required torque given by Equation 2.2.3 when the machine size is determined, instead of magnetic loading. The linear current density required to obtain the nominal torque have a larger acceptable range within the machine design. The air gap flux density value varies within a smaller scope and must adhere to given limits in order to avoid saturating [9]. Thus, the required linear current density is determined by implementing the torque obtained from Equation 2.2.1, as the torque in Equation 2.2.3. Nevertheless, the linear current density also have to adhere to limits in order to avoid unfeasible machine dimensions such as unsuitably large stator slots or high levels of current density [33].

The performance of the machine is associated with the torque density and machine efficiency. The torque density is a measurement of how effective the machine design is in terms of utilising size and volume to attain the nominal torque. Machines with concentrated windings, high pole number and with direct drive application often have a high torque density [6]. Torque density increase when the machine volume is minimised, which can be incorporated into the design process.

2.2.1 Torque Ripple

The torque is expected to vary in relation to time, thus creating a torque ripple. Torque ripple in a machine occurs due to several machine aspects, among these are space harmonics, magnetic saturation, cogging torque and machine eccentricities. Divergence from sinusoidal distribution of flux density in the air gap occurs due to the winding geometry and magnetic reluctance which varies on account of the stator slots [12]. Magnetic reluctance depend on the relationship between magneto-motive force harmonics and air gap flux density [29]. Increased saturation can contribute to variation of permanence and torque non-linearity. When saturation occurs in the stator tips, the flux leakage and cogging torque can also increase due to a greater reluctance torque [36]. Torque ripple is an inevitable occurrence in an electrical machine, but should be reduced as much as possible due to the effect it can have on the machine performance. Torque ripple can be linked to among other occurrences in the machine; vibration, and stress [4].

Cogging torque is a torque ripple contribution and is caused by the force between the stator teeth and magnets, which lead to variation in the permanence [15], [21]. The

magnetic forces in the machine seeks a position of minimum resistance and a stable position. This induce the cogging torque [15]. Thus, the force created between the stator teeth and the magnets counteract the rotation of the machine. The size of the cogging torque is dependent on the poles and stator slot combination. The worst case scenario occur if the number of poles and stator teeth are equal, which could make it difficult for the machine to rotate [30]. Each magnet would experience a magnetic attraction with a corresponding stator tooth. Nevertheless, a similar number of poles and stator slots for machines with concentrated windings yield a suitable cogging torque, given that the pole and slot combination is not equal. Other stator and rotor eccentricities can also contribute to torque ripple in the same manner as cogging torque [13]. The cogging torque occur for all load conditions since it is not dependent on the current. A large cogging torque could also affect the self start ability [21].

2.3 Machine Sizing

The magnetic loading is an important aspect in electrical machines. The magnetic flux is distributed in the machine and originate from the magnets. The magnetic flux is present in all core components of the machine and the flux distribution influence the geometric sizes required in order to obtain acceptable flux density levels.

2.3.1 Magnet Sizing

A PM machine has a given number of poles and stator slots. The frequency is determined based on the number of pole pairs (p_p) and the speed of the machine and given by Equation 2.3.1 [9].

$$p_p = \frac{60 f_e}{n_s}. \tag{2.3.1}$$

The relationship between the number of poles and the stator slots greatly influence the behaviour of the machine. Among the affected machine aspects are the phase layout, winding factor, modular structure and sub-harmonic magnetic fields. The slot and poles relationship is further explored in Section 2.5.

The magnets size influence the flux distribution and the dimensions of machine parameters. The magnet size and air gap thickness are often determined based on the resulting air gap flux density. Furthermore, the air gap flux density correlates with the flux distribution in the machine and is given by Equation 2.3.2 for open circuit conditions,

$$B_g = B_r \frac{l'_m}{l'_m + g'}, \tag{2.3.2}$$

where B_r is the remanence flux in the magnets determined by the material, l'_m is the magnet thickness when accounting for relative permeability and g' is the equivalent air gap thickness. The equivalent air gap thickness is the air gap thickness after altering in relation to the carter coefficient. The fundamental space component of the air gap flux density is given by Equation 2.3.3 [33].

$$B_{g1} = \frac{4}{\pi} B_g \cdot sin(\alpha_m \frac{\pi}{2}), \tag{2.3.3}$$

where the α_m is the relative magnet length. The magnet and air gap size must coincide to achieve a suitable air gap flux density. Thus, if the air gap thickness is decreased, the magnet size must also be decreased in order to maintain the same level of air gap flux density. The remanence flux in the magnets are temperature dependent. The effect of the magnets temperature can be found from Equation 2.3.4.

$$B_{r,T} = B_{r,T_0}(1 - \alpha_T(T - T_0)). \tag{2.3.4}$$

Magnets have a maximum operating temperature. Therefore, the machine design can account for expected temperature increase by utilising Equation 2.3.4. Magnets remanence flux is often given for 20°C. Thus, T_0 is equal to 20°C for the given level of remanence, T is the measured or expected temperature and α is the magnets temperature coefficient [28].

2.3.2 Core Sizing

The size of the core components for PM machines relates to the magnetic flux in the machine and the subsequent flux distribution. The flux density is determined by the magnetic flux distributed and the core volume. Thus, the size of the core components are dependent on flux density limits imposed on the machine design. A simplified analytical method can be utilised in order to determine the magnetic flux and flux densities in a PM machine. These calculations of flux and flux densities assumes that the iron components of the machine have infinite permeability. The reluctance is also assumed to be limited to the air gap and magnets [16]. Thus, such a model does not account for slot leakage or leakage between magnets. The magnetic flux produced per pole is given by Equation 2.3.5 and the corresponding fundamental component is given by Equation 2.3.7 [33].

$$\phi_p = B_g w_m L, \tag{2.3.5}$$

where w_m is the circumferential length of the magnets given by Equation 2.3.6.

$$w_m = \alpha_m \tau_p, \tag{2.3.6}$$

$$\phi_{p,1} = \frac{2}{\pi} B_{g,1} \tau_p L_{core}. \tag{2.3.7}$$

The total magnetic flux in a PM machine is given by Equation 2.3.8 and is the magnetic flux produced per pole times the number of magnets.

$$\phi_{total} = N_m \phi_p. \tag{2.3.8}$$

The total magnetic flux is distributed in the machine, and move through the stator and rotor due to the iron‘s ferromagnetic properties. The total magnetic flux produced by the magnets correlate with the air gap flux density and depend on the magnet dimensions as observed from Equation 2.3.5, 2.3.8, 2.3.3 and 2.3.2. The flux densities in the machine is given by the magnetic flux distributed in the iron core and the core dimensions. The iron core cannot have a flux density higher than a given limit due to the negative aspects

linked to over-saturation such as increased core losses [29]. Thus, the flux density limits are included as a machine design constraint. Furthermore, it can be observed that the magnets size indirectly determine the size of core dimensions such as the stator teeth, stator and rotor yoke thickness. The magnetic flux in the stator and rotor yoke are given by Equation 2.3.9 [9], [33].

$$\phi_{sy} = \phi_{ry} = \frac{\phi_p}{2}. \tag{2.3.9}$$

The flux enters the stator yoke through the stator teeth and are separated into two equal parts which moves in opposite direction in the stator yoke. The same phenomenon occurs in the rotor yoke, where the flux move from the magnet into the rotor yoke and are split into two parts that move in opposite directions. The magnetic flux moves through the stator teeth before it is distributed in the stator yoke. The magnetic flux in the stator teeth can be most prone to over-saturation due to the reduced core area compared to the stator and rotor yoke. The stator teeth flux density can be incorporated in the machine design by determining the stator teeth width on the basis of the desired flux density. Thus, the stator slot width is also determined indirectly by maximum stator teeth flux density. The stator tooth flux is given by Equation 2.3.10 given a predetermined stator tooth flux density limit. The stator teeth width required based on the maximum flux density is given by Equation 2.3.10 [33], [9].

$$w_{tt} = \frac{B_g}{B_{t,max} K_i} \cdot \left[\alpha_m \tau_p - \frac{\tau_s - \tau_p}{2} \right]. \tag{2.3.10}$$

The stator tooth width depend on the stator slot shape and can either be rectangular or trapezoidal. Rectangular stator teeth have a width corresponding to w_{tt}. The smallest width must correspond to w_{tt} for trapezoidal stator teeth. The smallest width of trapezoidal stator teeth for radial PM machines occur at the tip of the tooth. The stator slot width can be found by Equation 2.3.1 with rectangular stator slots and trapezoidal stator teeth. Thus, the stator slots width is constant along the height of the stator slots.

$$w_{st} = \frac{\pi 2 R_{si}}{N_s} - w_{tt}. \tag{2.3.11}$$

The open-circuit flux density in the stator and rotor yoke are given by Equation 2.3.12 and 2.3.13, respectively [9].

$$B_{sy} = \frac{\phi_p / 2}{h_{ys} L K_i}, \tag{2.3.12}$$

$$B_{ry} = \frac{\phi_p / 2}{h_{yr} L K_i}. \tag{2.3.13}$$

Suitable stator and rotor yoke thickness can be determined by the flux density obtained for the given yoke thickness. The flux density limits for the machine design are often assigned to the open circuit flux density. It is important to differentiate between the values of open circuit flux density and full load flux density when iron sizes are determined based on

the open circuit flux density values. The full load flux density is higher and the extent of an increase in flux density from no load to full load can be difficult to predict. The flux density for full load conditions depend on the H-B curve of the iron in relation to the machine dimensions. By constructing the machine based on acceptable open-circuit flux density limits, the full load flux density should be of a value determined by the H-B curves saturation point. Therefore, the material properties and machine dimensions both influence the full load flux density [29].

2.3.3 Modular Structure

A modular PM machine have a segmented stator that is physically split into different segments [32]. The stator segment partition leads to an air gap between the different stator segments, from this point onward called flux gap. The flux gap influence the behaviour of the machine. The alteration to the machine performance due to the flux gaps correlate with the stator slots and pole combination, flux gap width and number of flux gaps in addition to the general machine dimensions. The behaviour alteration on account of the flux gaps is different based on whether the number of poles are lower or higher compared to the number of stator slots [19].

The fundamental phase flux linkage for a modular machine initially increase when the number of slots are less than the number of poles before it start to decrease for a larger flux gap width. However, it constantly decrease when the number of stator slots are larger [19], [34]. The reasons behind the reduction and increase of flux linkage can be linked to three aspects given in [19] and presented in the following list.

- Winding factor alteration
- Flux focusing/defocusing effect
- Open-circuit flux density alteration

The flux focusing and defocusing effect alter the flux paths in the machine and especially in the stator teeth adjacent to the flux gaps. A modular machine with a higher number of poles compared to stator slots have a flux focusing effect, while a machine with more slots compared to poles experience a flux defocusing effect. The flux defocusing and focusing effect was observed in [19] for a 12 slot/10 pole machine and 12 slot/14 pole machine. A machine with a greater number of poles compared to slots experience a flux focusing effect since flux is forced into the stator teeth adjacent to the flux gap, which would have otherwise dissipated or become flux leakage. However, the flux has a greater difficulty of entering the stator teeth for a machine with a fewer number of poles since the flux has to pass through the flux gap which has a higher reluctance compared to iron [19]. The flux defocusing/focusing can be seen in relation to the slot pitch and the pole pitch, where a smaller pole pitch compared to slot pitch leads force the flux to enter the stator teeth.

A modular structure with flux gaps alters the winding factor [18], [19]. The winding factor alteration on account of the flux gaps are further explored in Section 2.5.5.1 Nevertheless, it can be noted that the winding factor is expected to initially increase and then decrease for a machine with a greater number of poles compared to stator slots. The winding factor decrease continuously for machines with a lower number of poles.

The open-circuit flux density in modular machines can be expected to decrease for both slot/pole combinations, since the relative air gap length increase when the flux gaps are implemented. The effect of an increased winding factor and flux focusing can have a

greater contribution on the phase flux linkage for a machine with a higher pole number. Therefore, increase the phase flux linkage when the flux gap width is small. Nevertheless, the phase flux linkage decrease when the open circuit air gap reduction exceed the contribution of a higher winding factor and flux focusing effect. Furthermore, the winding factor increase experienced by a machine with a higher number of poles also decrease when the flux gap exceed a certain limit, explored in Section 2.5.5.1. However, all three aspects presented in the list above contribute to a lower phase flux linkage for a machine with a greater number of slots compared to poles [19], [34].

2.3.3.1 Machine Behaviour

The flux gap implemented between the stator segments affect the behaviour of the machine due to the alteration to the phase flux linkage, winding factor, flux focusing/defocusing effect and air gap flux density as mentioned in the previous section [19]. Aspects that are affected include torque, phase back-EMF and flux density distribution. The phase back-EMF is proportional to the magnetic flux, and is therefore reduced if the phase flux linkage reduce. The load torque is dependent on the winding factor and air gap flux density. A reduction in the winding factor and air gap flux density cause a reduction in torque [20]. The cogging torque of a modular machine increase. The increase in cogging torque can be linked to stator eccentricities since the stator structure is degraded when flux gaps are implemented [18]. Furthermore, the flux gaps contribute to the cogging torque of the stator teeth adjacent to the flux gaps [18]. Thus, the cogging torque for a modular machine can be presented by Equation 2.3.14.

$$T_{cog} = C_{so} + C_{fg} + C_e, \tag{2.3.14}$$

where C_{so} is the cogging torque contribution from the stator slot openings, C_{fg} is the contribution from the flux gap and C_e is the slot opening contribution accounting for flux gap influence [18].

The torque ripple depend on the cogging torque, but an increase in cogging torque. Whether the torque ripple increase or decrease for the modular machines relates to the cogging torque and flux path alteration. Furthermore, [19] and [18] states that the torque ripple can be minimised if the machine can obtain a suitable flux gap width where cogging torque is the major torque ripple component, which occur when the phase back-EMF harmonics are reduced. Nevertheless, optimisation of this character is beyond the scope of this thesis. If a suitable flux gap width is not obtained the torque ripple is expected to increase [19].

The mutual and slot inductance can also be affected by the implementation of flux gap. This effect can be seen in relation to the relative air gap, which increase when the flux gap is implemented. Mutual inductance for the slots adjacent to the flux gap is reduced due to the flux not passing through the flux gap, which improves the fault tolerance since the interaction between the stator teeth affected by the flux gap are limited. The self inductance can be expected to reduce slightly due to the increase relative air gap flux density [19].

[19] also explore the flux gap effect on harmonic content. It is noted that the working harmonic is reduced for both slot combinations when a modular structure is implemented. Nevertheless, further studies of the machine harmonics are outside the scope of this thesis,

but should be included in further work. Alteration to the harmonic content can affect, among other aspects, the torque ripple and cogging torque and flux distribution.

2.3.3.2 Flux Gap Implementation

Flux gap between modules can be implemented utilising two different methods. The stator teeth affected by the flux gaps, can either have a readjusted or unaltered width. A machine that have readjusted the stator teeth width have altered the teeth width so the width on both side of the flux gaps are equal to the non-modular tooth width [19], [24]. [19] suggest that when the stator teeth width have been altered, the magnetic saturation does not increase greatly since the stator teeth area is unaltered. The slot width is reduced in order to readjust the stator teeth width. Empty slots are implemented in order to determine the new slot pitch. These empty slots represent the area lost due to the flux gap implementation. They correspond to the number of slots that could be included if the machine did not have a modular structure [24]. Thus, all slot widths are slightly reduced in order to maintain the stator teeth width. Machines with unaltered tooth width does not readjust the stator tooth width to compensate for the flux gap implementation. Thus, some of the stator teeth area is lost when the flux gaps are implemented. Machines without readjusted teeth width can expect a flux density increase in the affected stator teeth since the volume has decreased. Readjusted stator teeth and unaltered stator teeth are presented in Figure 2.3.1 and 2.3.2, respectively.

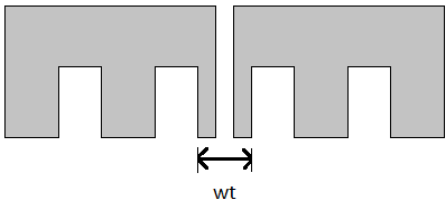

Figure 2.3.1: Flux Gap Construction without Tooth Width Compensation

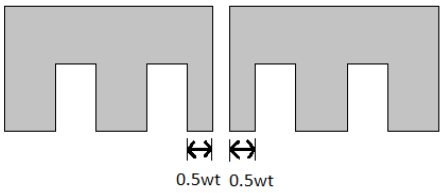

Figure 2.3.2: Flux Gap Construction with Tooth Width Compensation

2.3.4 Magnetic Field Harmonics

Magneto motive force (MMF) is the force occurring due to the current present in the stator coils. The MMF is often smaller compared to the magnetic field caused by the magnets. Nevertheless, the harmonic content of MMF can contribute to the rotor losses and torque ripple. A higher value of q lead to a more sinusoidal MMF and therefore less harmonic content. Machines with concentrated winding have a lower q compared to distributed winding which can result in higher harmonic content [20].

Sub-harmonic magnetic fields are more prominent for machines with concentrated windings. The magnetic flux density distribution in the machine is conducted on the basis of

open circuit flux densities, with the assumption that the flux density caused by the armature reaction is manageable. However, sub-harmonic contributions can increase above the flux present in the air gap. The increase in flux can lead to over-saturation [29]. Therefore, the full load flux density must be examined during machine design and testing. High sub-harmonic magnetic fields can also increase the iron losses. Sub-harmonic content can be observed by reduced flux density in some stator slots, which rotate counter actively to the rotation of the machine. The number of stator teeth affected by the flux density reduction relates to the slot and pole combination. The difference in the number of slots and poles denote the number of stator teeth affected [14], [16].

2.4 Electrical Parameters

The electrical parameter depend on the magnetic flux induced on account of the magnets [9]. Machine aspects of importance determined by electrical parameters include the number of conductors, conductor size, slot size, and winding structure. The electrical parameters included are the current, current density, induced voltage, resistance and inductance. The number of conductors is an important aspect, which influence the electrical parameters.

2.4.1 Voltage

Modular machines distribute the voltage across the number of stator segments. Each segment is connected to an individual converter. Therefore, a modular machine can be designed for a higher total voltage level since the electrical insulation requirements correlate with the voltage level of each module. Thus, the fill factor is not degraded. Nevertheless, the machine as a whole obtain a high voltage despite the segmentation. The converter topology can be reduced due to the high total voltage level for modular machines as explored in Section 2.1.

The voltage distribution across the modules facilitate the elimination of transformers and the simplified converter topology, in addition to reduced insulation requirements. The electrical insulation requirements for a modular machine is further elaborated in Section 2.4.6 [24]. The voltage affect the required number of conductors, which further influence the current, resistance and inductance. The voltage is found by Equation 2.4.1 given a current aligned with the q-axis, which is the current axis that denote maximum torque production [33].

$$V_r = E_0 + R_s \cdot I_s + jX_s \cdot I_s. \tag{2.4.1}$$

The relationship between the voltage and other electrical parameters are utilised to determine the number of conductors necessary in order to establish the required voltage. Thus, Equation 2.4.1 is rewritten in order to determine the number of conductor coils necessary to obtain the required voltage. The number of coils required for a specific voltage level and machine design is given by Equation 2.4.2.

$$n_{coil} = \frac{Vr}{\sqrt{((E_0' + R_s' I_s')^2 + (X_s' I_s')^2)}}, \tag{2.4.2}$$

where E_0', I_s', R_s', and X_s' is the corresponding value of E_0, I_s, R_s, and X_s divided by the order of the number of coils the given parameter depend on [33].

2.4.2 Electromotive Force

The no load phase back-EMF is the voltage induced in the coils due to the rotation of the machine and is closely linked to Faraday's law. The phase back-EMF in a machine counteracts the movement in the coils [16]. The phase back-EMF also contribute to the full voltage level as observed in the previous section. The phase back-EMF is given by Equation 2.4.3.

$$E_0 = \frac{4.44 f_e k_w n_{coil} \phi_1}{2}. \tag{2.4.3}$$

Phase back-EMF are linked to non-electric sources such as to the magnetic flux, frequency and winding factor, which can be deduced from Equation 2.4.3. The correlation between the phase back-EMF and magnetic flux can demonstrate the effect of the modular structure. Thus, a reduction in phase flux linkage is apparent from a reduced no load phase back-EMF [9].

2.4.3 Current

The phase current is determined based on the linear current density required to obtain maximum torque, and the maximum current density allowed in the stator slots. The first step is to determine the required stator slot size, given by Equation 2.4.4.

$$A_s = \frac{K_s \pi D_{is}}{J_{max} N_s k_{w1} k_{fill}}. \tag{2.4.4}$$

The stator slot is found by the relationship between the required linear current density and the maximum current density allowed. The slot area is determined based on electrical properties, while the stator slot width was found on account of the stator teeth maximum density. Furthermore, the stator slot height can be determined based on the stator slot area and width and can be found from Equation 2.4.5 given rectangular stator slots [33].

$$h_s = \frac{A_s}{w_{st}}. \tag{2.4.5}$$

When the slot area is determined the total phase current can be found from Equation based on the slot area determined by the linear current density and maximum current density.

$$I_r = J_{max} A_s k_{fill} \cdot \frac{N_s}{N_{ph} n_{coil}}. \tag{2.4.6}$$

The proposed method for determining the slot dimensions and current incorporates the maximum current density in the machine design. Thus, deterring a high current density which can contribute to temperature increase. The relationship between the winding factor, current and torque is apparent from Equation 2.4.4. A reduced winding factor increase the current required to induce the nominal torque. A lower fill factor, fewer slots, or smaller inner stator diameter also increase the required stator slot size. The total phase current is further divided by the number of modules. The phase current implemented for

each conductor in the stator slots are given by Equation 2.4.8 and the conductor area is given by Equation [33].

$$I_{ph} = \frac{J_{max} A_s k_{fill}}{n_{coil}}. \tag{2.4.7}$$

$$A_{wire} = A_s \frac{k_{fill}}{n_{coil}} \tag{2.4.8}$$

The maximum torque is obtained when the current is aligned with the q-axis, while current aligned with the d-axis indicate maximum flux and no torque production. The difference in angle between the d and q-axis is 90°. The current angle required to align the current with the q-axis is further elaborated in Section 2.5.3 [26].

2.4.4 Resistance

The resistance in the copper coils in a PM machine influence among other aspects the copper loss and indirectly relates to number of coils and voltage on account of Equation 2.4.2. The phase resistance for a PM machine is given by Equation 2.4.9.

$$R_{ph} = N_{sp}(R_s + R_e), \tag{2.4.9}$$

where R_s and R_e is the slot and end winding resistance respectively. The end winding resistance is determined based on Equation 2.4.10. The stator slots resistance is found from Equation 2.4.11.

$$R_e = \frac{\rho n_{coil}^2 \pi \tau_C}{2 k_{fill} A_s}, \tag{2.4.10}$$

$$R_s = \frac{\rho n_{coil}^2 L}{k_{fill} A_s}. \tag{2.4.11}$$

The phase resistance correspond with the copper resistivity. The copper resistivity is temperature dependent so by accounting for resistivity alterations in Equation 2.4.10 to 2.4.11, can the resistance and copper loss be determined for expected temperature levels. The copper resistivity relation to temperature level is given by Equation 2.4.12 [9].

$$R_s = R_{s0}(1 + \alpha_R(T_s - T_0)). \tag{2.4.12}$$

Here, R_s is the resistance at the given temperature and R_{s0} is the resistance at the reference temperature. The temperature corrections included in the machine design correspond to altering the machine in relation to expected machine temperatures. A heat transfer analysis would have to be conducted in order to determine the actual temperatures in the machine should . Furthermore, a heat transfer analysis is outside the scope of this thesis [3].

2.4.5 Inductance

The inductance in a PM machine can be divided into several sub-categories based on the cause of the inductance. The inductance present in the coils denote the magnetic energy in the slots [16]. Furthermore, the inductance also contribute to the number of coils required for the given electrical machine behaviour. The phase and slot leakage inductance is given by Equation 2.4.13 and 2.4.14, respectively.

$$L_{ph} = N_{sp}(L_e + L_g + L_s). \tag{2.4.13}$$

$$L_s = n_{coil}^2 \left(\frac{\mu_0 h_s^2 L}{3A_s} + \frac{\mu_0 d_2 L}{(w_{st} + w_{si})/2} + \frac{\mu_0 d_1 L}{w_{st}} \right). \tag{2.4.14}$$

The slot inductance depend on the slot shape. The parameters d_2 and d_1 are the stator slot opening height and width respectively. A rectangular stator slot does not necessarily have a stator slot opening. Thus, d_1 and d_2 are zero and the slot leakage inductance related to the stator slot opening are voided. This demonstrates the inductance relationship between the machines dimensions and electrical parameters. The air gap inductance also known as magnetising inductance is obtained form Equation 2.4.15 [9], [16].

$$L_g = \frac{n_{coil}^2 \mu_r \mu_0 L \tau_c k_d}{4(l_m + \mu_R k_c g)}. \tag{2.4.15}$$

The mutual inductance is the contribution from coils in other slots on the given slot and is included in the inductance measured in the slots. The end winding inductance can be determined using different methods and can be difficult to calculate correctly. Nevertheless, Equation 2.4.16 can give an approximation [9], [16].

$$L_e = \frac{n_{coil}^2 \mu_0 \tau_c}{8} ln \left(\frac{\tau_c^2 \pi}{4A_s} \right). \tag{2.4.16}$$

The end winding features of the machine cannot be measured utilising 2D simulations. Thus, end winding inductance and resistance are excluded for 2D FEM-simulations.

2.4.6 Insulation

2.4.6.1 Fill Factor

The fill factor is defined as the active material in the stator slots as a percentage of the total area. The fill factor give an indication of how effective the stator slots are utilised. Insulation is required in the stator slots in order to protect the copper coils. The inactive material are the insulation of the entire stator slot, the insulation of each individual copper coil and possible lost area between the copper coils. The fill factor is given by Equation 2.4.17 [23], [11].

$$k_{fill} = \frac{A_{cu}}{A_{slot}}. \tag{2.4.17}$$

When determining the fill factor several aspects must be taken into consideration. These are presented in the following list [23].

- Physical construction and assembly in stator slots
- Insulation requirements
- Copper coil insulation

When the coils are constructed and wound in the stator slots not all area can be utilised since smaller areas between the coils can be present and this space cannot be used by the conductors. A higher fill factor is beneficial since it indicate a more efficient use of the stator slots, a reduction in heat transfer and current density [17].

2.4.6.2 Modular Insulation

A modular structure alter the insulation required in the stator slots, and allow for a higher fill factor. The increase in fill factor for a modular machine is due to the distribution of the voltage as mentioned in Section 2.4.1. The insulation is also deconstructed and distributed in the stator modules [24]. Thus, some of the insulation is moved from the slots to the screens around the modules. The first step taken to determine the machine fill factor is the calculation of the insulation requirements on the basis of the number of segments and voltage level of the machine.

An equivalent fill factor presented in [24] is a factor that yields the insulation requirements for a modular machine. The insulation in the stator slots and around the stator module are incorporated in the equivalent fill factor expression. Furthermore, the factor can be used as a reference value for comparing the insulation required for different modular machines, in addition to the insulation required for increasing degree of modularity. It is important to note that the equivalent fill factor does not include the insulation required for each individual copper coil. The equivalent fill factor is determined based on the voltage level of each module, the stator slot dimension, number of modules and the voltage relationships presented in Table 2.4.1.

Table 2.4.1: Voltage distribution for modular and non-modular machines [24]

Voltage	**Non-modular Design**	**Modular Design**
Rated system voltage	U_{DC}	U_{DC}
U_{ph-ph}(max)	U_{DC}	U_{DC}/N_{segm}
U_{ph-scr}(max)	$0.5U_{DC}$	$0.5U_{DC}/N_{segm}$
U_{scr-e}	0	(U_{DC}-U_{DC}/N_{segm})/2
$U_{scr-scr}$	0	$2U_{DC}/N_{segm}$

The equivalent fill factor is found from Equation 2.4.18 given that there are no empty slots due to flux gaps between segments. An empty slot factor must be included in the equivalent fill factor expression if the slot pitch is reduced to accommodate the flux gaps between the stator segments as explored in Section 2.3.3.2. The empty slot factor is given by Equation 2.4.19, where $N_{Empty,slot}$ is the number of empty slots required to readjust the slot pitch to accommodate the flux gaps.

$$K_a = K_T K_R = \left[1 - \frac{U_{ph-ph}/E_{AC} + U_{scr-scr}/(N_{segm}E_{DC})}{w_{st}}\right] \cdot \left[1 - \frac{2(U_{ph-scr}/E_{AC} + U_{scr-e}/E_{DC})}{h_s}\right], \tag{2.4.18}$$

$$K_{EmptySlot} = 1 - \frac{N_{Empty,slot}N_{segm}}{N_s}. \tag{2.4.19}$$

The insulation requirements in the slots are determined based on the voltage level for each segment and the AC voltage level stress limit of the insulation. A safety factor can be included and are denoted as K. The insulation thickness for the stator slot walls are given by Equation 2.4.20 [24].

$$T_{slot} = \frac{K \cdot V_{ph,S}}{E_{AC}}. \tag{2.4.20}$$

The slot fill factor, excluding the coil insulation and lost area, is obtained based on the stator slot insulation thickness and is given by Equation 2.4.21.

$$f_{slot} = (1 - 2\frac{T_{slot}}{w_{st}})(1 - 2\frac{T_{slot}}{h_s}). \tag{2.4.21}$$

A modular machine requires insulation around each segment, on account of the DC potential being moved to the outside of the stator segment, to further reduce the slot insulation [24]. The insulation thickness between the segments and at the outer edge of the stator segments are given by Equation 2.4.22 and 2.4.23, respectively. The insulation distribution is presented Figure 2.4.1.

$$T_{segm} = \frac{2V_{DC,S}}{E_{DC}}, \tag{2.4.22}$$

$$T_{earth} = \frac{0.5V_{DC}}{E_{DC}}. \tag{2.4.23}$$

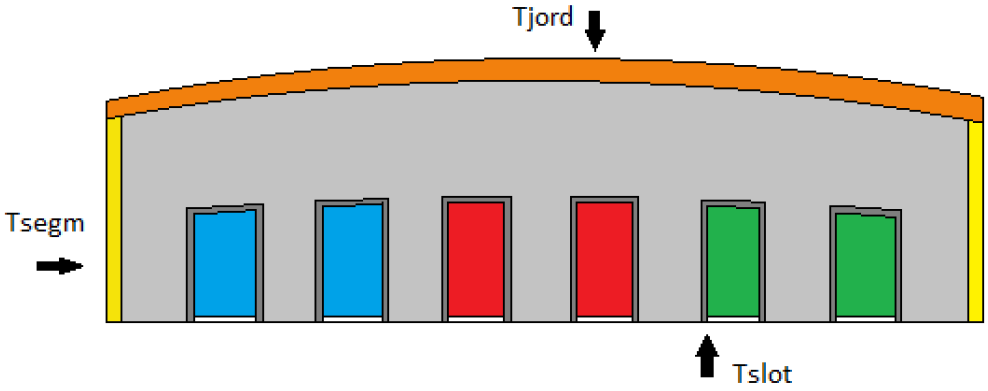

Figure 2.4.1: Illustration of Insulation Deconstruction

Figure 2.4.1 include the insulation requirement on account of the voltage level related to the modular structure. However, the presented insulation calculations does not account for the copper coils insulation, nor the area of the slot lost due to space that cannot be effectively utilised between the coils. Thus, further calculations are necessary to determine the copper fill factor. The fill factor can be defined by two terms, the slot fill factor and the copper fill factor. The slot fill factor includes the slot insulation, while the copper fill factor only consider the percentage of copper in the stator slots [23]. The method for determining the copper fill factor is further elaborated in Section 3.1.4.

Rectangular copper coils are expected to yield a higher fill factor compared to circular coils. Circular coils lead to a greater area of the stator slots being unusable as observed from Figure 2.4.2. Rectangular copper coils also contribute to shorter end windings, higher torque density, compact structure, and better heat dissipation, in addition to the higher fill factor[35].

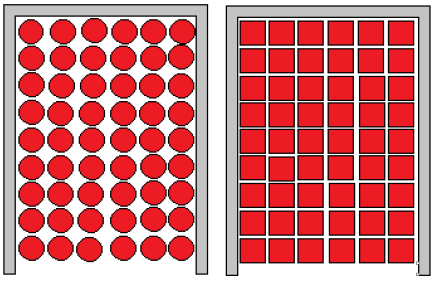

Figure 2.4.2: Left: Circular Coils, Right: Rectangular Coils

2.5 Winding Structure

2.5.1 Winding Configuration

There are two widely implemented winding structures; concentrated and distributed winding. Distributed winding divides the copper coils across several slots. Concentrated winding have a structure where the copper coils are centred around the stator teeth and can be non-overlapping. The conductors are connected in series and are wound around

the stator teeth [27]. Concentrated and distributed winding structure are presented in Figure 2.5.1

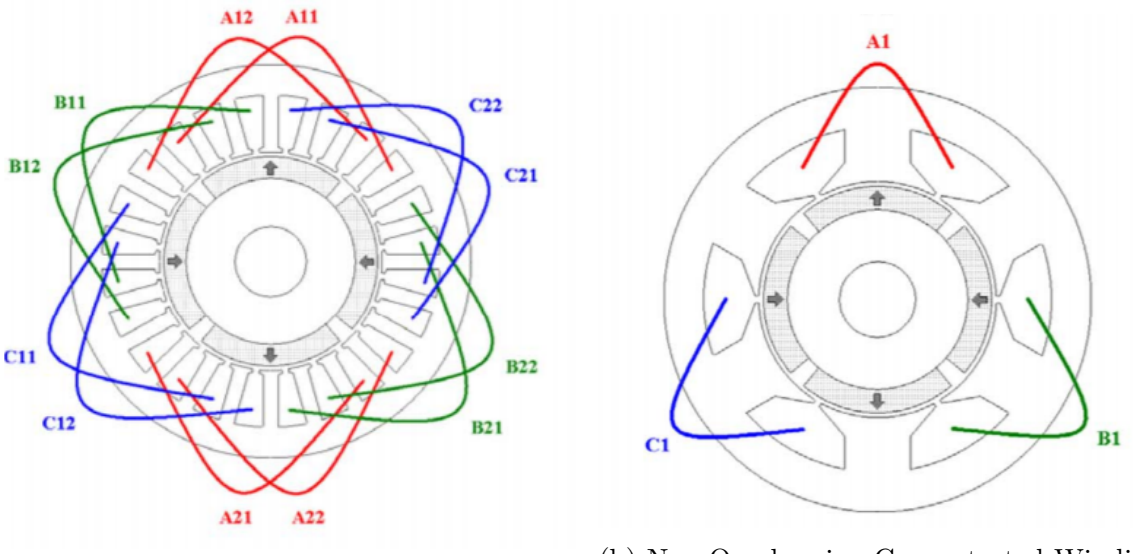

(a) Distributed Winding

(b) Non-Overlapping Concentrated Winding

Figure 2.5.1: Winding Configuration [27]

Concentrated and distributed winding structure have different benefits and disadvantages, which are considered when choosing a winding structure. There are lower costs associated with utilising concentrated windings compared to distributed windings. Concentrated winding also gives a lower cogging torque compared to distributed winding given a suitable slot and pole combination. Machines with concentrated windings can obtain a higher fill factor, which is further improved by a modular structure. A machine with concentrated windings also have a higher fault tolerance and power density. Nevertheless, a low winding factor can be associated with concentrated winding if the slot and pole combination is unsuitable. Nevertheless, the winding factor can be increased given a low difference in the slot and pole number. The winding factor for concentrated windings is further discussed in Section 2.5.5 Distributed winding obtain a more sinusoidal MMF distribution. Thus, concentrated winding structure can also have a greater degree of sub-harmonics magnetic flux due to the fractional winding structure [27].

Concentrated windings can be considered better suited for a modular machine since the winding structure must be limited within the machine modules. The winding structure is already centralised for concentrated windings. Some of the benefits obtained by implementing a modular structure such as higher fault tolerance and high fill factor is further improved by selecting a concentrated winding structure for the machine design. The slot/pole relationship required in order to construct modules with a symmetric phase layout is also easily obtained for concentrated windings as explored in Section 2.5.2. The winding structure is linked to the number of poles and stator slots, and the suitability of the slot and pole combination correlate with the of stator slot per pole per phase given by q in Equation 2.5.1.

$$q = \frac{N_s}{N_{ph} N_m} = \frac{z}{n}, \tag{2.5.1}$$

The winding structure is concentrated and feasible given a stator slot per pole per phase, q, between the values of 0.25 and 0.5. The performance of concentrated winding structure benefits from a value of q close to 1/3 since this yields a high winding factor. However, q cannot be equal to 1/3 since it indicates that the number of poles and stator slots are the same. A large force would occur between the poles and the stator teeth as mentioned in Section 2.2.1. The machine would also have only one phase[30].

2.5.1.1 Winding Rules

The winding structure designed for a machine must be feasible and fulfil general winding requirements. Thus, the winding design is conducted within the bounds of winding structure rules. The winding design constraints for a three phase modular PM machine are presented in the following list [30], [16];

- The number of poles must be even
- The number of stator slots must be dividable by 3
- The number of poles and stator slots cannot be equal
- The number of pole pairs for a section cannot be a multiplier of the number of phases
- Modular: The phase layout for each segment must be symmetrical
- Modular: The number of stator slots must be dividable by the number of modules divided by 2

The two last winding design constraints presented in the list above relates to a modular machine with concentrated windings and single layer. Since the coils are wound around the stator teeth then the phase of each side of a stator teeth wound must be the same phase.

2.5.1.2 Winding Layer

A concentrated winding can have either one or multiple layers, most often two layer. Single and double layer winding denote how the copper coils are wound around the teeth. A machine with a single layered concentrated winding have the copper coils wound around alternating teeth. Double layered windings have copper coils wound around every tooth. Single and double layered windings are presented in Figure 2.5.2.

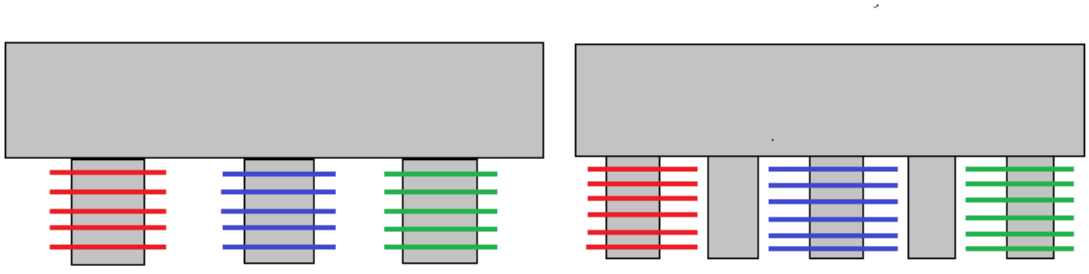

Figure 2.5.2: Left: Illustration of Double Layered Concentrated Winding, Right: Illustration of Single Layered Concentrated Winding

There are several advantages and drawback linked to single and double layered winding structure. These are presented in Table 2.5.1 [20], [25].

Table 2.5.1: Comparison of Machine Performance for Single and Double Layer Winding [20]

Machine Parameter	**Single Layer**	**Double Layer**
Winding factor	High	Low
Slot fill factor	High	Low
End winding length	High	Low
Slot inductance	High	Low
Resistance	Similar	Similar
Mutual inductance	Low	High
Fault tolerance	High	Low
EMF	Trapezoidal	Sinusoidal
MMF harmonics	Higher	Low
Torque ripple	Higher	Lower
Eddy current losses	Higher	Low

Single layered winding have a higher fault tolerance due to higher slot inductance and lower mutual inductance [25]. Double layered winding have a lower degree of harmonics and a higher fundamental harmonic order compared to single layered winding. A greater degree of winding harmonics also contribute to higher inductance and torque ripple for machines with single layers.

However, a single layered machine can obtain a higher winding factor. Higher fault tolerance can also be deduced from Figure 2.5.2. A single layered winding only have one coil wound around each stator slot. Thus, if a fault occur in a stator slot there is only one coil group affected. However, for a double layered winding two coil groups are present in a stator slot so if one coil group experience a fault the other coil group can be affected. One of the benefits related to modular machine is the increased fault tolerance and the possibility to run a machine with reduced modules even though this would require further study and are not included in the scope of thesis. Further fault tolerance improvement design steps are beneficial, such as selecting a single layered winding, for an offshore wind turbine where maintenance is difficult [25].

2.5.2 Modular Structure

A modular structure impose new restrictions on the winding design. Modular stator structures explored in this thesis is based on symmetric modularity. Thus, the number of phases must be equally represented in each stator segment. A symmetric phase distribution for a given number of stator modules are obtained by implementing a requirement of the difference in the number of stator slots and poles. Machines can be segmented based on sections (F1) or paths (F2). The choice of segmentation structure influence the difference in the number of stator slots and poles required. The sections (F1) for a machine are the number of equivalent independent machines the original machine can be divided into. The number of paths (F2) for a machine is defined as how many parallel phase paths that can exist in a machine. Thus, segmentation based on both sections or paths ensures symmetric phase layout. The number of paths possible in machine is given by Equation 2.5.2 [16].

$$F2 =\mid N_m - N_s \mid \tag{2.5.2}$$

F1 can be found by utilising Equation 2.5.2. If the number of poles divided by F2 is an even number then F1 is equal to F2. However, if the number of poles divided by F2 is odd, then F1 is equal to F2/2 [16]. The winding layout is limited by the difference in the number of poles and stator slot required for the modular machine, in addition to general rules relating to the winding structure as presented in the Section 2.5.1.1. A phase spread angle of 60° can be implemented if F1 and F2 is not equal. A phase angle for 60° benefits the machine performance since it results in a higher winding factor compared to a 120° phase spread [30]. Therefore, it is beneficial to design a machine were the number of paths and sections are not equal. The required difference in stator slots and poles given by Equation 2.5.2 can readily be included in the design of a machine with concentrated windings. The modular structure pole and slot design feature would have to be altered to be applied to machines with a distributed winding structure. The requirement of a given difference in the number of poles and slots, due to a given modular structure, reduce the pole/slot combinations possible to implement. Especially for a machine requiring a high number of modules, which indicates a greater difference in the slot and poles.

2.5.3 Star of Slots

The modular winding structure requirement presented in the previous section can be linked to universal winding terms. The number of section (F1) correspond to to the number of bases in a machine, and the number of parts (F1) correspond to half of a machine base given a phase angle of 60°. The phase spread angle denote the phase distribution within a winding base. A phase spread angle of 60° indicate that each phase occurs twice in each base winding. Thus, two paths per base winding are present with a phase angle of 60°. The number of bases in a machine is given by Equation 2.5.3. The number of slots and poles in a base is given by Equation 2.5.4 and 2.5.5, respectively. Equation 2.5.3 to 2.5.5 are viable given one winding layer [1], [30].

$$F1 = \frac{N_m}{2n} = GCD(N_s, N_m/2), \tag{2.5.3}$$

$$N_s^* = \frac{N_s}{t}, \tag{2.5.4}$$

$$N_m^* = \frac{N_m}{t} = n. \tag{2.5.5}$$

Star of slot is a phasor representation of the EMF harmonic and can be used to determine the winding layout for a machine with concentrated winding structure. The fundamental EMF harmonic is given by a star of slot phasor representation. The number of spokes in the phasor EMF representation is N_s/F1. The star of slot method also determine the current angle required to aligned the current with the q-axis. The slot angle is give by Equation 2.5.6. The angle between the phasors of two adjacent slots in the phasor representation are given by Equation 2.5.7, while the angle of two adjacent phasor spokes are given by Equation 2.5.8 [1].

$$\alpha = \frac{2\pi}{N_s}, \tag{2.5.6}$$

$$\alpha_e = \frac{N_m \pi}{N_s}, \tag{2.5.7}$$

$$\alpha_{ph} = \frac{2\pi}{N_s/F1} = \frac{\alpha_e}{N_m/2} t. \tag{2.5.8}$$

The current angle required to align the current with the d-axis is determined by Equation 2.5.7 divided by the number of phases. Therefore, the current angle necessary to align the phase current with the d-axis is phase shifted 90° to obtain the q-axis current angle.

2.5.4 Phase Layout

The phase layout in a PM machine depends on the number of slots and poles, number of winding layers and phase angle. The phase placement in a stator slot can be determined by utilising the average slot per pole per phase method, q_{avg}, given by Equation 2.5.9 to 2.5.10 [30], [31].

$$q_{avg} = \frac{1}{n} \sum q_1 = \frac{1}{n}(q_1 + q_2 + .. + q_n) = \frac{1}{n}(q_a + q_a + ... + q_b + q_b) = \frac{1}{n}(q_a z' + q_b(n - z')), \tag{2.5.9}$$

$$q_a = g + 1,$$
$$q_b = g,$$

$$q_{avg} = \frac{1}{n}((g+1)z' + g(n - z')). \tag{2.5.10}$$

The phase placement is determined based on the sequence obtained from q_{avg}, which consists of values of 1 and 0. The value of the sequence determine how the phases are distributed across the slots, a value of 1 or 0 indicates whether the phase is implemented for the respective stator slot or not implemented. The sequence obtained from q_{avg} is repeated until all stator slots have been assigned a phase. The phase angle and number of layers must be considered when utilising the average stator slot per pole per phase. If there is only one layer in the machine then each value in the sequence correspond to one specific slot. The sequence yielded by the q_{avg} also denote whether a phase spread angle of 60° are possible for the given slot/pole combination. The average stator slot per pole per phase method can be unreliable for single layered concentrated windings [20]. Therefore, the phase layout based on the average slot per pole per phase can be validated by utilising star of slot.

2.5.5 Winding Factor

A high winding factor increase the torque per ampere. Thus, a machine with a lower winding factor require higher current in order to obtain the same level of torque [20]. Concentrated winding would in general have a higher winding factor if the number of poles and stator slots are similar [30]. Smaller machines with a relatively low number of poles and stator slots can experience issues related to lower winding factor due to the

difference in slots and poles being a larger percentage of the total number of slots and poles. Thus, an advantage pertaining to a high number of poles and slots for concentrated windings are apparent by the improved winding factor. The highest winding factor would in general be obtained with the same number of stator slots and poles and thus a q = 1/3. However, as mentioned this is not a feasible combination. Therefore, the number of poles and stator slots should be as close as possible, but not equal. The winding factor is the product of the distribution and coil-pitch factor given by Equation 2.5.11,

$$k_{wn} = k_{dn} \cdot k_{en}, \tag{2.5.11}$$

where k_{dn} is the distribution factor and k_{en} is the coil pitch factor, n denotes the harmonic order [30], [16]. The distribution factor depends on the number of layers, The distribution factors is the sum of the phasor representation of EMF in relation to the arithmetic sum of EMF and is given by Equation 2.5.12 [16],

$$k_{dn} = \frac{sin(\frac{n \cdot \sigma}{2})}{z^* \cdot sin(\frac{n \cdot \sigma}{2 \cdot z^*})}, \tag{2.5.12}$$

where σ is the phase spread angle. The z* implemented in Equation 2.5.12 is the enumerator given by q with a double layered windings, while for a single layered winding z* is equal to z/2. The value of z* in relation to the number of winding layers given in Equation 2.5.12 is the reason for a higher winding factor with a single layer. A phase angle of 60° also contribute to a higher winding factor, which can be observed by Equation 2.5.12. The coil pitch factor is a measure of the flux in the coils and is given by Equation 3.1.1. The coil pitch factor is unchanged based on the number of layers [16], [1].

$$k_{en} = cos(\frac{1}{2} \cdot n \cdot \varepsilon), \tag{2.5.13}$$

where ε is the coil pitch angle given by Equation 2.5.14.

$$\varepsilon = \pi - \alpha_e. \tag{2.5.14}$$

The winding factor is dependent on the number of stator slots and poles and correlate with the value of q. The relationship between q and the winding factor is demonstrated in Figure 2.5.3 and 2.5.4 for double and single layered winding structures respectively. The premise for this correlation is a phase angle of 60° and unfeasible pole and slot combinations are not excluded [16].

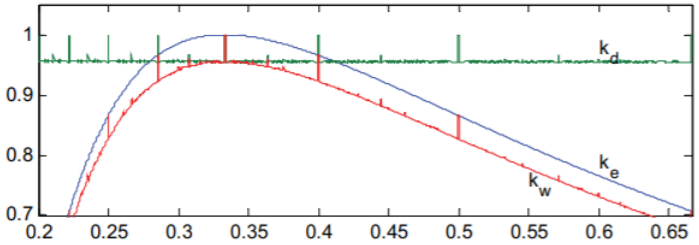

Figure 2.5.3: Winding Factor Compared to q for Single Layered Winding [16]

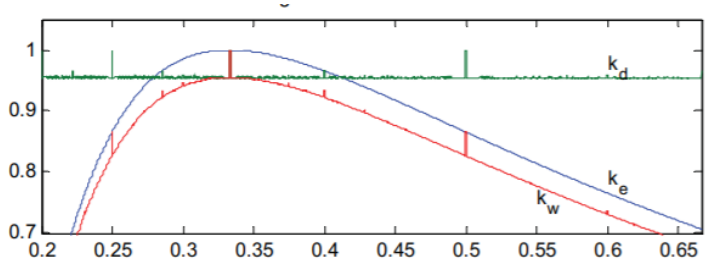

Figure 2.5.4: Winding Factor Compared to q for Double Layered Winding [16]

A single layered winding structure have the highest winding factor given a q = 2/5 and q = 2/7. This is demonstrated in Figure 2.5.3 and is due to the distribution factor being equal to 1 at this point [16]. Thus, single layered windings can exceed the presumed maximum winding factor given by q = 1/3. The frequency is determined based on the number of poles and speed, with a low speed a high number of poles can be suitable. A difference in the stator slots and poles affect the winding factor less with a higher number of poles and stator slots since the difference is a relative smaller percentage of the total number of poles and slots, with the exception of a slot/pole combination of q = 0.4 for single layered winding.

2.5.5.1 Modular Winding Factor

The flux gap of a modular structure affect the winding factor as previously mentioned in Section 2.3.3. The distribution factor is unaltered on account of the flux gap. The distribution factor is unaffected since the slot distribution is the same. However, the fundamental coil pitch factor (k_e) is affected, which can be observed from Equation 2.5.15 [19], [34].

$$k_e = sin(\frac{\tau_s - \delta}{\tau_p} \cdot \frac{\pi}{2}), \tag{2.5.15}$$

where δ is given by Equation 2.5.16 and correlate with the flux gap width, β, and the number of flux gap present in the machine, a.

$$\delta = a \cdot sin(\frac{\beta_0}{2 \cdot R_{si}}). \tag{2.5.16}$$

The increase or decrease in the winding factor is apparent from the relationship between the slot and pole pitch altered by δ. A greater number of stator slots compared to poles yield a larger pole pitch compared to the slot pitch. The difference in slot pitch and pole pitch increase when delta increase, which reduce the coil pitch factor. On the other hand, a machine with a greater number of poles compared to slots have a larger slot pitch. Thus, by reducing the slot pitch with the inclusion of a flux gap width the slot pitch and pole pitch converge. Nevertheless, as δ increase the nominator of Equation 2.5.15 eventually reduce below the value of the denominator and coil pitch decrease. A machine with fewer flux gaps compared to stator slots is expected to have a smaller winding factor alterations since fewer stator slots are affected.

2.6 Loss

The loss is divided into several subcategories based on the cause of the loss. These include core loss, copper loss and magnet loss.

2.6.1 Core Loss

The core losses in an electrical machine can be further divided into several categories based on the cause of the core loss. The total core loss is given by Equation 2.6.1, while the loss components that contribute to the total core loss are given by Equation 2.6.2 to 2.6.4. These equations are the basis for determining the core loss in PM machines.

$$P = P_h + P_e + P_a, \tag{2.6.1}$$

$$P_h = K_h \cdot \hat{B}^{\alpha_L} f, \tag{2.6.2}$$

$$P_e = K_e \cdot \hat{B}^2 f^2, \tag{2.6.3}$$

$$P_a = K_a \cdot \hat{B}^{1.5} f^{1.5}. \tag{2.6.4}$$

The hysteresis loss given by Equation 2.6.2 occurs due to the magnetisation of the iron for an altered operating point. The hysteresis loss is the energy lost when the a hysteresis loop is crossed as the machine rotates. The size of the energy lost is determined based on the size of the hysteresis loops given by the the relationship between flux density and magnetisation force in the core material. Hysteresis losses occur on a microscopic level while the dynamic loss, which include the eddy current losses and anomalous losses are of a larger scale. The core loss depend on the flux density in the machine core, which demonstrates the importance of avoiding over-saturation [10], [9].

The eddy current loss and the anomalous losses occur due to the rate of change of the flux in the iron core [10]. The eddy current and anomalous loss components are caused by the same phenomenon, but can be deconstructed and represented by Equation 2.6.3 and 2.6.4, respectively. Nevertheless, the anomalous loss expression can be included in the eddy current expression by assigning the hysteresis loss factor, α_L, as 2, otherwise it should be determined by curve fitting [3]. The eddy current and anomalous losses dominate in machines with a high frequency, while hysteresis losses contribute with a greater percentage for machines with lower frequencies, which can be deduced from Equation 2.6.2 to 2.6.4 [9], [10].

The core loss components given by Equation 2.6.2 to 2.6.4 are a based on a frequency domain model. The loss model can be transformed to a time dependent domain in order to implement the loss models in FEM simulation software, utilising time dependent analysis. The core loss for a time dependent domain is given by Equation 2.6.5 to 2.6.7 [10], [8].

$$P_e = K_e \frac{1}{2\pi^2 T} \int | \frac{dB}{dt} |^2 \, dt, \tag{2.6.5}$$

$$P_a = K_a \frac{1}{8.76T} \int | \frac{dB}{dt} |^{1.5} \, dt, \tag{2.6.6}$$

$$P_h = K_h \frac{1}{T} \hat{B}^{\alpha_L}. \tag{2.6.7}$$

The hysteresis loss depend on the peak flux density, while the eddy current and anomalous losses depend on the rate of cycling [10].

2.6.2 Copper Loss

Copper loss is the loss present in the copper coils in an electrical machine and is closely linked to the resistance in the copper coils. The total copper loss is given by Equation 2.6.8 [9].

$$P_{copper} = 3I_s^2 R_{ph}. \tag{2.6.8}$$

The copper loss depend on the resistance, which is temperature dependent as mentioned in Section 2.4.4. Copper loss reduction can include reducing the coil temperature. A higher fill factor contribute to better heat transfer between the coils leading to a temperature decrease [35]. A modular stator structure contributes to a higher fill factor as explored in Section 2.4.6 and could imply reduced copper loss. Reduced copper loss would be especially beneficial for low speed machines, which can expect a large copper loss contribution. The copper loss expression given by Equation 2.6.8 assumes ideal back-EMF. Thus, the true copper loss in machines can be assumed to be much larger.

The flux gaps for a modular machine can be implemented by two methods as explored in Section 2.3.3.2. The flux gap method that retain the stator teeth width despite the flux gaps implementation by utilising empty slots can experience an increase in copper loss [19]. This is because the stator slot area decrease as a result of the continued width of the stator teeth. Thus, the number or conductors or the conductor area would have to be reduced, which imply an increase in copper loss. Nevertheless, this factor could be negated by increasing the height of the stator slot in accordance with the slot width decrease.

2.6.3 Magnet Loss

The permanent magnets in a PM machine have a certain level of conductivity. Thus, the loss in the magnets are eddy current losses. Electrical conductivity in the permanent magnets can increase the temperature in the magnets, contribute to demagnetisation and magnet loss. Steps taken to limit magnetic losses include reduction of the current density presence in the magnets. The current density in permanent magnets can be limited by axial segmentation or an increase in the air gap. The electric current transfer through the length of the machines are limited with axial segmentation. Further magnet loss analysis are excluded from this thesis. Nevertheless, the current density in the magnets are observed in order to determine if it could pose a challenge [9].

Chapter 3

Modelling

The design process of a modular PM machine were based on given requirements and specification. The design process were divided into several sub-categories, which interact in order to determine the machine parameters. Some of the machine parameters had a greater degree of freedom and a parameter study was therefore conducted. The designed machine was implemented in FEM-software, COMSOL.

3.1 Design Process

This thesis includes the design of two modular machines, direct drive and geared machine, which must fulfil the same requirements related to machine performance. The design process is divided into several sub-categories, whom interacted during the machine design process. The overall design procedure is presented in Figure 3.1.1.

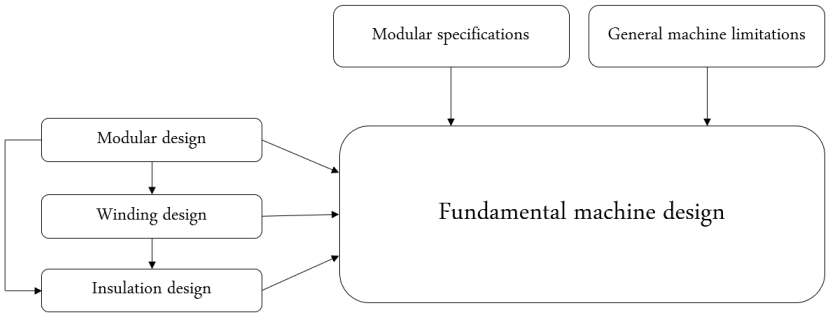

Figure 3.1.1: Overall Design Procedure

The starting point for the machine design is the predefined design specification and general machine limitations, given in in Table 3.2.1 and 3.2.2 for the specific machines designed in this thesis. These input parameters influence the machine construction and the aspects of the machine, such as magnetic and electrical parameters, in addition to the winding structure. The fundamental design is the design process utilised to determine the geometric sizes of the machine, in addition to the magnetic and electrical behaviour. The fundamental design relies on the three other design subcategories: winding, insulation and modular design. These sub-categories also interact as can be observed from the

flowchart presented in Figure 3.1.1. The modular design affect the winding structure and the insulation design. The cause of this relationship is the insulation design dependency on the voltage level for each module. The winding structure depends on the difference in number of poles and stator slots, which are determined based on the number of modules in order to obtain a feasible winding structure for modular machines with a given number of modules.

3.1.1 Fundamental Design

The procedure utilised in order to determine the fundamental machine parameters are closely linked to design methods presented in [9], [16], and [33]. The machine was designed based on the machine limitations and requirements. Parameter values had to be reconsidered if the limitations and specifications were not meet. The fundamental machine design incorporate the three aspects of machine dimension, magnetic and electrical behaviour. Thermal factors are also incorporated in relation to the magnets remanence flux density. The fundamental design process is conducted according to the diagram given in Figure 3.1.2.

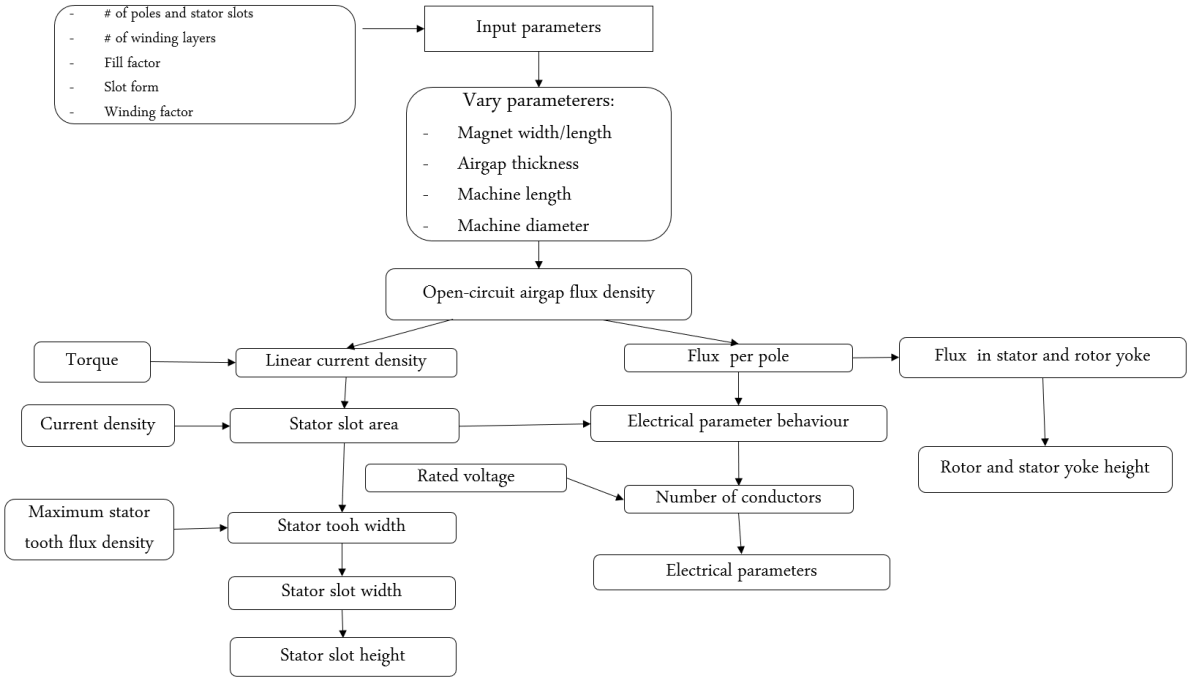

Figure 3.1.2: Fundamental Machine Design Procedure

Factors given by the other design sub-categories were also input parameters for the fundamental design, such as the number of stator slots and poles. There is a great degree of freedom present in the design process despite these input parameters. Machine components not limited by the input constraints were included in a parameter study to quantify the correlation between the parameter and the machines performance. The parameters included were the magnet width and length, air gap radius and machine size. The parameter study is presented in Section 3.1.6.

Some parameters were determined based on machine limitation. These limitations were incorporated in order to yield a feasible machine performance. The width of the stator teeth are determined based on the maximum allowed flux density, which can be observed

from Equation 2.3.10. The stator slot size were also determined based on the linear current density and the maximum current density allowed. This relationship can also be observed from Equation 2.2.3. The rotor and stator length are determined based on suitable flux density limits. The difference in the machine speed for the direct drive and geared machine contribute to a great difference in the diameter and length required for the machines since the torque levels are different. Furthermore, the speed influence the frequency level of the machine.

3.1.2 Modular Design

The modular design yields the difference in stator slots and poles required for a machine with a specified number of modules with symmetric phase placement. The number of modules required are determined by a given voltage limit for each module converter. The voltage level of each machine module must be below the voltage limit given by the converter. The modular design procedure is presented by Figure 3.1.3.

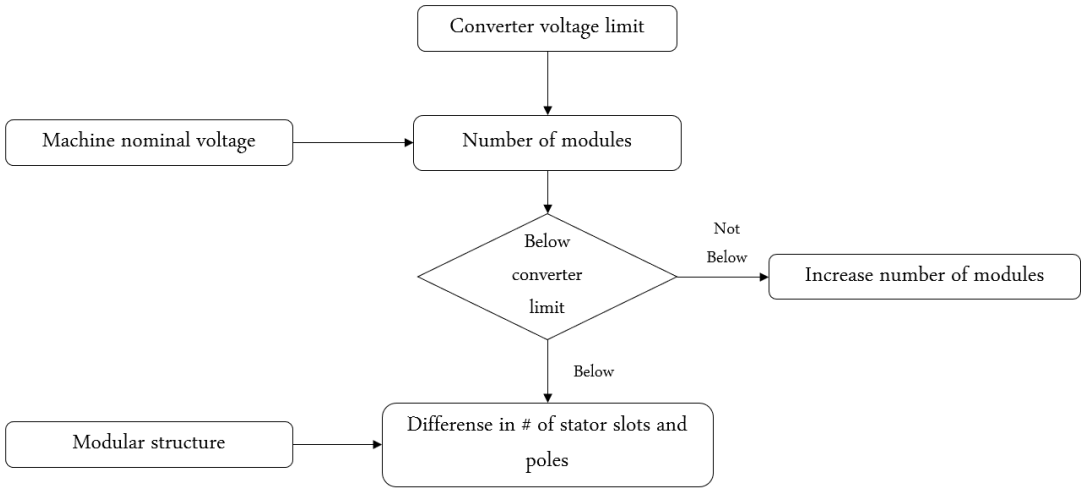

Figure 3.1.3: Modular Design Procedure

The voltage level for the machine and converter are specified, which determine the minimum number of modules. When the number of segments are determined the difference in the number of poles and stator slots can be found based on theory presented in Section 2.5.2. The segmentation is implemented on the basis of paths (F2) or sections (F1) in order to ensure symmetric phase distribution in each segment. The basis of the segmentation structure determine the difference in slots and poles required. The converter voltage limit and total nominal voltage for the machine is given in Table 3.2.1.

The direct drive machine were designed as a machine with a modular structure based on sections (F1). Thus, each segment could correspond to an individual machine. The machine with gear were designed with a modular structure implemented on the basis of paths (F2) and thus parallel paths possible in the machine. The basis of the modular structure for the direct drive and gear machine were different due to the speed of the machines, given in Table 3.2.1. The number of poles of the geared machine were limited to the largest degree possible for the number of modules required by the converter limit for

the geared machine. Thus, resulting in a modular structure based on paths. The direct drive machine allow for a higher number of poles compared to the geared machine due to the speed. The difference in modular structures for direct drive and geared machines could affect the machine performance on account of the number of flux gaps compared to number of stator slots. A special case occurs for pole/slot combinations where section (F1) are equal to parts (F2) since it indicates a phase angle of 120°. Therefore, the slot/pole combinations that lead to a phase angle of 120° are avoided when the number of slots and poles were determined.

3.1.3 Winding Design

The winding structures input constraint is the difference in the stator slots and poles required to obtain the number of modules determined by the modular design. The slot/pole difference is a defining winding design constraint for selecting the number of poles and stator slots. The number of stator slots and poles must also adhere to winding design rules given in Section 2.5.1.1. The winding design process is presented by Figure 3.1.4.

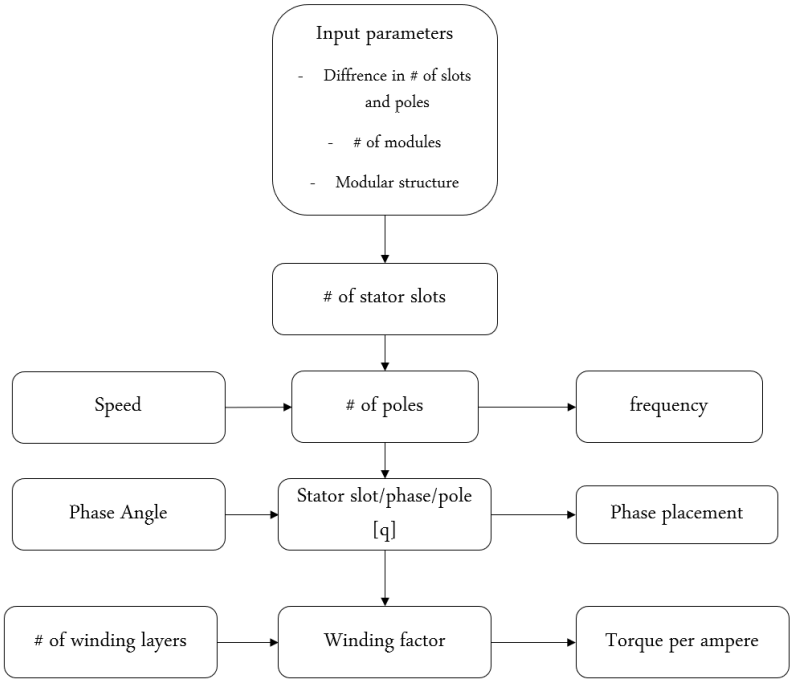

Figure 3.1.4: Winding Design Procedure

The winding structure is selected as concentrated due to the benefits obtained such as higher fill factor and higher fault tolerance, in addition to the correlation between concentrated windings and modular structure described in Section 2.5.2. The difference in stator slots and poles obtained from the modular design process relates to a concentrated windings structure. The machines are also preliminary selected with single layered winding structure. Single layered windings contribute to a higher fill factor and higher fault tolerance. Furthermore, the winding structure does not have to be modified in order to implement the flux gaps between the modules due to the alternating stator teeth without coils. High fill factor and high fault tolerance are some of the reasons behind implementing a modular stator structure. Therefore, a single layered concentrated winding further

improve these benefits. The winding design constraints are given by Table 3.1.1 for the winding design and depend on the machine specifications given by Table 3.2.1.

Table 3.1.1: Specifications for Winding Structure for Machine Structures

Winding Feature	**Condition**
# of segments	16
Difference in # of stator slots and poles (sections (F1))	32
Difference in # of stator slots and poles (paths (F2))	16
Phase angle	60
# of layers	1
Winding structure	Concentrated

The constraints given in Table 3.1.1, in addition to general winding design rules presented in Section 2.5.1.1 are the basis for the winding design. The stator slots are determined in relation the number modules, modular structure and phase angle. The number of poles are determined based on the number of stator slots and the required difference in stator slots and poles. The number of poles and stator slots must be reevaluated if the constraints and winding rules are not satisfied. The number of poles selected must be considered in relation to acceptable machine frequency. Nevertheless, constructing the winding design for the specified number of modules takes precedent over obtaining a suitable frequency. However, the winding structure and slot/pole combination can be modified within the given number of modules to obtain a suitable frequency. Thus, the geared machine is segmented based on paths instead of sections. The winding design for both machines yielded the results given by Table 3.1.2, when the machine design constraints of Table 3.1.1 were the basis for the winding layout.

Table 3.1.2: Winding Features for Direct Drive and Geared Machine

Winding Feature	**Direct Drive**	**Gear**
# of winding Bases	16	8
# of poles	160	80
# of stator slots	192	96
q	0.4	0.4
Winding factor	0.9659	0.9659
Frequency	13.333	266.667

The modules of the direct drive machine is based on sections and the geared machine are segmented on the basis of paths. Thus, the direct drive and geared machine required a difference in the number of poles and stator slots of 32 and 16, respectively. The fundamental winding factor for both machines are equal to the maximum value of 0.9659 due to q being equal to 0.4 with a single layer winding.

The number of stator slots and poles for the direct drive machine could be further increased to improve the frequency. The increase in slots and poles would not limit the modular winding design but rather increase the segmentation possibilities. The high

speed machine have a large frequency thus the limiting factor is the number of poles. An option were explored were the stator slots were the same as presented in Table 3.1.2, but the pole number were reduced to 64. This yielded a lower frequency, which were beneficial. However, the winding layout were unsuitable since the number of sections and paths were both equal to 32, leaving 3 slots for each base. Furthermore, the phase angle were also 120° resulting in a low winding factor. Thus the segmentation structure were altered and the machines modular structure were based on paths and not sections with a phase angle of 60°. This also allow for an exploration into segmentation choices since the premise of segmentation are different for the gear and direct drive machines.

3.1.3.1 Phase Layout

The phase layout is determined based on the average stator slot per pole per phase method explored in Section 2.5.4. The phase layout for the machines are given in Table 3.1.3.

Table 3.1.3: Phase Layout of One Base Winding for the Direct Drive Machine

Slot	1	2	3	4	5	6	7	8	9	10	11	12
Phase Placement	A	-A	-B	B	C	-C	-A	A	B	-B	-C	C

Table 3.1.4: Phase Layout of One Base Winding for the Geared Machine

Slot	1	2	3	4	5	6	7	8	9	10	11	12
Phase Placement	A	-A	-B	B	C	-C	-A	A	B	-B	-C	C

The phase layout for one base winding are repeated until all stator slots have been assigned a phase. The phase layout given for each machine demonstrates that symmetrical phase distribution have been obtained for both machines and modular structures. The direct drive machine could be further segmented on the basis of paths (F2) as observed from Table 3.1.3 were the phase layout of one base winding correspond to one module. The geared machine has reached the modular boundary limit and cannot be further divided for the given pole and slot combination since the phase layout of one base correspond to two modules. Therefore, The phase layout was corroborated by a star of slot representation.

3.1.4 Insulation Design

A modular structure alter the insulation required in the machine since the voltage is divided and distributed across the modules, as mentioned in Section 2.4.6. Some aspects of the insulation are also transported to the screens around the segments, which further reduce the insulation required in the stator slots [7]. The insulation design process is presented in Figure 3.1.5.

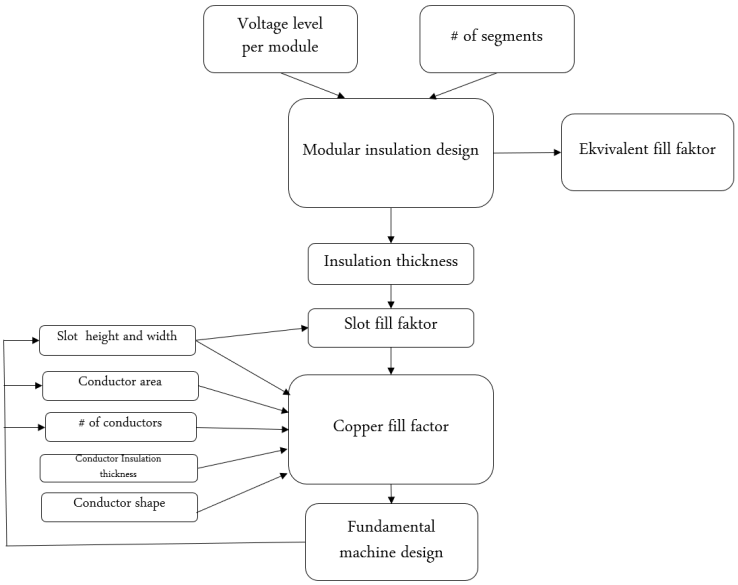

Figure 3.1.5: Insulation Design Procedure

The equivalent- and slot fill factor are dependent on the height and width of the slots and thus the stator slot area, as can be observed from Equation 2.4.18 and 2.4.21, respectively. The stator slots area are determined by linear current density required to obtain the necessary torque given by Equation 2.4.4. The modular insulation design determine insulation thickness of the slot walls on account of the voltage level and number of segments. Nevertheless, the coils require individual insulation. The conductor and slot insulation, in addition to possible air pockets are the inactive materials in the stator slot. The copper fill factor depend on the slot area, conductor area and number of conductors, in addition to the conductor and slot insulation and lost slot area. An iterative process is conducted for the slot-, copper fill factor and fundamental design until the fill factors for both design sub-categories converge. Therefore, the insulation design depends on the fundamental design of the machine. Furthermore, the fundamental design depends on the fill factor obtained from the insulation design. An iterative process is completed until the fill factor of the design sub-categories converge. It is important to note that the copper fill factor could possibly be increased further in an optimisation process.

The flux gaps were implemented with unaltered stator teeth width. Thus, the empty slot factor are not included and the stator slot width are not altered due to stator area lost. Thus, the effect of the flux gap implementation without alterations in relation to flux density and loss can be observed.

The copper conductors were designed as rectangular slots due to the benefits linked to this structure presented in Section 2.4.6. A factor of 1.1 were added to the copper conductor area and represented the insulation factor. Thus, the actual insulation requirement for the conductors might diverge from the given factor, but there were some challenges linked to finding suitable conductor insulation data. The factor was deduced from insulation data given by [23].

3.1.5 Core Loss Design

3.1.5.1 Loss Constants

The core loss depend on the ferromagnetic material proprieties of the iron core. These properties are incorporated into the loss model by the material constants, K_a, K_e, K_h and α as demonstrated by Equation 2.6.2 to 2.6.4. The material constants are determined by utilising curve fitting tools based on empirical power loss measurements for different frequencies given by Figure D.1.2. The empirical loss values should include a minimum of three frequency levels in the curve fit to obtain accurate constants [5]. The curve fit can include three or four variables given that the power loss is divided into the three categories hysteresis, eddy current and anomalous with four possible material constants. A four variable curve fit determine all four material constants. However, the eddy current constant can be determined by utilising material properties for the iron core. The eddy current constant is given by Equation 3.1.1 [8], [10].

$$K_e = \frac{\gamma_L \pi^2 t^2}{6\delta}. \tag{3.1.1}$$

The curve fit is implemented in Matlab to determine the material constants utilising Matlab's curve fitting tool. The curve fitting tool yields a factor, R, that indicate accuracy of the curve fit. Thus, the factor R can be utilised as an indication of the loss constant calculation and loss accuracy [10].

3.1.5.2 Core Loss Components

The modelling method presented in [10] and [5] includes the loss component, anomalous losses given by Equation 2.6.4. The anomalous losses can, as mentioned in Section 2.6.1, be seen as an extension of the eddy current losses and are included in order to consider the eddy current losses homogeneous in the iron core. However, the anomalous losses can be incorporated into the eddy current loss calculations by implementing an α value of 2 [10], [8]. The inclusion of the anomalous loss expression can negatively impact the robustness of the loss calculations. Core loss methodology presented in Section 2.6.1 includes anomalous losses by Equation 2.6.4 where B is to the power of 1.5.

The inclusion of the anomalous loss expression can lead to a non constant loss when utilising Cartesian components, which does not affect the hysteresis losses and the eddy current losses. Hysteresis losses depend on the maximum flux density and the flux density expression for the eddy current constant is to the power of 2 as observed by Equation 2.6.5 and 2.6.7, respectively. Thus, the eddy current and hysteresis losses are not affected by rotation variation. Excluding anomalous losses can be a more robust loss methodology [10], [5]. Therefore, the core losses components for this thesis is limited to eddy current loss and hysteresis loss with the material constant α_L is given as 2. The loss constants determined by the curve fit is limited to the hysteresis and eddy current constants. The direct drive and geared machine have utilise the same materials so the core loss constants are the same for both machines.

3.1.6 Parameter Study

Some machine parameters could vary within the machine constraints imposed, as mentioned in Section 3.1.1. The parameter study were included to discern suitable sizes for these parameters in relation to each other. The machine aspects included were related to geometrical, electrical and magnetic features.

The parameter study of the flux density in the air gap is given by Figure 3.1.6 for both machines. The air gap flux density is the first parameter studied since it mainly depend on the air gap and magnet properties and does not rely on the number of poles and stator slots, nor the machines diameters.

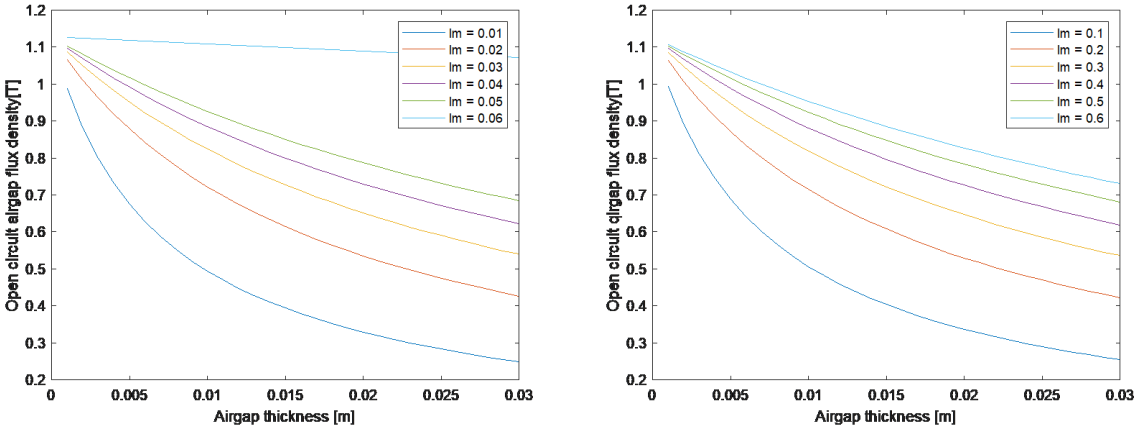

(a) Direct Drive (b) Gear

Figure 3.1.6: Open Circuit Air Gap Flux Density Value for Variable Magnet and Air Gap Thickness

The air gap flux density correlate with the fundamental air gap flux density space component as seen from Equation 2.3.3. The magnet thickness and air gap thickness are selected in order to yield a suitable open circuit air gap flux density. The geometrical sizes are included in the parameter study due to the size restrictions given by Table 3.2.1 for the machines. Furthermore, an important machine design feature is the torque and the corresponding linear current density, given by Equation 2.2.3. The linear current density, determined by the nominal torque, depend on the machine dimensions. The required linear current density relationship with the machine diameter and length is given by Figure 3.1.7 for the direct drive and geared machine.

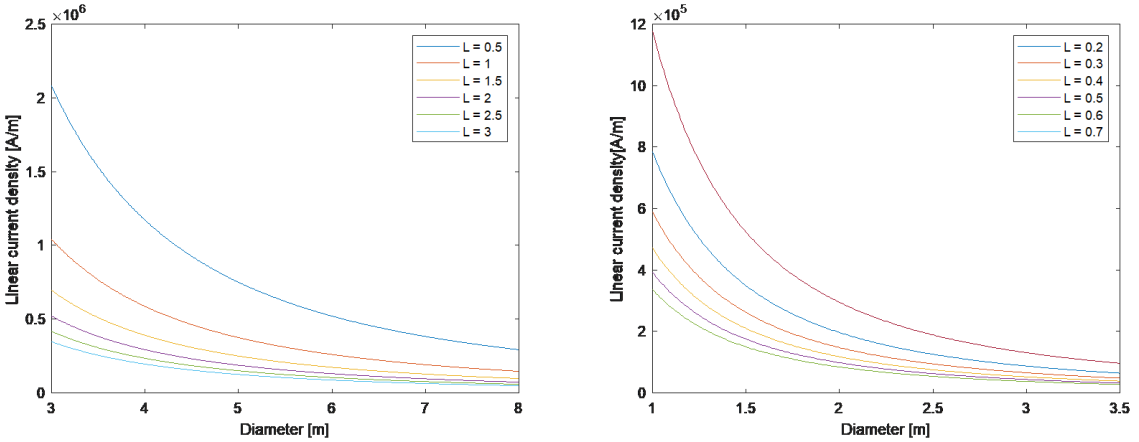

(a) Direct Drive (b) Gear

Figure 3.1.7: Diameter and Length Correlation with Linear Current Density

The length of the machines affect the weight so minimising the length is prioritised within the machines design constraint. The linear current density later contributes to determining the slot size. The machine size were selected so the slot area is of a reasonable size without exceeding the maximum current density. The width of the stator slot cannot be greater than the width allowed by the maximum limit imposed on the stator teeth flux density. Thus, the linear current density must be considered in relation to the stator slot area and height. A large linear current density can lead to abnormally long and difficult stator slots to manage.

The open circuit flux density in the iron structure determine the core sizes of the machines as explored in Section 2.3.2. The open circuit flux density in the air gap, stator and rotor, in addition to the stator teeth must be within acceptable limits of saturation. The open circuit maximum stator teeth width are, as mentioned given as a design limitation and thus the flux density in the stator teeth are not included for the parameter study. The rotor and stator yoke open circuit flux density compared to the yoke thickness is presented in Figure 3.1.8 and 3.1.9, respectively.

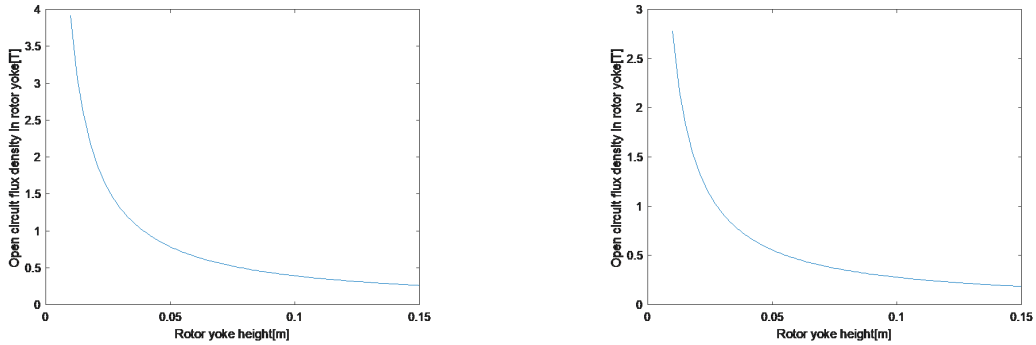

(a) Direct Drive (b) Gear

Figure 3.1.8: Rotor Yoke Thickness

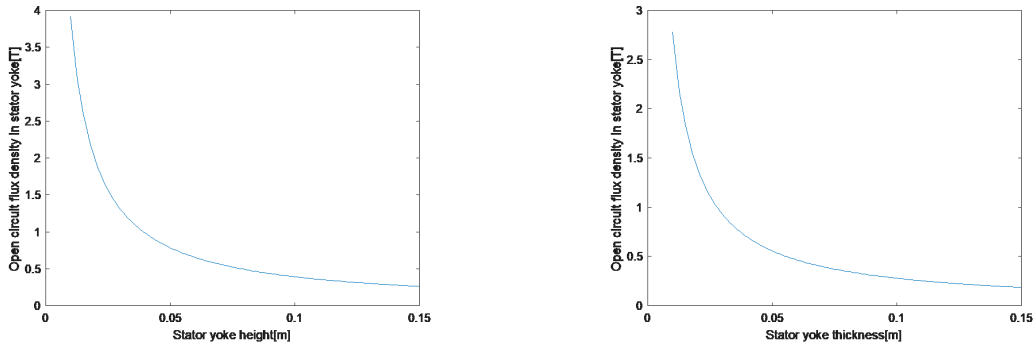

(a) Direct Drive (b) Gear

Figure 3.1.9: Stator Yoke Thickness

3.2 Analytical Design

The machine requirements and selections that were input constraints for the direct drive and geared machine design are given by Table 3.2.1. The machine specifications were

a preliminary requirement, while the machine selections were implemented due to the design benefits and behaviour yielded for these machine characteristics. The slot shape were implemented in order to simplify the machine design.

Table 3.2.1: Machine Design Origin

Machine Specification	**Feature**
Topology	Radial
Power	10 MW
Line to line Voltage [$V_{l-l,rms}$]	74 kV
Speed	10 rpm
Gear ratio	1:40
Maximum Diameter	8 m
Maximum length	3 m
Converter voltage limit [rms]	2.8 kV
Machine Design Selections	**Feature**
Winding structure	Concentrated
Winding layer	Single
Slot shape	Rectangular
Coil shape	Rectangular
# of segments	16

General machine limitations are incorporated in the machine design in order to obtain a feasible machine structure. The machine limitations relates to the machine performance and are presented in Table 3.2.2.

Table 3.2.2: Machine Design Constraints

Machine Design Constraint	**Value**
Maximum open circuit air gap flux density	1.1 T
Maximum open circuit stator yoke flux density	1.5 T
Maximum open circuit rotor yoke flux density	1.5 T
Maximum open circuit stator teeth flux density	1.5 T
Maximum current density	$3{\cdot}10^6 A/m^2$
Slots per pole per phase	$0.25 < \mathrm{q} < 0.5$
Maximum magnet temperature	80°

The flux density requirements are implemented in the machine design in order to avoid over-saturation. The maximum current density ensures a suitable stator slot temperature given that the constructed machine adhere to the given limit. The slots per pole per phase range ensures a feasible concentrated winding structure. The temperature limit for the magnet are incorporated in order to avoid demagnetisation. Machine design constants utilised to obtain the machine performance are given by Table 3.2.3.

Table 3.2.3: Machine Parameters that Remains Constant in the Design

Machine Design Constant	**Value**
Current angle for d-axis [θ_d]	-25°
Eddy current constant [K_e]	0.0001225
Hysteresis constant [K_h]	0.01437
α_L	2

The eddy current and hysteresis constant were determined by curve fitting. α_L is given as 2 due to the core loss expression utilised. The Matlab curve fitting tool is given in Appendix D.2. The d-axis current angle were determined based on the star of slot method given in Section 2.5.3. The q-axis angle, θ_q, is 90° phase shifted from the d-axis angle. The analytical design method presented in Section 3.1 based on the machines specifications and constraints yielded the machine parameters and performance presented in Table 3.2.4 and 3.2.5.

Table 3.2.4: Geometric Machine Parameters

Parameter	**Direct Drive**	**Gear**
Outer stator radius [R_{so}]	3.7552 m	1.4687 m
Inner stator radius [R_{si}]	3.5170 m	1.2560 m
Inner air gap radius [R_{ag}]	3.507 m	1.2500 m
Outer rotor radius [R_{ro}]	3.4770 m	1.2320 m
Inner rotor radius [R_{ri}]	3.3770 m	1.1520 m
Machine length [L]	1.500 m	0.3800 m
Air gap length [g]	0.010 m	0.006 m
Relative magnet length [α_m]	0.7	0.7
Magnet circumferential length [w_m]	0.0967 m	0.0691 m
Magnet thickness [l_m]	0.03 m	0.018 m
Slot pitch [τ_s]	0.1151 m	0.0822 m
Pole pitch [τ_p]	0.1381 m	0.0986 m
Stator slot area [A_s]	0.0067 m^2	0.0038 m^2
Stator slot height [h_s]	0.1182 m	0.0927 m
Stator slot width [w_{st}]	0.0567 m	0.0407 m
Stator tooth width [w_{tt}]	0.0584 m	0.0414 m

Table 3.2.5: Machine Parameters and Performance

Electrical Parameter	**Direct Drive**	**Gear**
Open circuit air gap density [B_g]	0.8091 T	0.8046 T
Fundamental air gap density [B_g]	0.9179 T	0.9127 T
Flux per pole [ϕ_m]	0.1173 Mx	0.0211 Mx
Total flux [ϕ_{total}]	18.736 Mx	1.688 Mx
Equivalent fill factor [K_A]	0.8686	0.8299
Slot fill factor [f_{slot}]	0.9316	0.9078
Copper fill factor[k_{fill}]	0.7627	0.7448
Segment insulation thickness [T_{segm}]	2.0833 mm	2.0833 mm
Screen insulation thickness[T_{eart}]	5.0 mm	5.0 mm
Slot wall insulation thickness[T_{slot}]	1.33 mm	1.33 mm
Peak voltage pr phase	60 481 V	60 481 V
# of conductors pr. slot	130	78
Copper conductor area [A_{wire}]	$3.8778{\cdot}10^{-5}$ m^2	$3.6061\cot^{-5} m^2$
Total conductor diameter [A_{ins}]	$4.2656{\cdot}10^{-5}$ m^2	$3.9667{\cdot}10^{-5} m^2$
Peak Phase current pr. coil [I_{ph}]	164.5207 A	152.9923 A
Peak phase back-EMF [E_0]	$4.073{\cdot}10^4$ V	$4.397{\cdot}10^4$ V
Slot resistance [R_s]	5.4068 Ω	0.4419 Ω
Slot inductance [L_s]	1.4160 H	0.1590 H
Fundamental winding factor [k_w]	0.9659	0.9659
Nominal Torque [τ_r]	$9.549{\cdot}10^6 Nm$	$2.387{\cdot}10^5 Nm$

The machine was constructed in COMSOL based on the analytical design, in order to study the machine behaviour with the benefit of FEM-simulation tool and flux gaps. Thus, the modular structure is also implemented in the FEM-software. The direct drive and geared machine were first constructed as a non-modular machine to validate the analytical design. The non-modular machine performance is presented in Section 3.2.2. The machine behaviour is compared to the analytical design, the direct drive and geared machine is also compared.

3.2.1 Validation

The machine parameters and performance for the geared and direct drive machine were obtained from the analytical design based on theoretical calculations. The machines were constructed by utilising FEM simulation software, COMSOL, after suitable results had been obtained by the analytical model. The model was validated by comparing the expected behaviour of analytical design and the result gained from FEM simulations for non-modular machines. Laboratory testing of the machine are not included in the scope of this thesis. The validation is limited but substantiates the final results presented in the next chapter. Validation aspects are presented in the list below. The machine validation yielded several observations, which are explored further in this chapter.

- Feasible design
- Expected behaviour compared to behaviour from FEM simulations

- Modular comparison to non-modular structure
- Flux gap implementation

3.2.1.1 Feasible Design

The machine must uphold the machine constraints given by Table 3.2.2. The analytical design is conducted in order to adhere to the electrical and magnetic limitations that ensure suitable temperatures and reduce losses, respectively. The limitations included in the analytical design process can be verified in COMSOL and can be a factor utilised to observe if the analytical design and the resulting FEM simulations converge.

The slot area is determined on account of the allowed current density and linear current density required to obtain the given torque levels, while the stator slot width is indirectly determined based on the maximum stator teeth flux density. A consequence of this design method could be stator slots, which are long and thin making it physically difficult to implement the copper coils. If the analytical machine design result in an unsuitable stator slot shape then the machines parameters must be reevaluated. Steps taken to counteract this phenomenon included increasing the stator slot diameter or other factors that limit the required linear current density.

The scope of this thesis relates to constructing a feasible machine. Nevertheless, the parameters determined might not yield the best result and an optimisation of the machine design should be completed in order to improve the machine. The analytical design is also limited and does not tackle all aspects related to the machine performance, such as heat transfer in the machine. It can therefore be assumed that the results gained from FEM simulations and the analytical design will vary within a certain scope.

3.2.2 Analytical Design Compared to FEM Simulation for Non-modular Machines

The modular structure affects the machine behaviour due to the flux gaps. Therefore, the machines were initially constructed without flux gap. However, it is important to note that the the copper fill factor implemented for the non-modular machines were based on the modular structure, even though these machines would have a lower fill factor. The simplified models are constructed in order to compare the analytical design and the FEM simulations. The machine performance measured by the FEM software and the corresponding deviation from the analytically calculated values are given in Table 3.2.6 and the FEM simulations are presented in Appendix B.

Table 3.2.6: Non-Modular Machine Performance with % Correlation Against Analytical Results

Machine Parameter	**Direct Drive [% corr.]**	**Gear [% corr.]**	**Unit**
Peak Phase Voltage [V_{pk}]	57160 [94.51%]	55011 [90.96%]	V
Tot. Peak Phase Back-EMF [E_0]	39 515 [97.02%]	43 380 [98.67%]	V
Resistance [R_s]	5.365 [99.2%]	0.4385 [99.23%]	Ω
Nominal Torque [τ_r]	$9.3757{\cdot}10^6$[98.15%]	$2.5134{\cdot}10^5$[105.29%]	Nm
Cogging Torque [$\triangle T_{cog}$]	17070	870	Nm
Torque ripple [$\triangle T_{rip}$]	$5.82{\cdot}10^5$	$3.50{\cdot}10^4$	Nm
Peak copper loss [P_c]	435 500	30 795	W
Hysteresis loss [P_h]	10604	12097	W
Eddy current loss [P_e]	35 661	380 664	W

The % correlation noted in Table 3.2.6 are the percentage size of the non-modular results compared to the analytical value. The modular results are later compared to the result obtained from the non-modular machine and not the analytical design results.

Table 3.2.6 demonstrates that the FEM-simulation results deviate from the calculated values to an acceptable degree and the values converge. Thought, the result vary differently for the direct drive and geared machines. The current density is not presented in Table 3.2.4 but given by in Appendix B and it can be observed that the machine adheres to the current density limit. The open circuit flux density in the iron core correspond to the given limits as observed from the plots in Appendix B. Thus, the FEM-models were further constructed with the implementation of flux gaps.

3.2.2.1 Flux Gap Implementation

The modular machines are implemented with three different flux gaps with a width of 1cm, 1.5 cm and 2cm in order to observe the effect of an increased flux gap width. The smallest flux gap width of 1 cm are the main focus of the result, but the other flux gap widths are included to observe possible negative effect linked to flux gap implementation and increased flux gap width. The parameters affected by an increase in flux gaps are included in Appendix C.1 and C.2 for the machines with a flux gap width of 1.5 cm and 2 cm, respectively. As mentioned in Section 3.1.4, were the flux gaps implemented directly without including an empty slot factor and readjusting the stator teeth width.

3.3 FEM-software

The FEM-software utilised for this thesis was COMSOL Multiphysics. The machine geometry was constructed in COMSOL and assigned the material properties and behaviour for each machine component. The machines performance was analysed utilising stationary and time dependent.

3.3.1 Model Setup

A machine segment were constructed for each machine. The segment built corresponded to one base winding for both machines, which is one module of the direct drive machine and two modules of the geared machine. The geometry was limited to one base winding in

order to limit simulation time and construction required. The base winding modules are repeated according to the number of bases. Therefore, the machine construction could be limited to one base winding. The machine geometry is presented in Figure 3.3.1 and 3.3.2 the modular machines with a flux gap width of 1.5 cm.

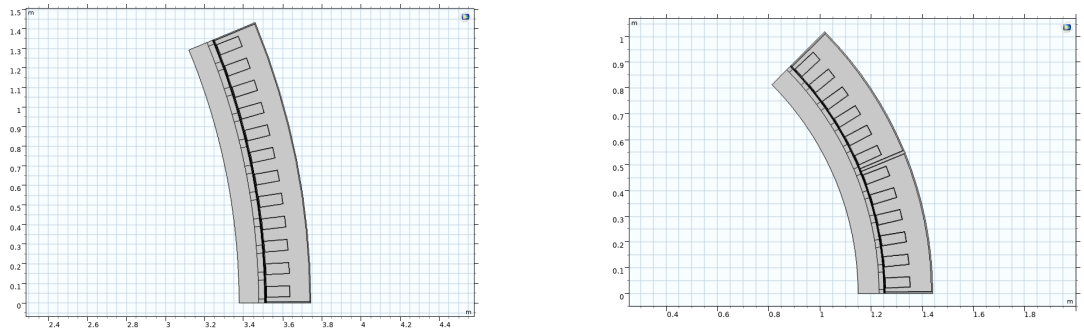

(a) Direct Drive

(b) Gear

Figure 3.3.1: COMSOL Construction of Modular Machine with a Flux Gap Width of 1 cm

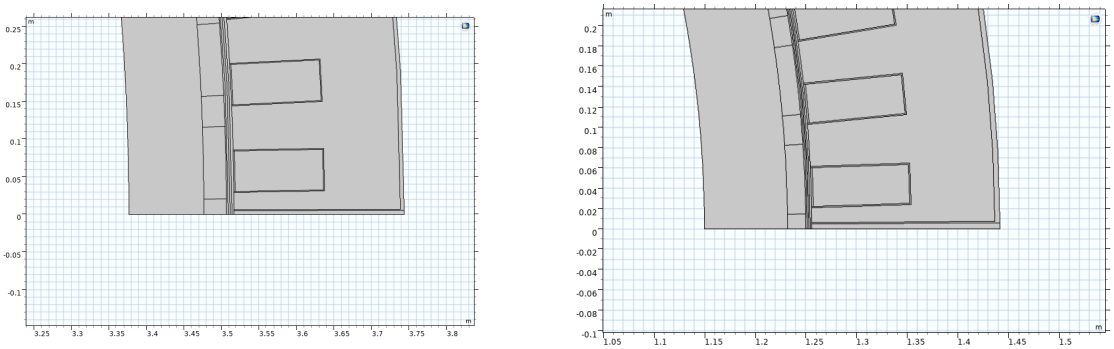

(a) Direct Drive

(b) Gear

Figure 3.3.2: COMSOL Construction of Modular Machine with a Flux Gap Width of 1 cm, Close up

The other machines constructed are the same as the machines given by Figure 3.3.1, with the exception of the flux gap width, which are excluded for the non-modular machine, and increased for an increased flux gap width. The air gap was constructed as four different segments as observed in order to improve the air gap mesh and implement the necessary boundary conditions in the air gap. The model was constructed as a 2D model in order to limit simulation time. The machine length was included as the depth of the model. However, a 2D model affect the machine implementation. Lamination is not included for a 2D model and the cores electrical conductivity is given as zero. Thus, lamination stack coefficient is equal to 1. Furthermore, end winding electrical parameters are also excluded.

The relevant material properties implemented in COMSOL are presented in Appendix D.1. It is important to note that there were some issues related to obtaining good machine data for some cases. For these cases approximations were included. One example of this is the B-H curve presented in Appendix D.1. Furthermore, the insulation thickness of

the stator structure around the screen and in the stator slots were based on theoretical calculations and sources. Thus, these limits are not incorporated.

3.3.1.1 Rotating Magnetic Machinery

The machine constructed in COMSOL are assigned a physical behaviour according to the structure constructed. The physic, rotating magnetic machinery, was utilised in order to include electrical machine behaviour related to the different components. Rotating machinery features included are, among other, coils, magnets, iron and air gap utilising amperes law in relation to the machine features. The coil feature denote the conductor area, current, phase and material properties related to copper. The magnets feature include remanence flux density and polarity direction. The temperature increase in the magnets were included by altering the remanence flux according to Equation 2.3.4. The current implemented in the coil features denote the sinusoidal current with the desired amplitude, phase, phase shift, number of conductors, conductor area and current direction. Boundaries are also incorporated in the rotating magnetic machinery physics. These include boundary conditions for the edge of the machine segments, which denote the repetitive nature of the segment built. Sector symmetry is defined between the rotor and stator segments. The boundary conditions implemented in COMSOL was continuous due to the repetitive nature of the machine segments constructed. The rotation of the machine is also denoted in the rotating magnetic machinery [22].

3.3.1.2 Mesh

A mesh features is included in COMSOL in order to analyse the machine performance. The mesh is implemented in the constructing in order to study the structures using finite elements which correspond to the mesh components. The accuracy of the mesh is an important since it denote the finite element structure. A close up of the mesh for the direct drive and geared machine are given in Figure 3.3.3. Furthermore, a close up of the air gap is included in Figure 3.3.4.

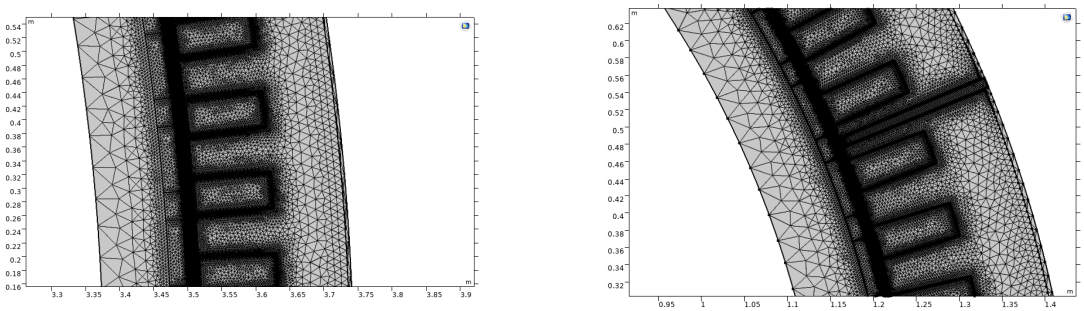

(a) Direct Drive

(b) Gear

Figure 3.3.3: Mesh Distribution for the Modular Machine with a Flux Gap of 1 cm

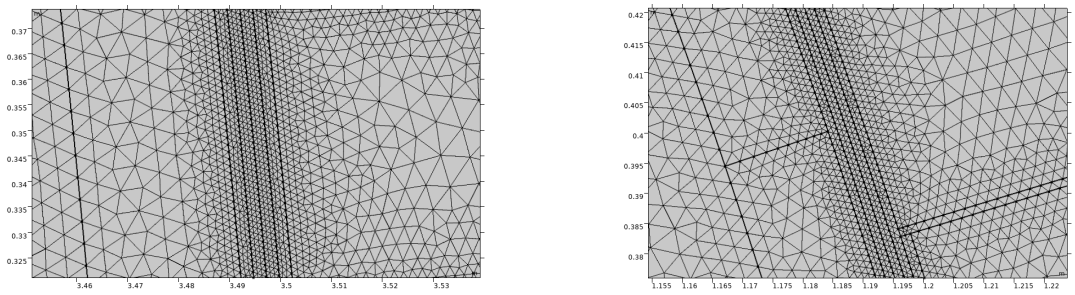

(a) Direct Drive (b) Gear

Figure 3.3.4: Mesh Distribution for the Modular Machine with a Flux Gap of 1 cm

The mesh size in the air gap was specified in order to ensure an acceptable air gap mesh distribution. Furthermore, the mesh in the air gap and flux gaps are improved by including a distribution factor, which improve the mesh distribution. Mesh boundary conditions were also included in the mesh and were implemented for the deconstructed air gap, inner and outer radius, in addition to the boundary of the segments. A more accurate mesh structure increase the computational time considerably since more elements are incorporated. the mesh distribution size was limited.

3.3.1.3 Loss Model

The copper loss calculations were implemented by combining the parameters the copper loss depend on in a plot, according to Equation 2.6.8. The core loss however required a more sophisticated simulation implementation. The core loss expressions given for a time dependent model was utilised and implemented in the feature know as Derived Values. The surface integration feature were utilised and the time dependent core loss equation were implemented in the surface integral expression and the machine segment of the rotor and stator core were selected as the surface. Nevertheless, the expression also had to account for the total number of modules, weight of the iron and length of the machine. These factors were included in the integral expression.

The surface integral expression were further specified according to the core loss component. The integral method were given as integral for both eddy current and hysteresis loss. However, the data series operation were given as absolute for the hysteresis loss and integral for the eddy current loss. The simulation were also specified to be for one period for both machines, which was required due to the time dependent core loss expressions given in Section 2.6.1, which are specified for one time period.

3.3.2 Analysis

The FEM analysis was conducted utilising stationary, time dependent and frequency domain studies in COMSOL, as mentioned earlier. The studies were conducted with an error of 0.1%. The time dependent study was conducted for three time periods, with a time step of T/100, with the exception of the core loss simulations. The core loss simulations required a simulation time equal to one period due to the expressions, as mentioned in the previous section. The stationary and time dependent analysis components were included in one study. The simulations conducted were for no load and full load conditions. Performance obtained under no-load condition are presented in the following list.

- Open circuit flux density

- Open circuit air gap flux density
- Phase back-EMF
- Cogging torque

It is important to note that the no-load results are obtained without conductivity in the materials in addition to no current. The full load machine performances have a three phase current implemented in the coils. The current induced in the slots are given by Equation 3.3.1 to 3.3.3.

$$I_a = I_{ph} sin(2\pi ft + \theta_q), \tag{3.3.1}$$

$$I_b = I_{ph} sin(2\pi ft + 2\pi/3 + \theta_q), \tag{3.3.2}$$

$$I_c = I_{ph} sin(2\pi ft + 4\pi/3 + \theta_q). \tag{3.3.3}$$

θ_q denote the current angle required to align the currents with the q-axis and was 90° phase shifted from θ_d. The phase currents are implemented in the COMSOL model according to the phase layout presented in Section 3.1.3.1. The full load performance included the following results [22]:

- Nominal torque
- Voltage
- Resistance
- Full load flux density
- Current density
- Copper loss
- Core loss

Chapter 4

Results

A modular machine structure influence the machine design and alter the machine performance. The design procedure for modular machines are further explored in general in relation to the degree of modularity. The modular direct drive and geared machine is presented and studied utilising FEM simulation software, COMSOL. Furthermore, the altered behaviour is compared to the FEM-simulation results for the non-modular machines presented in Section 3.2.2 based on the results given in Appendix B.

4.1 Modular Structure

A modular machine alters certain aspects of the machine design as previously explored. Design aspects of a modular machine affected are insulation, possible winding structure and flux gaps. These design features change in relation to the degree of modularity.

4.1.1 Insulation

The insulation size depend on the number of modules and the relationship between the modules and insulation is of great interest. An increase in the number of modules limits the feasible pole and slot combinations and affect the winding structure, which is further elaborated in Section 4.1.1.1. Therefore, the relationship between the insulation reduction and imposed winding structure constrains should be studied during a design process. The relationship between the number of modules and the resulting equivalent fill factor are presented in Figure 4.1.1 for the direct drive and geared machine, respectively. It is important to note that the equivalent fill factor value relates to the given voltage level and stator slot shape for the direct drive and geared machine.

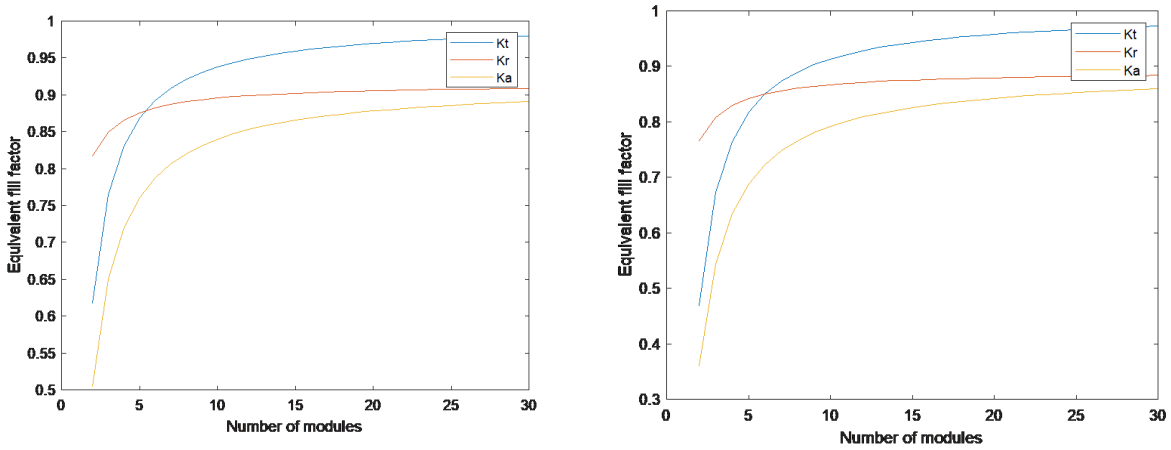

(a) Direct Drive

(b) Gear

Figure 4.1.1: Equivalent Fill Factor Obtained for an Increase in the Number of Modules

Figure 4.1.1 present the equivalent fill factor given as K_a, and the factors the equivalent fill factor depend on K_t and K_r. In addition, empty slot factor is excluded. The equivalent fill factor increase to a great degree when a modular structure is implemented and initially increased. However, the equivalent fill factor start to converge when the number of modules increase as observed from Figure 4.1.1. Thus, the benefits of a modular structure in relation to decreased insulation stagnate for a high degree of segmentation. Nevertheless, there can be other benefits related to a large number of modules in a machine such as, for this thesis, and is linked to the converter voltage limit.

The relationship between the equivalent fill factor and modularity are given in Figure A.0.1 and A.0.2 in Appendix A for a DC voltage level of 200 kV and 300 kV. The equivalent fill factor for a higher voltage also converge. However, equivalent fill factor converge toward a lower value compared to the equivalent fill factor with a voltage level of 100 kV given by Figure 4.1.1. Nevertheless, the equivalent fill factor convergence start to occur at the same number of modules for all voltage levels. Machine aspects that could indicate another point of convergence is the stator slot area. The equivalent fill factor obtained at 30 modules are given in Table 4.1.1.

Table 4.1.1: Equivalent Fill Factor Convergence Values

DC Voltage Level	**Direct Drive**	**Gear**
100 kV	0.8902	0.8575
200 kV	0.79494	0.7248
300 kV	0.6829	0.5969

The insulation thickness for the stator slots, outer rotor radius and between segments for different number of modules are presented in Figure 4.1.2.

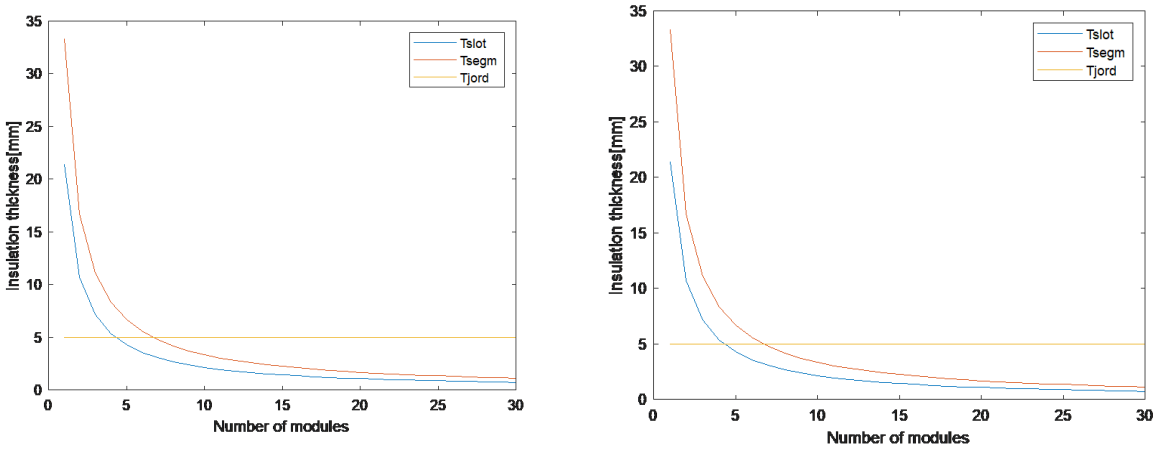

(a) Direct Drive

(b) Gear

Figure 4.1.2: Segment Insulation

The outer screen insulation does not depend on the number of modules, which can be observed from Equation 2.4.23. However, the insulation thickness between the segments and in the stator slots decrease with an increase in the number of segment. The modular insulation for an increased number of segments presented in Figure 4.1.2 demonstrates the same trend as the equivalent fill factor. The effect of implementing modules are great when modularity is initially implemented. However, the insulation thickness converge when the number of segments increase substantially. Nevertheless, the correlation between the insulation thickness, equivalent fill factor and number of modules demonstrates the benefits of a modular structure in relation to insulation reduction. The geared and direct drive machine required the same insulation thickness in the stator slots and around the modules since the insulation properties and voltage level are the same. However, the equivalent fill factor and slot fill factor depend on the stator slots size and are therefore marginally different.

4.1.1.1 Winding Structure

Symmetric modular machines require a symmetric phase layout in each machine module. The phase layout is dependent on the pole/slot combination as explored in Section 2.5.2. Therefore, the slot/pole combination required to obtain a feasible winding layout alter according to the number of modules. Table 4.1.2 yield the minimum number of slots and poles, the required difference in poles and slots, and the resulting winding factor for different degrees of modularity. Table 4.1.2 yields the minimum pole/slot combination required for a modular machine given a phase angle of 60°, a single layer and a modular structure equal to sections (F1). The slot/pole combination allow for further segmentation if the modular structure is based on paths (F2) instead of sections (F1) due to the phase angle of 60°.

Table 4.1.2: Modular Parameter Study

# of segments	In pole/slot	Min. pole #	Min. slot #	Winding factor	q
2	4	20	24	0.9659	0.4
4	8	40	48	0.9659	0.4
8	16	80	96	0.9659	0.4
10	20	100	120	0.9659	0.4
12	24	120	144	0.9659	0.4
14	28	140	168	0.9659	0.4
16	32	160	192	0.9659	0.4
18	36	180	216	0.9659	0.4
20	40	200	240	0.9659	0.4

The machine structures presented in Table 4.1.2 are the lower limit of possible slot/pole combination as mentioned previously. It can be observed that the minimum number of slots and poles for different degrees of modularity all obtain the same winding factor due to the winding structure culminating in a q = 4. Both machines designed for the given thesis are present in Table 4.1.2, and are the structures given for 8 segments and 16 segments for the geared and direct drive machine, respectively. The geared machine have 16 number of segments since the modular structure is based on the paths (F2) instead of sections (F1). The minimum number of stator slots and poles increase with an increase in the number of modules. Thus, a higher degree of modularity require a higher pole and slot number in order to yield a feasible modular structure. The star of slot and EMF phasor representation for all slot and pole combinations presented in Table 4.1.2 are given by Figure 4.1.3 for one base winding.

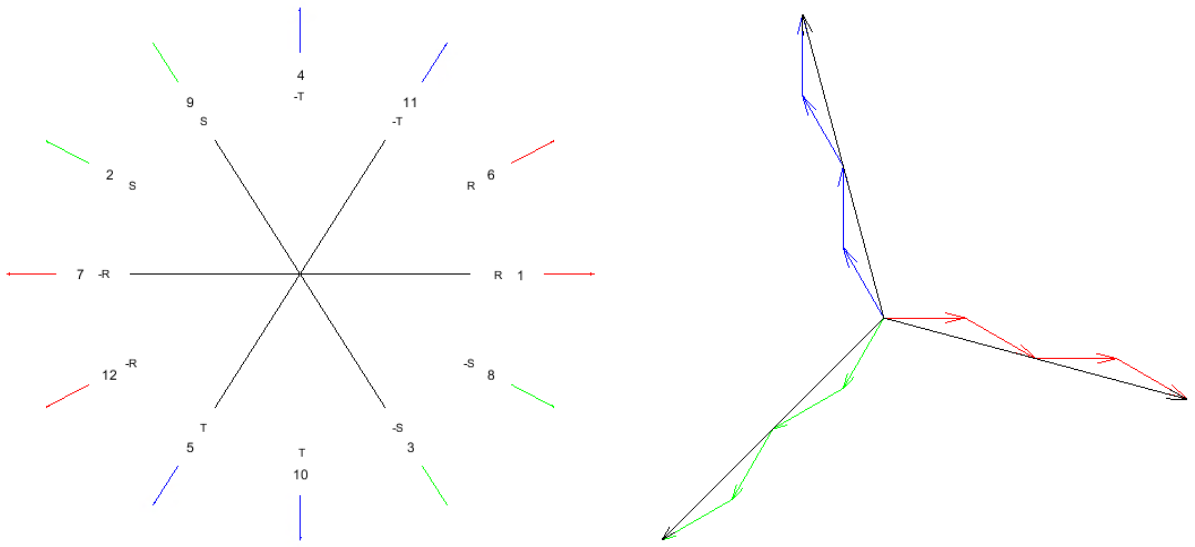

(a) Star of Slot for One Base Winding

(b) Phase EMF

Figure 4.1.3: EMF Phasor Representation

Figure 4.1.3 demonstrates that the modular winding structure presented in Table 4.1.2

has the minimum number of stator slot per base given a phase spread angle of 60° and a single layer. The phases occurs twice in the base winding with only two stator slots per phase. Thus, the base winding is at the minimum limit since two adjacent slot have the same phase and they correspond to the same coil wound around one stator tooth. Figure 4.1.3 also demonstrate that the base winding could be further segmented by paths (F2) by dividing the base winding as two modules. The phase distribution for a modular structure based on paths would be symmetrical.

Table 4.1.3 yield the frequency increase for an increase in the number of stator slots relative to the number of modules with a speed of 10 and 400 rpm, respectively. The values $2N_{s,min}$, $3N_{s,min}$ and $4N_{s,min}$, given in Table 4.1.3, denote the slot number compared to the minimum number of stator slots required for the number of modules given in Table 4.1.2. The number of stator slots were increased with the minimum stator slots times the integer denoted.

Table 4.1.3: Frequency Dependence of Modular Structure

Direct Drive [10 rpm]	$N_{s,min}$	$2{\cdot}N_{s,min}$	$3{\cdot}N_{s,min}$	$4{\cdot}N_{s,min}$
2 Segments	1.6667 Hz	3.6667 Hz	5.6667 Hz	7.6667 Hz
10 segments	8.333 Hz	18.333 Hz	28.333 Hz	38.333 Hz
20 segments	16.6667 Hz	36.6667 Hz	56.6667 Hz	76.667 Hz
Gear [400 rpm]	$N_{s,min}$	$2{\cdot}N_{s,min}$	$3{\cdot}N_{s,min}$	$4{\cdot}N_{s,min}$
2 Segments	66.667 Hz	183.335 Hz	283.335 Hz	383.335 Hz
10 segments	333.33 Hz	733.33 Hz	1133 Hz	1533.33 Hz
20 segments	666.667 Hz	1466.68 Hz	2266.68 Hz	3066 Hz

The frequency increase to a greater degree when the speed is higher for an equal increase within a given modular structure. The frequency also increase to a greater degree when the number of modules are higher for all speeds, as observed by comparing the frequency increase for a machine with 2 and 20 modules. This occurs since a greater increase in the stator slots are necessary for a machine with a higher degree of segmentation. The number of poles are determined by the number of stator slots required for the given number of modules and the difference in stator slots and poles in order to obtain a feasible phase layout. Thus, for symmetric modular structures it is the number of stator slots that are the defining modular constraint and the pole number must be chosen in accordance with the number of stator slots and the required difference in the number of stator slots and poles. As a result, the frequency have a greater increase for a higher degree of modularity in order to obtain a feasible slot number.

4.1.1.2 Winding Factor

The flux gap required between the stator modules reduce the effective slot pitch for the adjacent stator slots and thus the coil pitch, as given by Equation 2.5.15 in Section 2.5.5.1. The winding factor reduction due to the flux gap width is given by Figure 4.1.4 for the direct drive and geared machine.

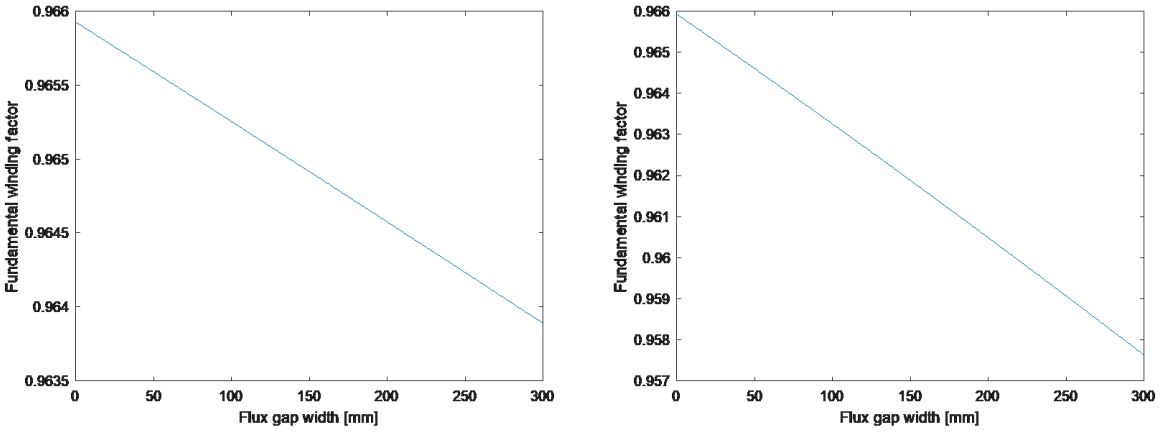

(a) Direct Drive (b) Gear

Figure 4.1.4: Effect of Flux Gap on the Fundamental Winding Factor

The winding factor is reduced when the flux gap between the stator modules increase with the given machine pole/slot combination for the direct drive and geared machine. The geared machine experience a greater reduction in the winding factor compared to the direct drive machine. This can be linked to the slot and pole pitch in relation to the size of the inner stator slot radius and the number of flux gaps compared to stator slots. The reduced winding factor is linked to the modular structure and therefore the number of poles and stator slot compared to the number of modules. Thus, the greater reduction of winding factor for the geared machine is partially caused by the modular structure based on paths compared to the direct drive with a modular structure given by sections. To summarise, the decrease in winding factor is linked to four aspects, the number of flux gaps, flux gap width, slot/pole pitch, and machine dimensions. The geared machine has both a smaller inner stator radius, fewer slots and poles compared to the number of modules and a smaller stator tooth width, which result in a greater winding factor reduction.

4.2 FEM Analysis

The FEM analysis was conducted for two load conditions; no-load and full load for the direct drive an geared machine structure. The FEM analysis included the performance of non-modular machines, which are the non-modular counterparts to the modular machines constructed for this thesis. The FEM-simulation results of the non-modular machines were presented in Table 3.2.6. The non-modular results were included to compare the non-modular and modular machine performance, in addition to validate the analytical machine design without the effect of flux gaps. The FEM analysis presented in this section relates to the modular machines with a flux gap width of 1 cm. Selected machine parameters affected by the flux gap are given in in Appendix C.1 and C.2 for a flux gap width of 1.5 and 2 cm, respectively, and are included to further observe the machine performance deviation from non-modular machines for an increased flux gap width.

4.2.1 Flux Density

4.2.1.1 No-load Flux Density

The open circuit flux densities are obtained under no load conditions. The machine design limitations included open circuit flux density, given by Table 3.2.2. The open circuit flux

density limits are utilised in order to avoid over saturation for full load conditions. The direct drive and geared machine are booth designed for the same open circuit flux density limits. No load flux density distribution for the direct drive and geared machine are given by Figure 4.2.1 for the modular machine with a flux gap of 1 cm.

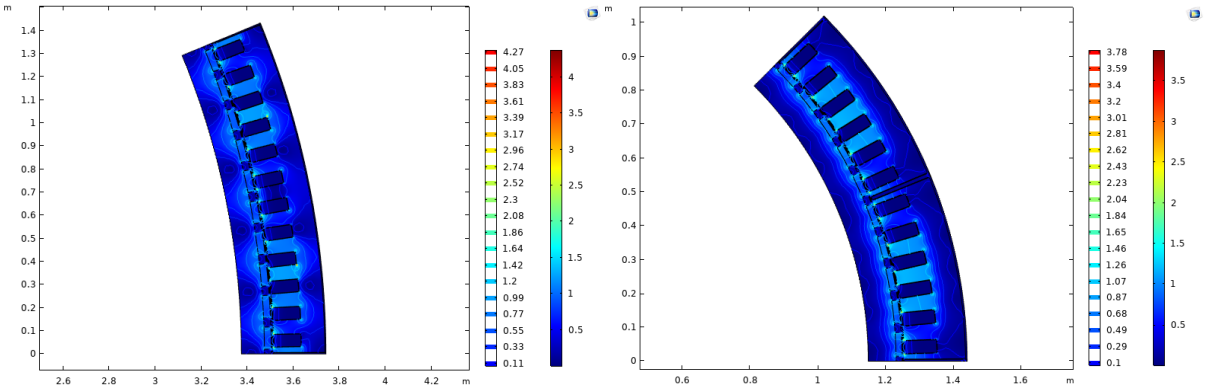

(a) Direct Drive (b) Gear

Figure 4.2.1: No-load Flux Density

The flux density in the stator and rotor yoke, in addition to the stator teeth coincide with the given limits by Table 3.2.2. The flux density in the stator teeth are 1.5 T at maximum, with the exception of the edge of the stator teeth. The stator teeth edges experience a very high flux density in a limited area. The open circuit flux density in the stator and rotor yoke are lower and varies between the value of 0.2 and 1.3 T, according to the varying magnetic field distribution. It can be observed from Figure 4.2.1 that the flux density level in the flux gap between the segments are approximately equal to zero. The flux gaps isolate the segments in regards to flux, and no magnetic fields move between the modules for no load conditions. The flux gap takes up some of the volume of the stator teeth between the segments.

The flux density in the air gap implemented between the stator and rotor affect the flux density distribution in the machine and influence other machine aspects such as the torque. The open circuit air gap density is given by Figure 4.2.2.

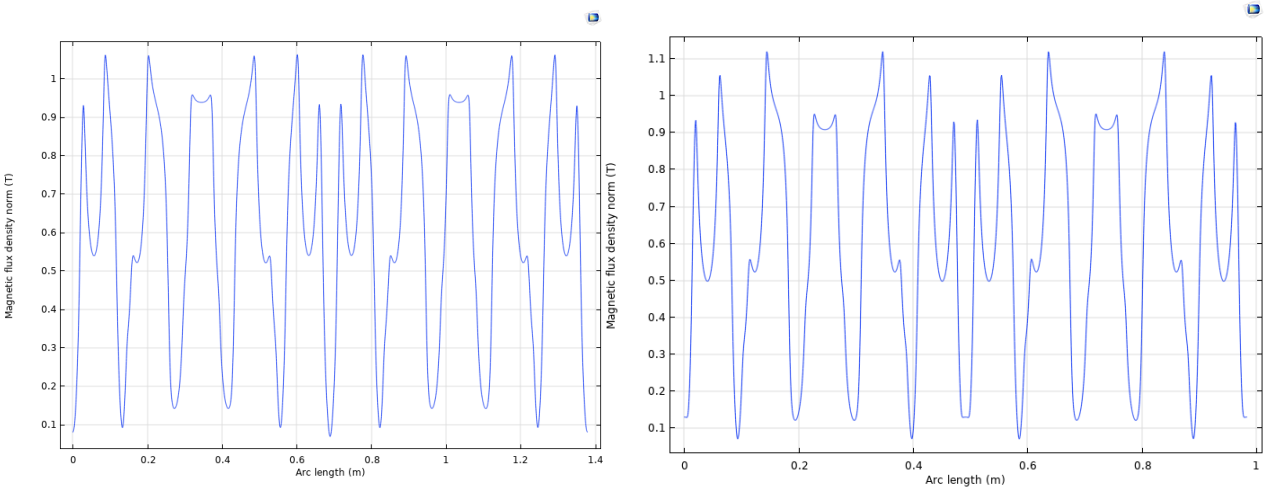

(a) Direct Drive

(b) Gear

Figure 4.2.2: Open Circuit Air Gap Flux Density

The no-load air gap flux density correspond with the given flux density limits with an exception for some areas of the geared machine. The geared machine exceed the limits at some points and thus improvements to the machine design could be considered in order to reduce the open circuit flux density slightly. The air gap flux density is affected by the flux gap present in a modular machine, and are reduced for both machines. The air gap flux density of the non-modular direct drive and geared machine are given in Appendix B. The difference in open circuit air gap flux density have a 99.98% and 96.01 % correlation with the non-modular machine for the direct drive and geared machine, respectively. Thus, the direct drive machine experience an negligible reduction, while the reduction of open circuit air gap flux density for the geared machine is prominent compared to the non-modular open circuit flux density.

4.2.1.2 Full Load Flux Density

The machine flux density in the core for full load conditions increase compared to the open circuit flux density. The full load flux density is given in Figure 4.2.3.

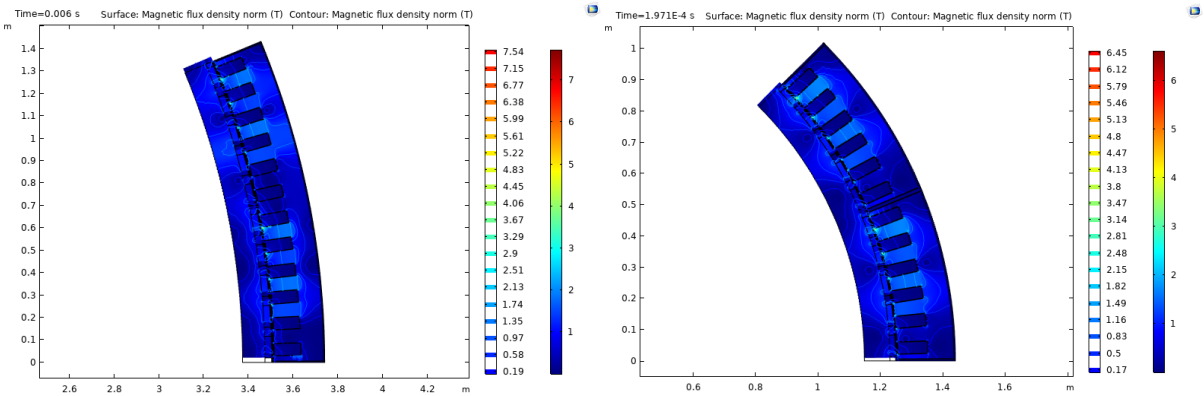

(a) Direct Drive

(b) Gear

Figure 4.2.3: Full Load Flux Density

The flux density in the stator teeth for both machines approaches saturation at a value

of 2 T, which correlate with saturation given by the B-H curve for the soft iron, given in Appendix D.1 The flux density in the rotor and stator yoke also approach saturation for some areas. However, there are larger areas with lower flux density compared to the stator teeth. There are also points in the machine that exceeds the saturation value of 2 T. The stator teeth edges experience a larger flux density as observed under no - load conditions, which can be linked to flux leakage.

Open circuit flux density and full load flux density experience an alternating magnetic field, which is especially apparent from the flux density in the stator teeth. This alteration in the flux density can be linked to sub-harmonic magnetic fields correlating to the difference in slots and poles for each base machine. The number of teeth covered by the reduced magnetic flux correlate with the difference in slots and poles for each basis winding. The harmonic is also apparent from the magnetic field lines that cross several stator slots.

The stator teeth adjacent to the flux gap also experience a high flux density given by Figure 4.2.4. The flux gaps for modular machines were implemented directly in the stator teeth without readjusting the stator tooth width. The stator teeth disrupted by the flux gaps have a reduced teeth width, since the flux gap and insulation between the segments make demands on some of the tooth width. The flux density of these stator teeth exceed the allowed limit. Steps can be taken to avoid this by either designing the machine for a lower open circuit flux density than the absolute limit or increase the stator teeth width by implementing empty slots, as explored in Section 2.3.3. A close up of the flux gap is presented in Figure 4.2.4, which present over-saturation occurring in the stator teeth adjacent to the flux gap. The increased flux density of the stator teeth adjacent to the flux gap is observed from this figure.

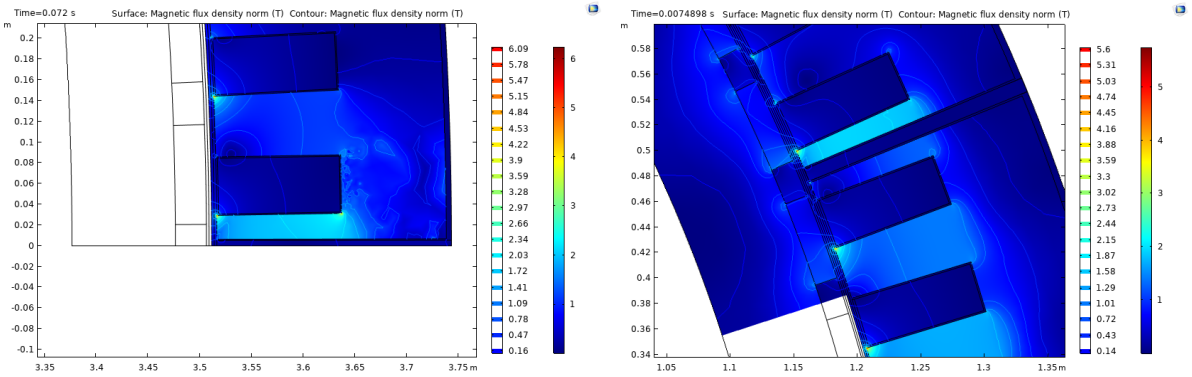

(a) Direct Drive (b) Gear

Figure 4.2.4: Close up of Full Load Flux Density

4.2.2 Electrical Parameters

The electrical parameters of the machine greatly depend on the fill factor and number of coils implemented in the machine. The modular machine structure was an integral part in the electrical design due to the influence on the fill factor and insulation.

4.2.2.1 Voltage

The phase back-EMF can be determined from the FEM simulations for voltage under no-load conditions without conductivity present. The phase back-EMF for the geared

and direct drive machine segment is given by Figure 4.2.5 with a flux gap width of 1 cm.

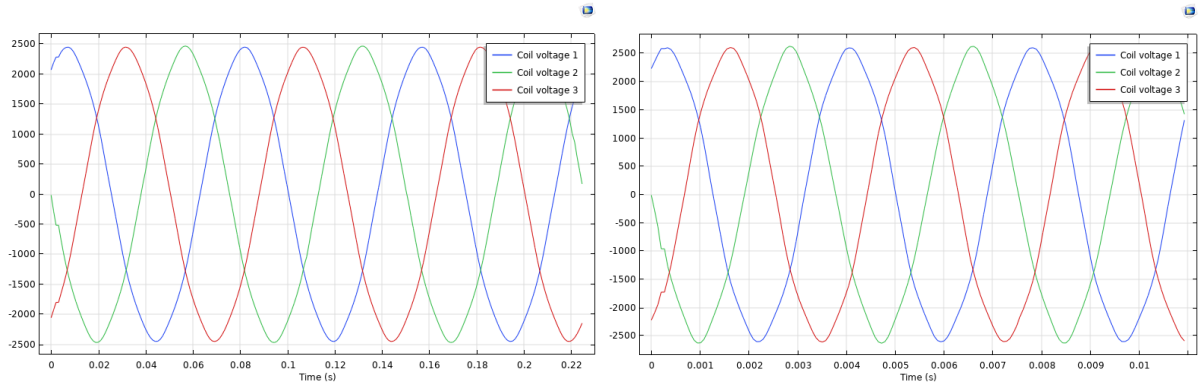

(a) Direct Drive (b) Gear

Figure 4.2.5: No-load Phase Back-EMF

The phase back-EMF for the modular machines presented in Figure 4.2.5 have a lower value compared to the non-modular machines. The phase back-EMF for modular machines with flux gap widths of 1.5 cm and 2cm are given in Appendix C.1 and C.2 for direct drive and geared machines. The value of the phase back-EMF for modular machines compared to non-modular machines are presented in Table 4.2.1 and included the % correlation with non-modular machines.

Table 4.2.1: No Load Phase Back-EMF [V] with % Correlation to Non-modular Results

E_0 pr. Module	$\beta = 1$ cm [% corr.]	$\beta = 1.5$ cm [% corr.]	$\beta = 2$ cm [% corr.]
Direct Drive	2449.75 [99.1%]	2445 [99.00%]	2437 [98.58%]
Geared	2629 [96.96%]	2542 [93.74%]	2481 [91.50%]

The phase back-EMF reduce with an increase in the flux gap width. The geared machine decrease with a greater percentage compared to the direct drive machine. The reduction of phase back-EMF depend on the machine dimensions compared to the flux gap size. The flux gap width is a relatively larger for the geared machine compared to the direct drive machine, as observed from Table **??**. The full load voltage for the modular machines are presented in Figure 4.2.6 for one module.

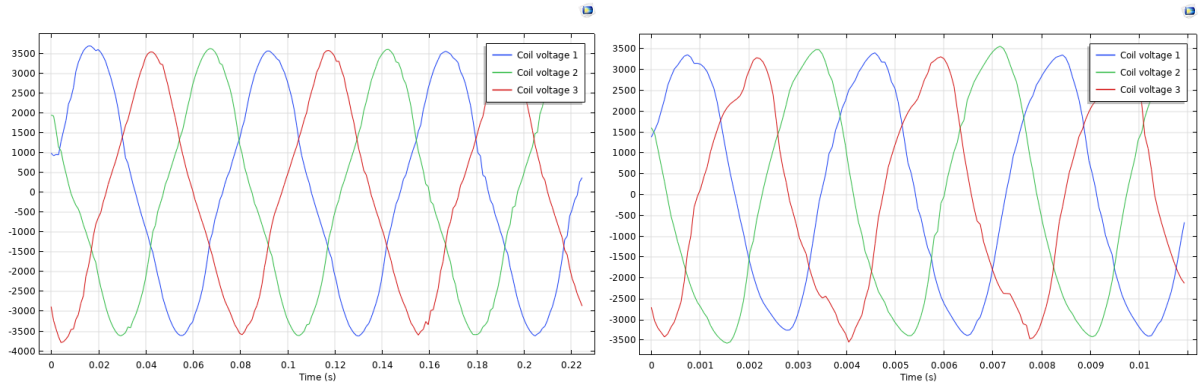

(a) Direct Drive (b) Gear

Figure 4.2.6: Nominal Voltage

The voltage for each module correspond with the required voltage to a reasonable degree for both machines. The % correlation is approximately 100.2% and 99.1% for the direct drive and geared machine respectively. Nevertheless, the peak load full voltage vary slightly for the different phases, which is especially apparent from the geared machine and can be a source of error.

4.2.2.2 Current

The current densities for the modular machines are given by Figure 4.2.7, with a flux gap of 1 cm during full load operations.

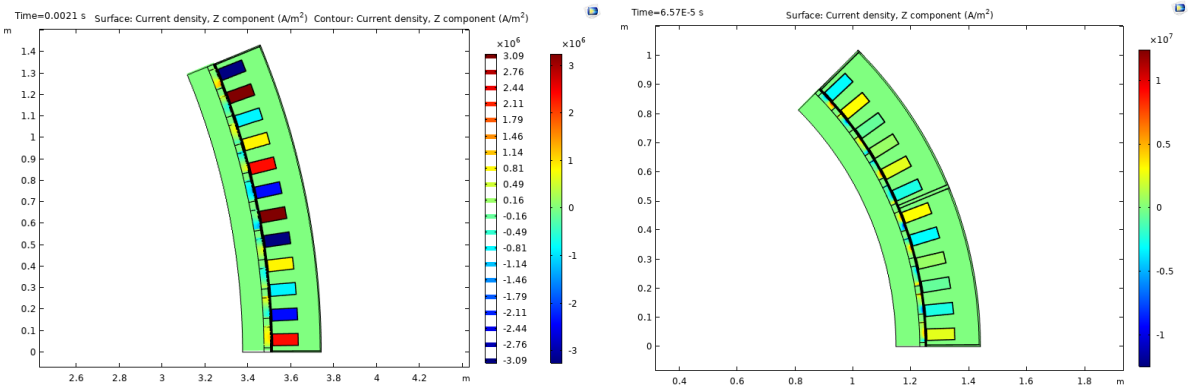

(a) Direct Drive (b) Gear

Figure 4.2.7: Current Density for Full Load Operation

The maximum current density was incorporated into the design process, as mentioned in Section 2.4.3. The measured current density does not exceed the maximum limit for any of the machines. It can be observed from Figure 4.2.7 that the current density for the modular machines are unaltered compared to the current density measure for the non-modular machines given in Appendix B. Furthermore, the coil characteristics such as the current, conductor area and fill factor are determined in relation to a modular structure. Thus, the current and current density are the same for non-modular and modular machines.

The measured full load current density of the whole module demonstrates that there are electric conductivity present in the magnets for both machines. The geared machine experience a large current density in the magnets, which can pose an issue and contribute to magnet loss. The conductivity in the magnets are further discussed in Section 5.3.3

4.2.2.3 Machine Resistance

The resistance measured in COMSOL is the phase resistance per module. The measure resistance correspond to the total slot resistance per phase for each module, since the end windings are excluded in the 2D model. The resistance is presented by Figure 4.2.8 for modular machines with a flux gap of 1 cm.

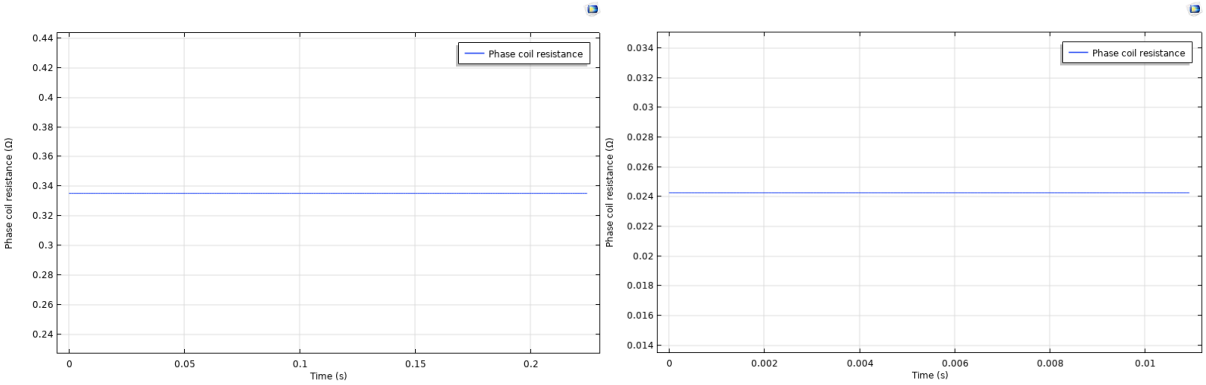

(a) Direct Drive (b) Gear

Figure 4.2.8: Slot Resistance

The non-modular resistance deviation is minimal for the direct drove machine, with a correlation value corresponding to 100.01%. However, the slot resistance of the geared machine converge to a lesser degree, with a percentage of 89%.

4.2.3 Torque

The torque produced for full load conditions, with a flux gap width of 1 cm between each module, are presented in Figure 4.2.9. The full load torque with a flux gap of 1.5 and 2 cm are given in Appendix C.1 and C.2, respectively.

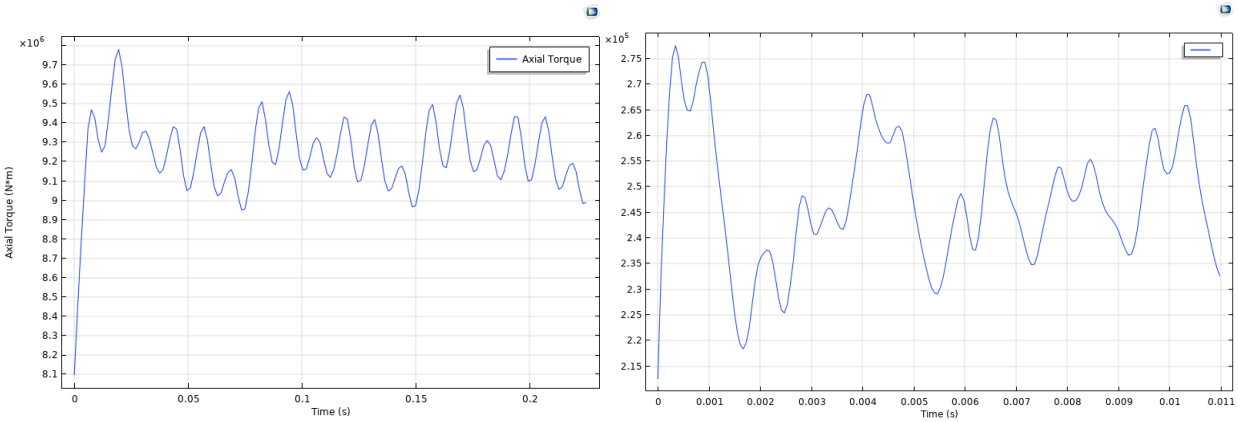

(a) Direct Drive (b) Gear

Figure 4.2.9: Nominal Torque

The power produced correlate with the torque. Thus, a reduction in torque, reduce the power output. The nominal torque for the non-modular machines converged with the analytical nominal torque to a reasonable degree, as observed in Table 3.2.6. The nominal torque for the modular machines are compared against the analytical obtained torque in order to determine the effect of implementing flux gaps between the modules. The nominal torque for the different flux gap widths are given in Table 4.2.2 and 4.2.3 for the direct drive and geared machine, respectively. The cogging torque are measured under no-load conditions with no electrical conductivity present in the machine and given by Figure 4.2.10 for the modular machines with a flux gap width of 1 cm are. The cogging torque with a flux gap of 1.5 and 2 cm are also given in Appendix C.1 and C.2, respectively.

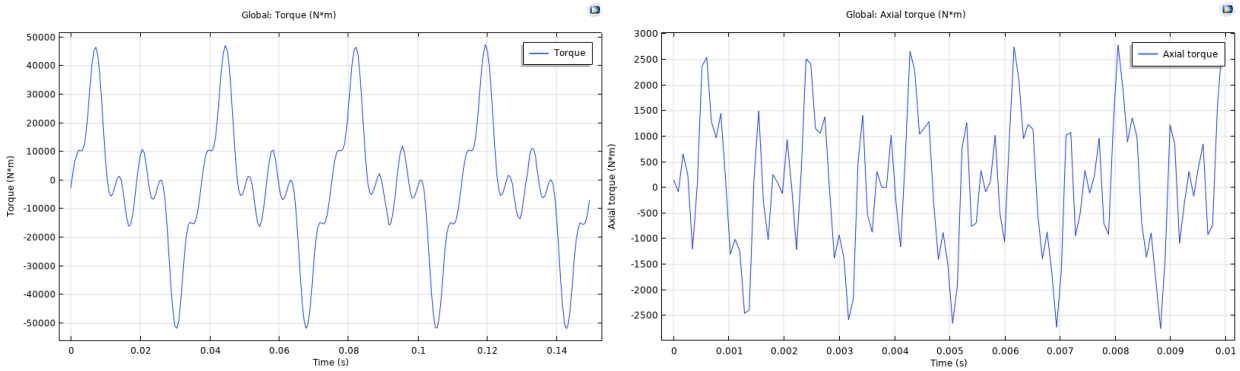

(a) Direct Drive (b) Gear

Figure 4.2.10: Cogging Torque

The amplitude value of the cogging torque for the modular machines compared to the non-modular machines are also presented in Table 4.2.2 and 4.2.3 with different flux gap width for the geared and direct drive machine, respectively.

Table 4.2.2: Torque Performance for Direct Drive Machine [Nm] with % Correlation to Non-modular Results

Torque Result	$\beta = 1cm[\%corr.]$	$\beta = 1.5cm[\%corr.]$	$\beta = 2cm[\%corr.]$
Nominal Torque	$9.262{\cdot}10^6[98.78\%]$	$9.219{\cdot}10^6[98.32\%]$	$9.156{\cdot}10^6[97.65\%]$
Torque ripple $[\triangle T_{rip}]$	$6.23{\cdot}10^5[107\%]$	$7.14{\cdot}10^5[122.7\%]$	$7.985{\cdot}10^5[137.2\%]$
Cogging Torque $[\triangle T_{cog}]$	92 900 [544.2 %]	153 000 [896.3 %]	266 200 [1550 %]

Table 4.2.3: Torque Performance for Geared Machine [Nm] with % Correlation to Non-modular Results

Torque Result	$\beta = 1cm[\%corr.]$	$\beta = 1.5cm[\%corr.]$	$\beta = 2cm[\%corr.]$
Nominal torque	$2.432{\cdot}10^5[95.8\%]$	$2.371{\cdot}10^5[93.4\%]$	$2.3065{\cdot}10^5[90.135\%]$
Torque ripple $[\triangle T_{rip}]$	$4.969{\cdot}10^4[139.9\%]$	$6.407{\cdot}10^4[180\%]$	$8.09{\cdot}10^4[227.9\%]$
Cogging Torque $[\triangle T_{cog}]$	5040 [579.3 %]	8900 [1022.9%]	18180 [2089.6%]

The nominal torque and torque ripple decrease and increase respectively when the flux gaps are implemented for direct drive and geared machines. A higher flux gap result in an increase of the torque ripple and decrease of the nominal torque. Thus, the machines benefit from a smaller flux gap width based on the torque performance. Nevertheless, the nominal torque reduction for the modular machines in relation to the non-modular machines are relatively small compared to the size of the torque, as observed from the deviation in percentage for both direct drive and geared machine. The torque ripple increase significantly compared to the non-modular machine, but are still relatively small relative to the nominal load torque for both machines. The most prominent effect of the flux gap implementation and increase of flux gap width is the cogging torque behaviour. The cogging torque increased to a large degree compared to the cogging torque of the non-modular machines. Nevertheless, the cogging torque is relatively small compared to the nominal torque and torque ripple for both machines. Nevertheless, the increase in torque ripple in absolute value closely correlate with the cogging torque.

It is apparent from Table 3.2.5, that the flux gap implementation had a greater effect on the geared machine compared to the direct drive machine. The nominal torque of the geared machine with different flux gap width, had a larger relative decrease compared to the direct drive machine, as observed from the percentage correlation. The torque ripple and cogging torques increase relative to the initial size of the non-modular machine were also larger for the geared machine. The greater negative effect of the flux gap implementation on the geared machine compared to the direct drive machine can be linked to the machine dimensions, pole and slot number, modular structure and winding factor, which is further discussed in Section 5.3.2.

4.2.4 Loss

The copper loss for the direct drive and geared are assumed unaffected by the modular structure and is therefore given by Table 3.2.6, as 435 500 W and 30 79 W for the direct drive and geared machine, respectively. The copper loss of the direct drive machine is much larger compared to the copper loss of the geared machine due to the higher slot resistance for the machines. The resistance in the direct drive machine is much larger compared to the geared machine due to the machine design and the higher torque which result in a higher electrical loading required.

The core loss obtained from the FEM-simulations are presented in Figure 4.2.11, denote the flux gap width. The corresponding values of the core loss components presented in Figure 4.2.11 are summarised in Table 4.2.4.

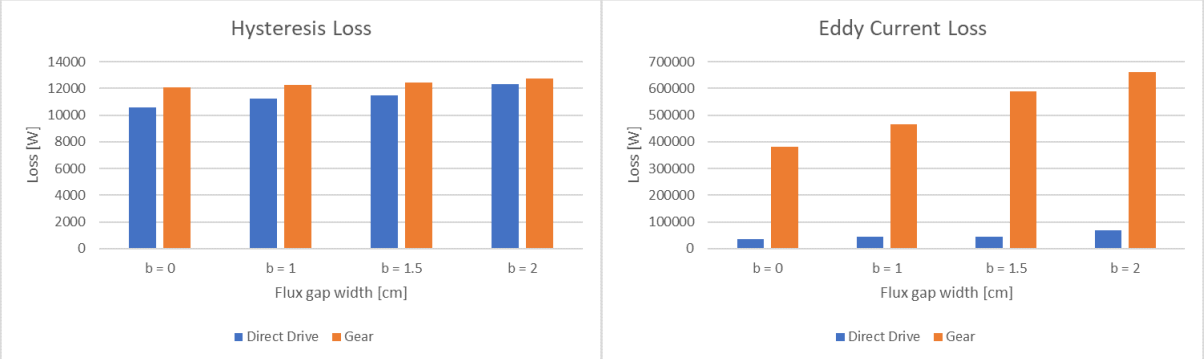

(a) Eddy current Loss

(b) Hysteresis Loss

Figure 4.2.11: Core Loss from FEM simulations

Table 4.2.4: Core Loss [W] with % Correlation to Non-modular Results

	Core Loss	$\beta = 1cm[\%corr.]$	$\beta = 1.5cm[\%corr.]$	$\beta = 2cm[\%corr.]$
Direct Drive	Hysteresis loss	11 220 [105.62 %]	11 482 [108.28 %]	12 318 [116.16%]
	Eddy current loss	44 317 [124.27%]	44 587 [125.03 %]	67 685 [189.8%]
Gear	Hysteresis loss	12 274 [101.46 %]	12 455 [102.96 %]	12 751 [105.4 %]
	Eddy current loss	465 284 [122.22 %]	590 924 [155.23 %]	660 554 [173.52 %]

The copper loss is the greatest loss contribution for the direct drive machine for all non-modular and modular machines. The eddy current and hysteresis losses are substantially lower compared to the copper loss. The eddy current loss component was the most prominent loss contribution for the geared machine. The copper loss and hysteresis loss were significantly lower compared to the eddy current loss contribution.

The modular machines experience greater core losses compared to the non-modular machines. The core loss increased for an increase in flux gap width for both the direct drive and geared machine, which can be observed from the % correlation to the non-modular machine given by Table 3.2.6. Furthermore, the direct drive and geared machine experience a similar relative increase compared to the initial core loss size for the non-modular machines. Thus, the machines increased relative to the initial size, but with similar percentage increase. Nevertheless, the geared machine have the greatest total loss increase due to the initially large eddy current loss. The increase in core loss can be linked to the increase in flux density for the teeth adjacent to the flux gap, which occurs due to the reduced width of these stator teeth. The loss are further discussed in Section 5.4.

Chapter 5

Discussion

5.1 Modular Structure

5.1.1 Winding Structure

A modular structure can negatively affect the performance of the machine and limit the winding design possibilities, as explored in Section 4.1.1.1. A high number of machine modules, with a symmetric phase layout, reduce the possible slot and pole combinations. The difference in poles and stator slots required to obtain a symmetric phase layout increase, in addition to the slot number required to obtain a feasible winding structure.

The minimum feasible number of poles and stator slots increase with an increase in number of modules, in addition the required difference in the number of poles and stator slots increase, as observed from Table 4.1.2. Therefore, the pole/slot combination limitations increase with an increase in the number of modules given a feasible symmetric modular winding structure. Nevertheless, the winding factor were equal for all minimum slot and pole combination for different degrees of segmentation, in addition to being very suitable due to the high value. However, the winding factor deviate from the value obtained in 4.1.2 as the slots and poles increase within a modular structure. Nevertheless, the winding factor is expected to remain high, since a greater number of slots and pole combined, in general results in a high winding factor. Thus, a high winding factor would be obtained for modular machines due the correlation between the number of segments required and the difference in slots and poles. A high winding factor is also probable given a single layer with a phase spread angle of 60° within the modular structure. The modular structure correlates with the expression of base winding, which is present in all concentrated wound machines. Nevertheless, modular winding design could prioritise the number of bases required in the machine winding, which might not be an emphasised design feature for non-modular machines.

A higher degree of modularity contribute to greater frequency limitations compared to a lower number of modules, due to the difference in frequency obtained for each possible slot/pole combination with a given number of modules, as observed from Table 4.1.3. The frequency limitations must be considered against the benefits of modularity. If the number of modules necessary are determined then the frequency is determined in relation to modularity and the necessary number of stator slot to construct a feasible winding structure. A higher speed also contributed to greater frequency with a given modular structure. It could prove challenging to obtain a high number of modules with

symmetrical phase layout for machines with a frequency limit and high speed. Therefore, a symmetric modular structure can be acquired at the expense of preferred frequency values. A higher degree of segmentation can be more easily implemented for low speed machines. Whether a suitable frequency level or a high degree of modularity is favoured for high speed machines have to be considered from case to case.

5.1.2 Insulation

The insulation benefits are substantial when the number of modules initially are implemented and increased. However, the equivalent fill factor converge as the number of modules increase significantly. Thus, the incentive for implementing a high degree of modularity decrease as the number of modules increase. A high degree of segmentation can still be beneficial due to aspects such as power electronic limitation. The minimum number of poles and slots increase linearly with the increased degree of modularity as observed from Table 4.1.2. Thus, there is not necessary an even trade of in relation to the insulation benefits and winding design constraints. It can be argued that the benefits of insulation outweighs the slot/pole constraint for a low number of segments due to the insulation reduction observed from the direct drive and geared machine. However,the insulation benefits must be considered against the winding structure limitations imposed for a greater number of modules, and additionally other possible constraints.

The insulation behaviour presented in Section 4.1.1 relates to the direct drive and geared machines constructed in this thesis. Aspects that could alter this behaviour is the stator slots sizes, number of stator slots and voltage level. The insulation thickness converge toward a value based on the voltage level and insulation properties. The fill factors for higher voltage levels given Appendix A also observed a convergence. These equivalent fill factor converged toward a lower fill factor, but followed the same behaviour. The direct drive machine converged toward a higher value than the geared machine. The difference in the stator slot area of the direct drive and geared machine were prominent and is the cause of the difference. However, the equivalent fill factors converged toward similar values for both machines despite the difference in slot size. The equivalent fill factor for higher voltage level were considerably lower. Thus, the voltage level had a greater influence since the difference in equivalent fill factor is greater for different voltage level compared to the difference of direct drive and geared machine.

5.2 Machine Design

The machine design incorporated the modular structure in some aspects. The insulation and fill factor, determined based on the modularity, contributed to the electrical machine design. The number of poles and stator slots were selected based on the number of modules and a feasible winding layout. Thus, the modular structure became an integral part of the machine design. However, further steps to include the modularity could be considered such as including the expected reduced winding factor in the design process to find the torque per ampere and altering the affected stator teeth width on account of the flux gap with the implementation of empty slots. Nevertheless, the machine design utilised to construct the machine make it possible to study the effect of implementing a modular machine structure compared to a non-modular machine since modular design steps relating to the flux gaps have not been included. Despite the similarities in machine design for the direct drive and geared machine there were some prominent differences, which relates to the machines speed. The modular structure were different due to the

high speed of the geared machine and the steps included to limit the frequency within the modular structure.

The machine design method created feasible machines. However, there can be some weaknesses related to the machine design procedure. These include among other the omission of in dept studies related to sub-harmonic and harmonic behaviour of the EMF and MMF. Especially since it is noted in literature that some of the effects of modular structures relates to harmonic behaviour [19], [34]. The magnetic modelling of the machine were also based on simplified calculations. As mentioned in Section 3.1.4, some assumptions were included in relation to the coil insulation due to lack of material requirements, which could be further improved in order to determine the absolute maximum copper fill factor possible for both machines. Furthermore, the machine design could be further optimised to improve the machine performance.

Heat transfer modelling should also be conducted. A higher temperature in the copper coils increase the resistance and therefore copper loss, which reduce the efficiency of the machine. A heat transfer model could yield important information about the behaviour of the two machines and indicate if one modular machine structure resulted in a better machine performance. The flux gaps could be a possible cooling mechanism for the machines, which would benefit the machine performance. Modular machines with physically separated modules also require a universal yoke which fasten the modules. Thus, a new manufacturing step is included for modular machines. Nevertheless, the manufacturing process also becomes easier once modularity is implemented. Each segment can be wound and constructed separately before assembly.

5.2.1 Direct Drive and Geared Machine Design

The machine constraints and selections were the same for both machines and, given by Table 3.2.1. The winding design are similar since the machines have the same base winding, number of layer, winding factor and stator slot per pole per phase. However, the number of base winding and number of segments are different. The difference in the machine design are caused by the difference in speed of the machines, as mentioned in the previous section. The greater speed for the geared machine influenced the segmentation structure and resulted in different numbers of poles and slots. The required torque is also lower for the geared machine, which influenced the size of the machine.

The frequency for the geared and direct drive machine varied greatly. The design of the machines had different limitations in relation to frequency due to the speed. The direct drive machine could easily increase the number of stator slots and poles with an unaltered modular structure in order to increase the frequency. However, the geared machine was designed with the slot and pole number combination for the absolute limit of a modular machine with 16 segments. The geared machine segmentation structure were based on paths (F2) instead of sections (F1). If the geared machine were to be segmented on the basis of sections (F1), the frequency would be 400 Hz and the two machines would have the same winding structure. A reduction in frequency for the geared machine would require a reduction in either the number of modules or speed, given a symmetric phase layout within the modules. Thus, the difficulties for high speed symmetric machines are demonstrated by the geared machine. Low speed machines can more easily accommodate a high degree of segmentation, which allow a higher number of poles. If a high frequency is not an issue then a high degree of segmentation is not a definitive constraint for high speed machines.

The equivalent fill factor in relation to the number of modules and the voltage level were above the convergence break point in, as observed by Figure 4.1.1. Therefore, the number of segments could be reduced and still obtain a high equivalent fill factor for the direct drive and geared machine if the degree of modularity is only implemented to ensure reduced insulation. A reduction of the number of modules could benefit the geared machine design since it would allow for a lower frequency. However, the number of modules should not be reduced below 8 segments for both machines since the equivalent fill factor drops drastically below this level of modularity.

The flux gaps implemented in the modular machines were of the same size despite the difference in machine dimensions. Thus, the flux gaps were expected to affect the machine performance by different degree. Furthermore, this is supported by the expected reduced winding factor presented in Figure 4.1.4b. The modular geared winding factor reduced to a greater degree compared to the direct drive machine.

5.3 FEM Simulations

The results obtained from FEM simulations for the machines yielded information that relates to the modular machine performance. Some of the simulations yielded unfavourable results and must be studied further.

5.3.1 Analytical Design Compared to FEM-simulations

The non-modular machines were constructed as a first step to validate the machine design and use as a benchmark to observe the effect of modularity and flux gap. However, whether it can be considered an adequate benchmark is up for discussion since the machines does not have a feasible fill factor and insulation structure. Thus, these machines can only be utilised in relation to the equivalent modular machines and could not be constructed for lab testing. Nevertheless, the non-modular machines presented are the non-modular machines with the greatest similarities compared to the modular machines constructed. Thus, the difference in behaviour could be more fine tuned. However, it could be beneficial to compare the machines to a feasible non-modular machine in order to further compare the performance of modular and non-modular machines.

The non-modular FEM-simulation and calculated values converged to a reasonable degree with only a small deviation for some parameters. However, the direct drive and geared machine varied differently from the calculated values. The direct drive machine‘s torque were below the calculated value, while the geared were above, which can indicate some inconsistencies in the modelling process. The voltage levels obtained also varied slightly. The voltage and torque were the two values that differed from calculated values to the greatest degree. The deviation can be linked to the calculation tools utilised. COMSOL have more sophisticated calculation methods compared to the analytical method and it is therefore reasonable to expected some variations. Furthermore, the analytical design does not account for torque ripple or cogging torque. The cogging torque of the non-modular machines accounted fro a small part of the total torque ripple, which suggest that other torque ripple contributions are significant. Furthermore, the torque ripple for the non-modular results varied slightly around zero which could be a source of error.

There was a high torque ripple at the start of the simulation period and it is a possibility that it could be linked to high start up cogging or inconsistencies in the models. The current density limit is observed to be upheld by the non-modular machines, which further

support the convergence of the analytical model and the model constructed in COMSOL. However, the machine parameters related to the current density, such as current, number of conductors and area of the conductors, are input parameters in COMSOL.

5.3.2 Modular Performance Compared to Non-Modular Performance

The modular structure affect the machine performance, which can be observed form the FEM-simulation results presented in Section 4.2. The most prominent aspects altered are the phase back-EMF, torque and loss, in addition to the flux density increase in the stator teeth affected by the flux gap. These alterations can be observed in relation to the parameters affected. The phase back-EMF correlate with the flux linkage, the torque depend on the winding factor and air gap flux density and the loss correlate with the flux density in the machines. The deviation in torque and loss is especially important since the torque produced at a given speed determine the power output and the loss determine reduce power output. Thus, the machine efficiency is affected by implementing a modular structure. Phase flux linkage is reduced by the implementation of flux gaps for the pole/slot combinations of these machines and so is the winding factor and open circuit air gap flux density as discussed in Section 2.3.3.

5.3.2.1 Torque

The torque decreased with the implementation of the flux gaps. Nevertheless, the decrease in nominal torque can be considered minimal as seen from percentage deviation from non-modular machines given in Table 4.2.2 and 4.2.3 for the direct drive and geared machine, respectively. The reduction in percentage of nominal torque for increased flux gap widths are also relatively small in relation to the total size of torque produced. The size of the torque reduction can be linked to the modular structure, machine size and number of flux gaps. The winding factor reduction is presented in Figure 4.1.4. The winding factor reduction is minimal, due to the minimal increase in flux gaps width and number of flux gaps, which correlate with a relatively low torque reduction. Furthermore, the air gap flux density is reduced, which also contribute to the reduced torque. Thus, the torque reduction is small since it depend on the winding factor and air gap flux density who both experience a slight reduction. There are few flux gaps compared to the number of slots due to modularity being symmetric, which imply that the flux gaps are implemented on the edge of the winding bases. The most fundamental alteration in relation to torque characteristics was the cogging torque increase. The cogging torque increase is large compared to the non-modular cogging torque. Thus, the size of the cogging torque increase indicate that the flux gap have a great effect on this parameter despite the few number of flux gaps compared to stator teeth and the relative size of the flux gaps compared to the machines diameter. The increase in torque ripple for increased modularity was of a same size as the cogging torque for both machines. Thus, it can be assumed that other torque ripple contributions are not greatly affected by the flux gaps for symmetric modular machines, when they have been implemented. Nevertheless, an harmonic study should be conducted in order to confirms this assumption.

The reduction of nominal torque for modular machines can be considered significant when it is compared to the relationship between the machine dimensions and flux gap width given by Table 4.2.2 and 4.2.3. Flux gaps width of 1, 1.5 and 2 cm cause a noticeable decrease in torque an thus power production for both machines if one consider the absolute power lost, when the nominal torque is reduced. Moreover, if the nominal

torque reduction is considered in relation to the losses in the machine it is apparent that the torque reduction is significant since the loss and torque reduction are of the same size order, when observing the torque in relation to the speed. Thus, the torque performance for modular machines compared to non-modular machines demonstrated the importance of limiting the flux gap width to further limit the torque reduction, given a slot pole combination with a greater number of slots compared to poles. Accurately predicting the nominal torque before a prototype is constructed yield important information related to the power production since a variation in the flux gap width affect the nominal torque to a considerable degree. Thus, determining and limiting the flux gap width before the machine is constructed will be a new manufacture challenge related to modular machines. The torque reduction on account of flux gap could be considered a form of modular machine loss since they reduce the power produced by the machine compared to non-modular machines.

5.3.2.2 Electrical Parameters

The no-load phase back-EMF deviated from non-modular machine performance with a % reduction similar to the the nominal torque deviation when the flux gaps were implemented, as observed from Table 4.2.1. The no-load phase back-EMF depend on the winding factor and the flux linkage. The winding factor also affect the no load phase Back-EMF, as observed from Equation 2.4.3. The electrical parameters, with the exception of EMF, experience little alteration by the implementation of modularity as observed in Section 2.4, which can be seen in relation to the flux gap implementation method utilised. The stator slots were not altered to accommodate the flux gaps. Thus, the slot width were not reduced. The current and conductor behaviour were input parameters and were similar for the modular and non-modular machines. Alteration to electrical performance could be expected with the use of the empty slots method for flux gap implementation due to the reduced slot width and equivalent fill factor decrease. The voltage depend on the phase back-EMF, which correlate with the flux gap implementation. Nevertheless, this affected the full load voltage to small degrees. However, it could be observed that the peak phase voltage and phase back-EMF varied for modular machines, which were not as widespread for the non-modular simulation. The cause of this could be that the coils of only two phases have slot adjacent to the flux gaps, but further studies would have to be conducted in order to conclude. The variation can also be contributed to errors in the COMSOL set up or other unknown cause.

5.3.2.3 Magnetic Loading

The flux density distribution remained similar for both non-modular and modular machines with the exception of the stator teeth adjacent to the flux gaps, which increased above given limits. Thus, the magnetic behaviour in the entire modules did not appear to be greatly affected by the flux gaps implementation. The increase in the flux density of the stator teeth adjacent to the flux gaps occur due to the reduction in teeth width without including steps to compensate for the stator teeth width lost. Nevertheless, there are few flux teeth affected by the increased flux density since the number of stator slots are much higher compared to the flux gaps. The increase can be linked to an increase in core losses, which are further discussed in Section 5.4.

Different approaches could be utilised in order to improve the flux gap implementation and reduce the flux density in the stator teeth affected by the modular structure. Flux gap implementation methods include reduction of the flux density limit of the stator

teeth for the entire machine and increasing the affected stator teeth width by empty slot implementation as explored in Section 2.3.3.2. Advantages and disadvantages can be linked to both methods. Reducing the flux density limit does not affect the equivalent and slot fill factor, stator slot characteristics or the winding factor, but it can require a larger stator yoke to meet the reduced flux density limit constraints. Furthermore, it could be difficult to ensure a suitable full load flux density of the affected stator teeth by utilising a reduced open circuit flux densities to determine the machine dimensions. The stator area removed are small and it could be hard to the magnetic behaviour in these stator slots.

The empty slot method does not reduce the open circuit flux density limit given so the machine size would remain the same. Nevertheless, the added factor of empty slots cause a reduction in the equivalent slot fill factor and reduce the slot fill factor, if the height of the stator slots are not increased to compensate for the lost width. Some of the negative aspects related to the empty slot method could be negated by increasing the stator slot height in relation to the stator width lost. Therefore, the stator slots could become unsuitably long if the width is reduced considerably. Copper loss could also become more prominent. A possible slot width reduction can be considered small and there are relative few flux gaps compared to stator teeth for the direct drive and geared machine. A slight flux density increase in stator teeth could possibly be accepted, when only a few teeth are affected. Thus, not altering the stator teeth structure for symmetric modular machines could be an acceptable design choice. However, as the flux gaps increase the magnetic saturation is also expected to increase. Thus, direct flux gap implementation become increasingly unsuitable with the increase in flux gap width.

5.3.3 Comparison of Gear and Direct Drive Modular Machines

The flux gaps included in the geared and direct drive modular machines were of equal size, despite their difference in machine size. The flux gaps are larger for the geared machine relative to the machine size and parameters. The relative flux gap size compared to machine performance correlate with the increased deviations of the geared machine for the torque characteristics, phase back-EMF and losses. A proportionally larger flux gap width compared to the stator teeth width indicate a greater relative reduction in stator slot area for the geared machine, which can increase the flux density. The relationship between the inner stator radius, slot pitch and number of stator slots compared to flux gap can cause a greater winding factor reduction, due to the relationship between these parameters and the modular winding factor. It was expected that the winding factor was reduced more for the geared machine, as described in Section 4.1.1.2. This is corroborated by the higher level of torque reduction for the geared machine. The geared machine experience a greater drop in the back-EMF compared to the direct drive machine, which can also be linked to the relationship between the machines and the flux gap width.

The geared machine experienced in general a higher deviation from non-modular result. Nevertheless, the machine might be able to support smaller flux gaps compared to the larger direct drive machine. The flux gap is present due to the implementation of physically separated machine modules when the machine is manually assembled. The size of the machine could indicate the size of the required flux gap, which would indicate that a smaller machine in diameter could support a smaller flux gap. Though mechanically construction or testing would have to be studied to verify this possibility. Nevertheless, the insulation between the modules must be included and is of an equal size for both

machines and contribute to the absolute flux gap width.

The flux density for the no load and full load conditions for both machines, experienced a rotating field caused by harmonic content. The sub-harmonic is still present when the modularity have been included and it appears as though it has not been affected to a great degree by the modularity. Nevertheless, further studies in relation to harmonic behaviour should be conducted in order to make an accurate conclusion. It is also important to note that the direct drive machine were segmented in relation to the sections (F1) and thus the harmonic structure is presented by the whole segments. The geared machine has one base winding separated into two modules. The harmonic behaviour of machines with different modular structure based on sections and paths could be studied further, in order to observe any difference in the machine performance.

5.4 Loss

The copper loss dominates the loss contributions for the direct drive machine, in accordance with expected behaviour for low frequency machines. The geared machines most dominant loss contribution was the eddy current loss. The frequency of the geared machine was above 100 Hz and can be considered a high frequency machine. Thus, the machine design and FEM results correspond with expected behaviour for the machines frequency levels.

The direct drive non-modular machine had marginally higher total loss compared to the geared machine. However, eddy current losses for the gear machine increase drastically when the modular structure is included. The relative core loss increase in % are similar for both machines. Nevertheless, the eddy currents obtained for the non-modular machines were initially high and with the increase in percentage contributed to a large loss increase for the geared machine. Nevertheless, the copper losses can be expected to increase with an increase in temperature, which would affect the direct drive machine to a the larger degree due to the higher copper loss for the direct drive machine.

The core loss measured for the modular machines increased with flux gap implementation and with increased flux gap width, which can be linked to the increased flux density in the stator teeth adjacent to the flux gaps. Thus, this could indicate an increase in core losses for modular machines with direct flux gap implementation. The empty slot method negate the reduced stator teeth flux density and the core loss could possibly be avoided. However, as noted in Section 2.6.1, the empty slot method could be linked to increased core losses. Therefore, further work could include a comparison of direct flux gap and empty slot implementation to determine the most beneficial method for loss reduction for different machine structures. The preferred flux gap implementation method could be linked to the machine size and frequency. An increase in copper loss could contribute to a greater degree of loss increase for low speed machines, while the core loss increase could contribute to a greater degree of the total loss increase for the high speed machines.

The increase in core loss with a modular structure was substantial for both machines, which could indicate additional factors, that contribute to the core loss increase with a modular structure. Furthermore, core loss estimations can be inaccurate when used in FEM-software due to the mesh feature and time step. During the simulations it was observed that alterations to the mesh or time step influenced the core loss values to a large degree. Therefore, more sophisticated loss simulations is required in order to determine accurate core losses and loss increase on account of flux gap implementation. However,

the loss simulation presented in this thesis can give an indication of the possible core loss behaviour related to flux gap implementation since the mesh and time step were the similar, accounting for the frequency and size of the machines. There is also a possibility that the meshing around the flux gaps could contribute to the core loss results. The copper loss can also be expected to increase drastically due to a possible increase in temperature and the simplified expression used to determine the copper loss.

A study of the loss in the magnets are not included, but would contribute to the total loss to some degree due to the conductivity present in the magnets, especially for the geared machine as observed by Figure 4.2.7. However, axial segmentation could limit the conductivity as previously mention in Section 2.6.3. The core loss constants were determined based on four frequency levels. However, the direct drive machine have lower operating frequency than the frequencies included in the loss matrix given by Figure D.1.2. This could indicate an unsuitability related to determining the constant for the direct drive and lower frequencies.

Chapter 6

Conclusion

Two symmetric modular machines were designed, as direct drive and with a gear. The machines were implemented and studied utilising the FEM-simulation software, COMSOL. Two functional modular machines were designed based on the given specifications. The introduction of flux gaps decreased the performance of the modular machines compared to the non-modular machines. This implementation was done without readjusting the stator tooth width. The reduced machine performances were mainly caused by a reduction in torque and phase back-EMF, in addition to increased core loss, flux density and torque ripple.

The reduction of torque were relatively small compared to the nominal torque value. Nevertheless, the torque reduction could be considered a substantial cause of reduced power output. Higher core losses were also present in the modular machines compared to non-modular machines. The core loss increased further when the flux gap width and the flux density increased. The flux density increased mainly in the stator teeth adjacent to the flux gap. The most prominent increase in core loss was the eddy current loss. Further loss calculations should be conducted before definitive conclusions are drawn in terms modular machine versus non-modular machine efficiency, due shortcomings and inconsistencies related to the core loss results.

The geared machine performance was affected by the flux gap implementation to a larger degree, compared to the direct drive machine. This was caused by the relative size of the machine compared to the flux gap width. Nevertheless, other causes could also contribute to the difference in machine performance between the geared and direct drive machines. Therefore, further studies should be conducted. The requirement of the flux gap size from a mechanical point of view, might lead to a smaller machine, requiring a smaller flux gap. Additionally, the core losses were greater for the geared machine compared to the direct drive machine.

For the design process, modular winding design constraints were included. A high degree of modularity could indicate a shift towards the number of stator slots being the defining winding structure constraint. Furthermore, a high number of stator modules could impose restrictions on the possible frequency values, especially for machines with a higher speed. The geared machine design demonstrated the difficulty related to a high speed and a high degree of modularity. On the other hand, the direct drive machine could further increase the number of poles and stator slots to obtain a higher frequency, without jeopardising

the number of symmetric modules.

The required insulation in the machine is reduced as the number of modules increase. However, an insulation convergence were observed when the number of modules increased to a large degree. Thus, the trade-off between the insulation design and the winding structure constraints are not necessarily equal. However, the insulation behaviour would have to be verified by laboratory testing.

6.1 Further Work

Symmetric modular machines should be studied further in order to explore specific machine characteristics pertaining to the modular structure. The machines constructed and studied in this thesis also require further testing, in order to draw conclusions about the machine design suitability. Aspects that should be studied for modular structure in general and the machine designed for this thesis, are presented in the following list.

- The performance for machines with different number of modules could be constructed and compared. For example by designing the machine for a given number of modules and then decreasing the number of modules to compare the behaviour. Thus, effect of physical segmentation and flux gaps can be studied.
- Harmonic study of the modular machines should be conducted in order to further draw conclusions about the machine behaviours. Harmonic content could be affected by the modular structure and further affect the machine performance. Thus, the harmonic alteration on account of the modular structure is an important aspects, which require further studies. The harmonic content of non-modular and modular machines could be compared to quantify the harmonic behaviour for symmetrical modular machines.
- The flux gap implementation method denoted as empty slots could be included in the machine design in order to study how it alters the machine performance and design. Thus, the behaviour of the machines with and without adjusted flux width can be compared and studied. An aspect that would be of particular interest is core loss alterations on account of the flux gaps with readjusted flux teeth.
- Thermal study of the machines designed: The temperature in the machine affects the machine performance and high temperatures can greatly increase the losses. Aspect such as demagnetisation of the magnets and increased copper loss could occur for higher temperatures. Furthermore, the flux gaps could be a possible cooling mechanism and it could be interesting to observe how the flux gap could benefit the heat transfer. A modular machine can also support a higher fill factor which contribute to a better heat transfer.
- The flux gap implementation affected the level of cogging torque and torque ripple, which can influence the level of vibration in the machine. The stator modules must be connected to a universal yoke. Therefore, the behaviour of the machine in relation to the universal yoke should be studied to ensure that the yoke can support the machines rotation with increased cogging torque an torque ripple. Furthermore, a mechanical study should be conducted in relation to the minimum size of the flux gaps the machine can support physically. Since the flux gaps width are very small compared to the general size of the machines.

- The proposed modular insulation design should be tested in order to ensure that the machines are capable of supporting the level of insulation during operation. Testing could include both simulations and lab testing.
- The machine design should be further optimised in order to improve the performance within the given modular structure. Optimisation steps could include the stator slot design, fill factor improvements beyond modular implementation and machine dimensions combinations.
- Laboratory testing of the machines designed could be conducted. The analytical study and FEM simulations are both based on calculations, though the FEM-simulations can be considered sophisticated analytical simulation. Nevertheless, laboratory testing would have to be conducted in order to make any definitive conclusions related to the machine performance. A laboratory scaled machine would then have to be designed.

Bibliography

[1] N Bianchi and M Dai Pre. "Use of the star of slots in designing fractional-slot single-layer synchronous motors". In: *IEE Proceedings-Electric Power Applications* 150.2 (2003), pp. 139–145.

[2] L. Castellini and M. D'Andrea. "High speed surface PM synchronous machine for wobble laser welding". In: *Proceedings - 2015 IEEE International Electric Machines and Drives Conference, IEMDC 2015* October 2017 (2016), pp. 1600–1606. DOI: 10.1109/IEMDC.2015.7409277.

[3] Lester Chong, Rukmi Dutta, and M. F. Rahman. "Design and thermal consideration of an interior permanent magnet machine with concentrated windings". In: *Proceedings - The 12th International Conference on Electrical Machines and Systems, ICEMS 2009* (2009).

[4] Min Dai, Ali Keyhani, and Tomy Sebastian. "Torque ripple analysis of a permanent magnet brushless DC motor using finite element method". In: *IEMDC 2001 - IEEE International Electric Machines and Drives Conference* 19.1 (2001), pp. 241–245.

[5] Mircea Fratila et al. "Iron Loss Calculation in a Synchronous Generator Using Finite Element Analysis". In: *IEEE Transactions on Energy Conversion* 32.2 (2017), pp. 640–648.

[6] Chris Gerada et al. "High torque density PM machines for high performance operation". In: *IECON Proceedings (Industrial Electronics Conference)* (2007), pp. 210–215.

[7] Sverre S. Gjerde, Paal Keim Olsen, and Tore M. Undeland. "A transformerless generator-converter concept making feasible a 100 kV low weight offshore wind turbine Part II - The converter". In: *2012 IEEE Energy Conversion Congress and Exposition, ECCE 2012* (2012), pp. 253–260.

[8] Seok Hee Han, Thomas M. Jahns, and Z. Q. Zhu. "Analysis of rotor core eddy-current losses in interior permanent-magnet synchronous machines". In: *IEEE Transactions on Industry Applications* 46.1 (2010), pp. 196–205.

[9] Dr. Duane Hanselman. *Brushless Permanent Magnet Motor Design*. Magna Physics publishing, 2006.

[10] Philip A. Hargreaves, Barrie C. Mecrow, and Ross Hall. "Calculation of iron loss in electrical generators using finite-element analysis". In: *IEEE Transactions on Industry Applications* 48.5 (2012), pp. 1460–1466.

[11] Greg Heins, Dan M. Ionel, and Mark Thiele. "Winding Factors and Magnetic Fields in Permanent-Magnet Brushless Machines With Concentrated Windings and Modular Stator Cores". In: *IEEE Transactions on Industry Applications* 51.4 (2015).

[12] Joachim Holtz and Lothar Springob. "Identification and compensation of torque ripple in high-precision permanent magnet motor drives". In: *IEEE Transactions on Industrial Electronics* 43.2 (1996), pp. 309–320.

[13] Joachim Holtz and Lothar Springob. “Identification and compensation of torque ripple in high-precision permanent magnet motor drives”. In: *IEEE Transactions on Industrial Electronics* 43.2 (1996), pp. 309–320.

[14] Marta Karoline Husebø. “Segmented Stator of a PM Machine with Concentrated Windings Masteroppgave i Energi og miljo”. In: *Master Thesis, Norges teknisk-naturvitenskapelig universitet, Fakultet for informasjonsteknologi og elektronikk, Institutt for elkraftteknikk* (2019).

[15] Mohammad S. Islam et al. “Design considerations of sinusoidally excited permanent magnet machines for low torque ripple applications”. In: *Conference Record - IAS Annual Meeting (IEEE Industry Applications Society)* 3 (2004), pp. 1723–1730.

[16] Oystein Krovel. “Design of Large Permanent Magnetized Synchronous Electric Machines”. In: (2011).

[17] M. C. Kulan, N. J. Baker, and J. D. Widmer. “Design of a high fill factor permanent magnet integrated starter generator with compressed stator windings”. In: *Proceedings - 2016 22nd International Conference on Electrical Machines, ICEM 2016* (2016), pp. 1513–1519.

[18] G. J. Li et al. “Cogging Torque Mitigation of Modular Permanent Magnet Machines”. In: *IEEE Transactions on Magnetics* 52.1 (2016).

[19] G. J. Li et al. “Influence of flux gaps on electromagnetic performance of novel modular pm machines”. In: *IEEE Transactions on Energy Conversion* 29.3 (2014), pp. 716–726.

[20] Florence Meier. *Permanent-Magnet Synchronous Machines with Non-Overlapping Concentrated Windings for*. 2008, pp. 1–177.

[21] E. Muljadi and J. Green. “Cogging torque reduction in a permanent magnet wind turbine generator”. In: *2002 ASME Wind Energy Symposium* January (2002), pp. 340–344.

[22] COMSOL Multiphysics. “AC / DC Module User ’ s Guide”. In: *Comsol* 5.2 (2015).

[23] C. Nevoloso et al. “Fast procedure for the calculation of maximum slot filling factors in electrical machines”. In: *12th International Conference on Ecological Vehicles and Renewable Energies, EVER 2017* (2017).

[24] Paal Keim Olsen et al. “A Transformerless generator-converter concept making feasible a 100 kV light weight offshore wind turbine: Part i - The generator”. In: *2012 IEEE Energy Conversion Congress and Exposition, ECCE 2012* (2012).

[25] Mircea Popescu et al. “Single and double layer windings in fractional slot-per-pole PM machines - Effects on motor performance”. In: *IECON Proceedings (Industrial Electronics Conference)* (2008), pp. 2055–2060.

[26] Jayarama Pradeep and R. Devanathan. “Adoption of Park’s transformation for inverter fed drive”. In: *International Journal of Power Electronics and Drive Systems* 5.3 (2015), pp. 366–373.

[27] Ayman M. EL-Refaie. “Fractional-slot concentrated-windings synchronous permanent magnet machines: Opportunities and challenges”. In: *IEEE Transactions on Industrial Electronics* 57.1 (2010), pp. 107–121.

[28] David Reigosa et al. “Magnet temperature estimation in permanent magnet synchronous machines using the high frequency inductance”. In: *IEEE Transactions on Industry Applications* 55.3 (2019), pp. 2750–2757.

[29] Astrid Rokke and Robert Nilssen. “Analytical Calculation of Yoke Flux Patterns in Fractional-Slot Permanent Magnet Machines”. In: *IEEE Transactions on Magnetics* 53.4 (2017).

[30] S.E. Skaar, O. Krovel, and R. Nilssen. “Distribution, coil-span and winding factors for PM machines with concentrated windings”. In: *XVII International Conference on Electrical Machines, ICEM 2006* (2006), p. 346.

[31] T. D. Strous, H. Polinder, and J. A. Ferreira. “Inductance calculations for PM machines with concentrated windings”. In: *2011 IEEE International Electric Machines and Drives Conference, IEMDC 2011* (2011), pp. 447–452.

[32] Junzi Sun. *Open Aircraft Performance Modeling Based on an Analysis of Aircraft Surveillance Data*. 2019, p. 289.

[33] Silvio Vaschetto, Alberto Tenconi, and Gerd Bramerdorfer. “Sizing procedure of surface mounted PM machines for fast analytical evaluations”. In: *2017 IEEE International Electric Machines and Drives Conference, IEMDC 2017* 63 (2017).

[34] Y. Yao, Q. Lu, and Y. Ye. “Comparative study of E-core and C-core modular PM linear machines with different slot/pole combinations”. In: *2017 IEEE International Magnetics Conference, INTERMAG 2017* 53.11 (2017).

[35] Yu Zhao et al. “Overview of the Rectangular Wire Windings AC Electrical Machine”. In: *China Electrotechnical Society Transactions on Electrical Machines and Systems* 3.2 (2019), pp. 160–169.

[36] Z. Q. Zhu and David Howe. “Influence of design parameters on cogging torque in permanent magnet machines”. In: *IEEE Transactions on Energy Conversion* 15.4 (2000), pp. 407–412.

Appendix A

Modular Structure

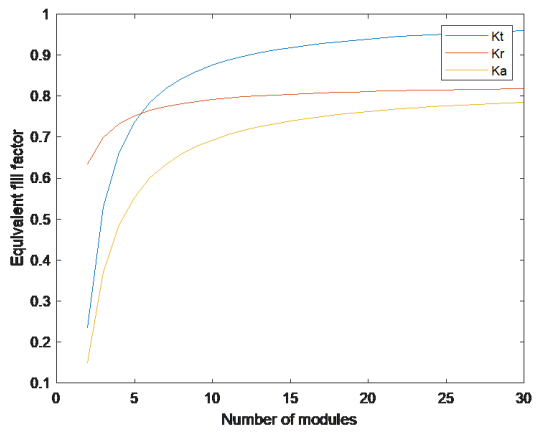

(a) 200 kV

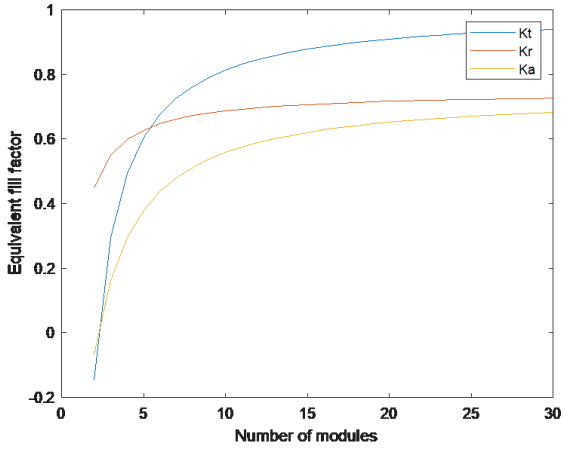

(b) 300 kV

Figure A.0.1: Equivalent Fill Factor, Direct Drive Machine

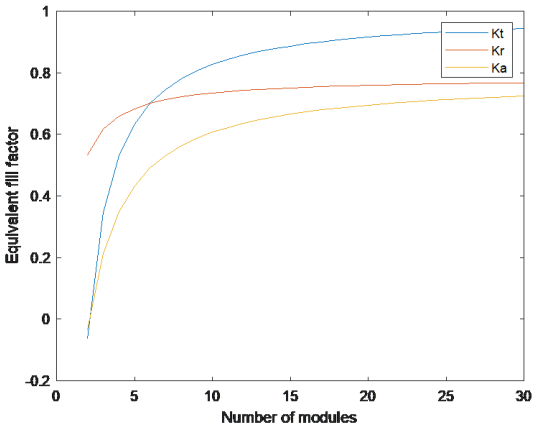

(a) 200 kV

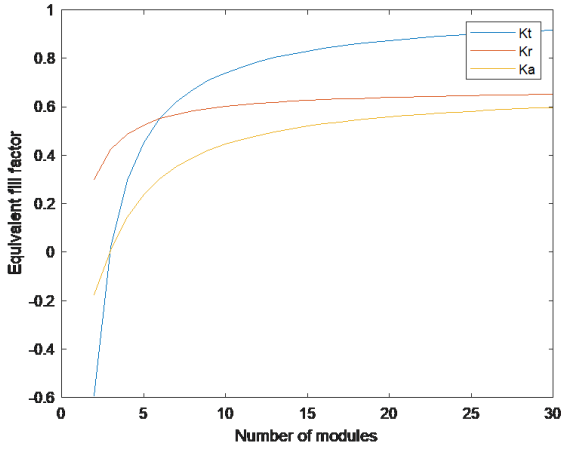

(b) 300 kV

Figure A.0.2: Equivalent Fill Factor, Geared Machine

Appendix B

Non-modular Machine

B.1 Direct Drive Machine

B.1.1 Flux Density

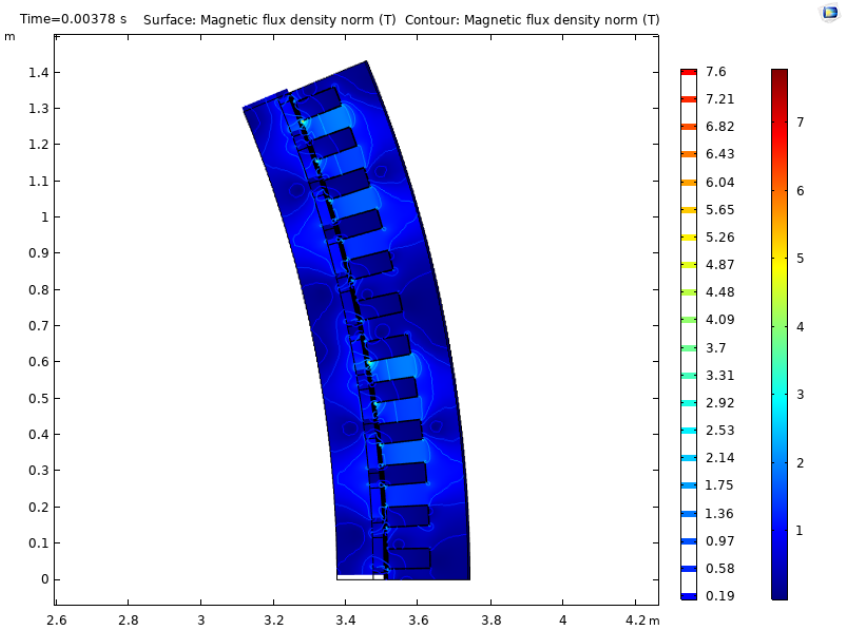

Figure B.1.1: Full Load Flux Density for Non-Modular Machine, Direct Drive

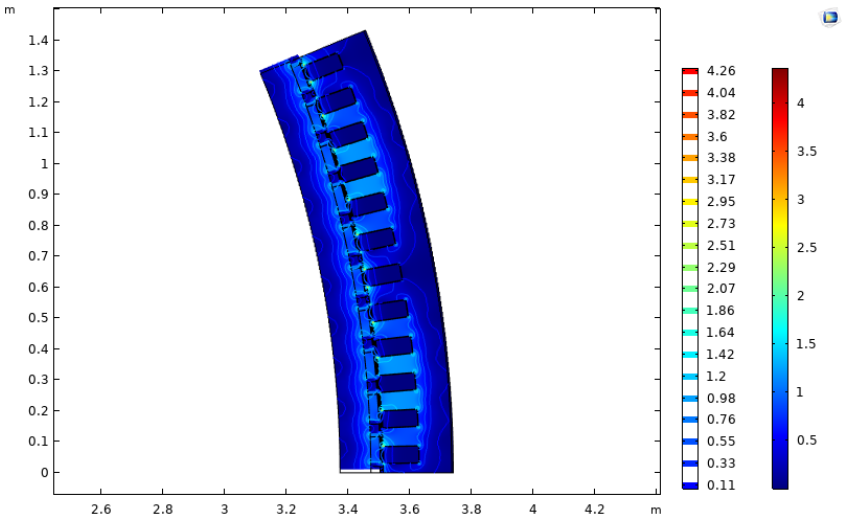

Figure B.1.2: No Load Flux Density for Non-Modular Machine, Direct Drive

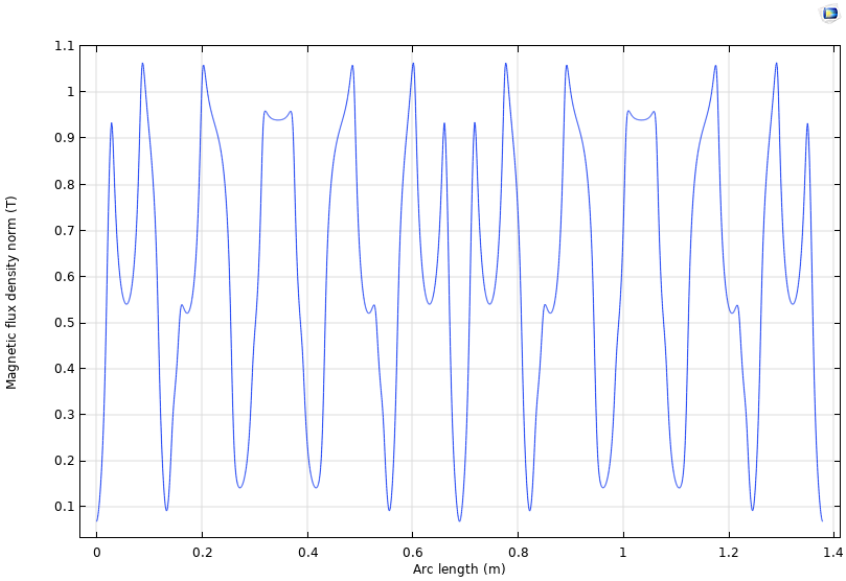

Figure B.1.3: No-load Air Gap Flux Density for Non-Modular Machine, Direct Drive

B.1.2 Electrical Parameters

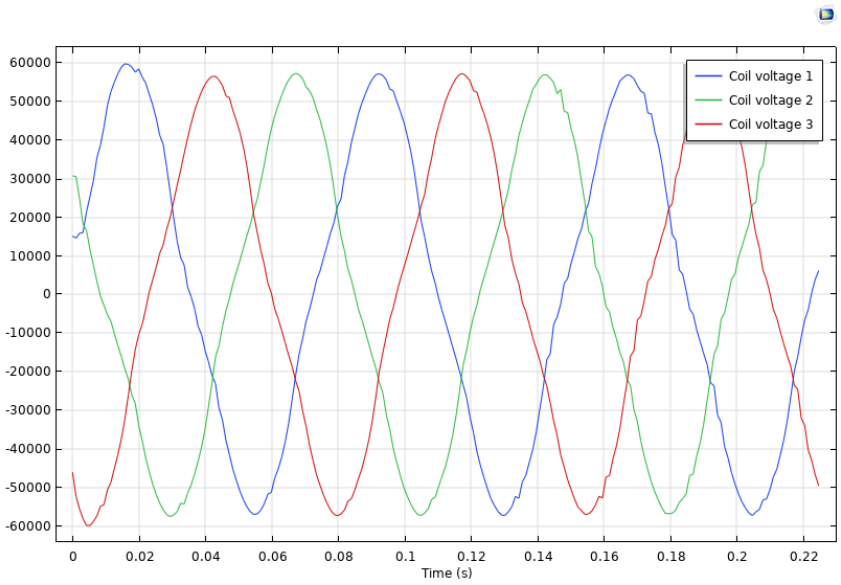

Figure B.1.4: Nominal Voltage for Non-Modular Machine, Direct Drive

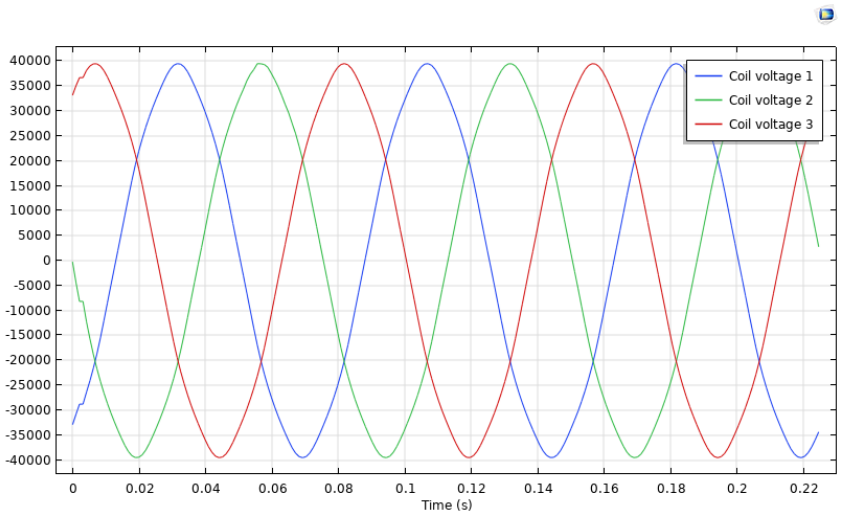

Figure B.1.5: Phase Back-EMF for Non-Modular Machine, Direct Drive

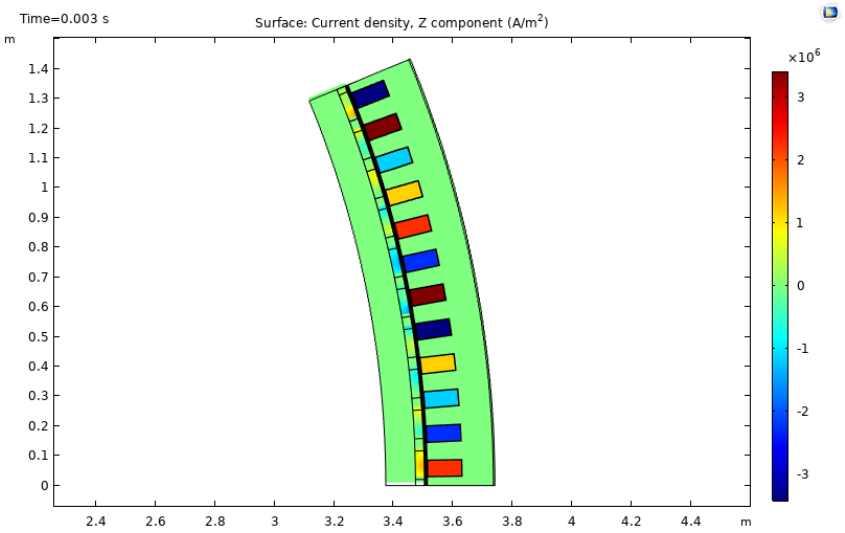

Figure B.1.6: Full Load Current Density for Non-Modular Machine, Direct Drive

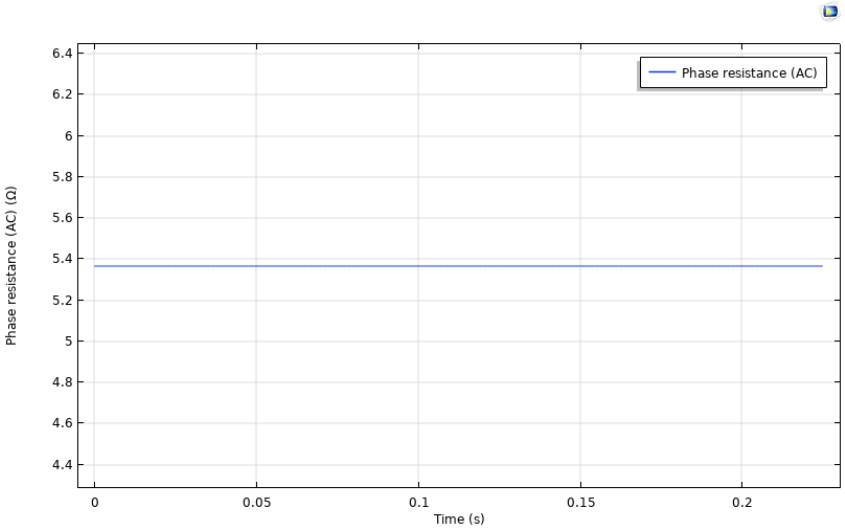

Figure B.1.7: Total Slot Resistance for Non-Modular Machine per Phase, Direct Drive

B.1.3 Torque

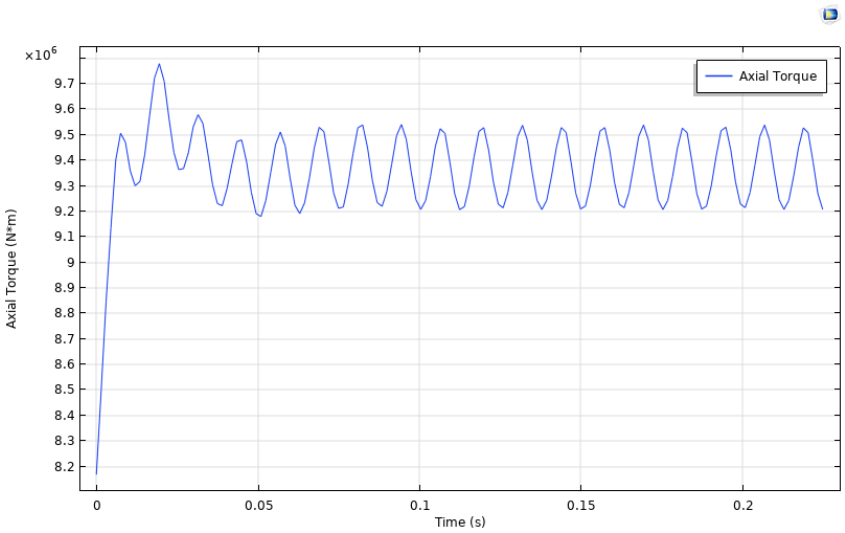

Figure B.1.8: Full Load Torque for Non-Modular Machine, Direct Drive

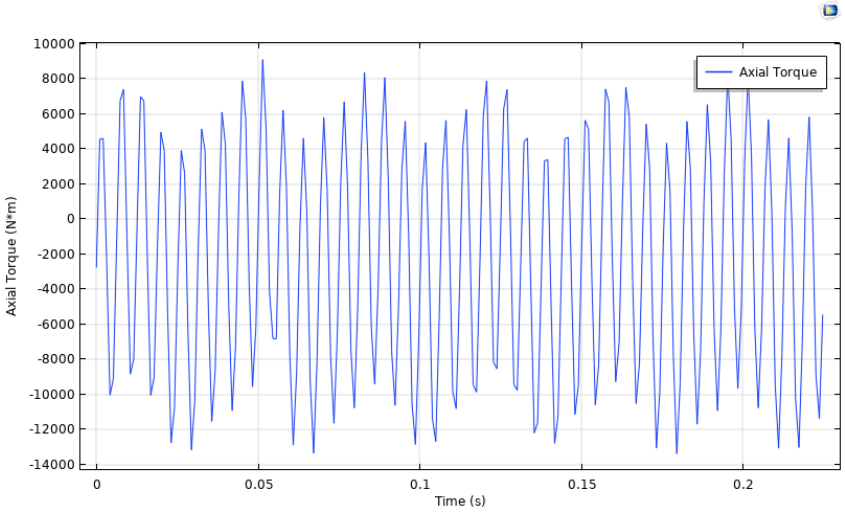

Figure B.1.9: Cogging Torque for Non-Modular Machine, Direct Drive

B.1.4 Loss

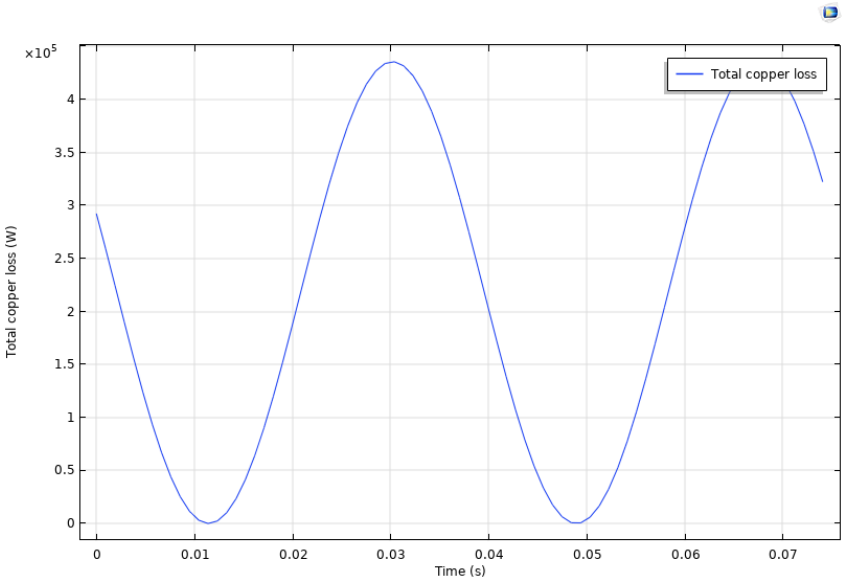

Figure B.1.10: Phase Copper Loss for Non-modular Machine, Direct Drive (4.355)

B.2 Gear

B.2.1 Flux Density

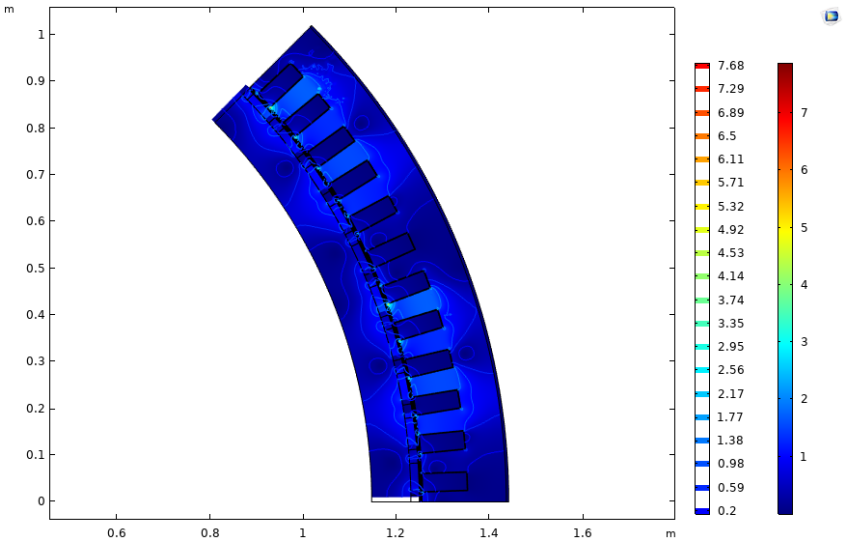

Figure B.2.1: Full Load Flux Density for Non-Modular Machine, Gear

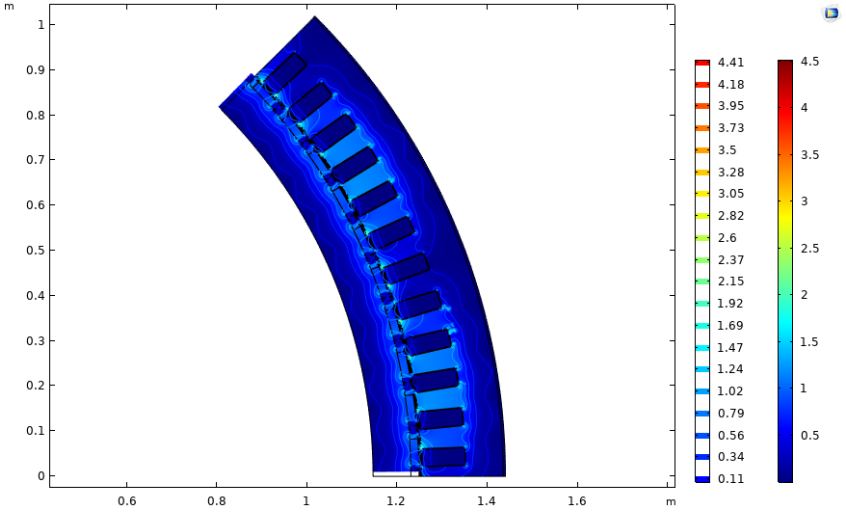

Figure B.2.2: No Load Flux Density for Non-Modular Machine, Gear

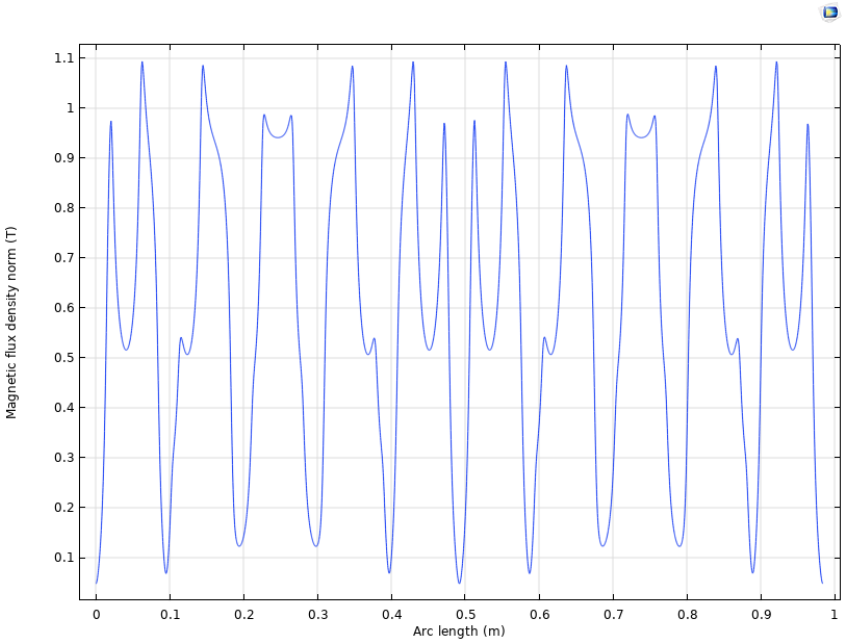

Figure B.2.3: No Load Air Gap Flux Density for Non-Modular Machine, Gear

B.2.2 Electrical Parameters

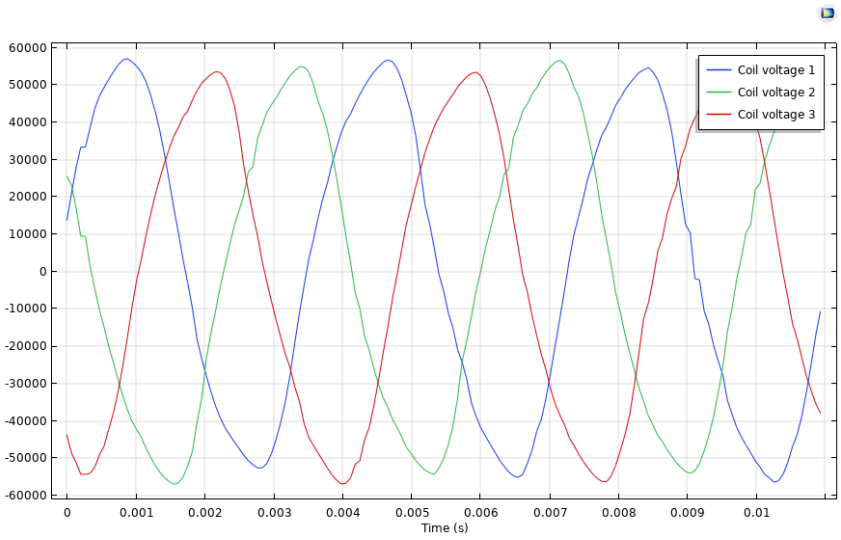

Figure B.2.4: Nominal Voltage for Non-Modular Machine, Gear

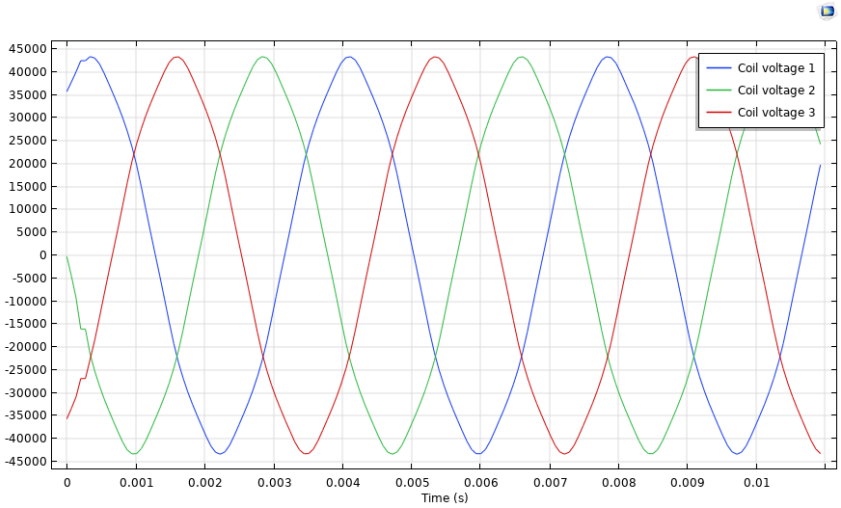

Figure B.2.5: Phase Back-EMF for Non-Modular Machine, Gear

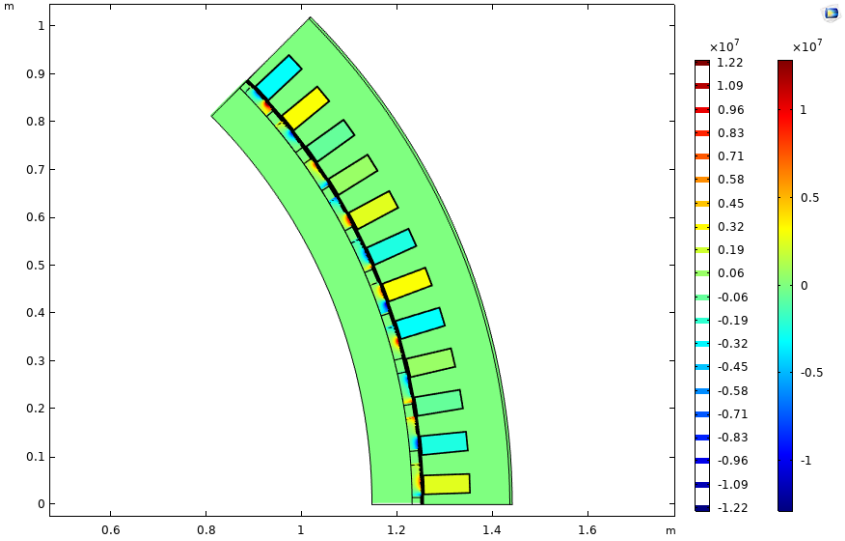

Figure B.2.6: Full Load Current Density for Non-Modular Machine, Gear

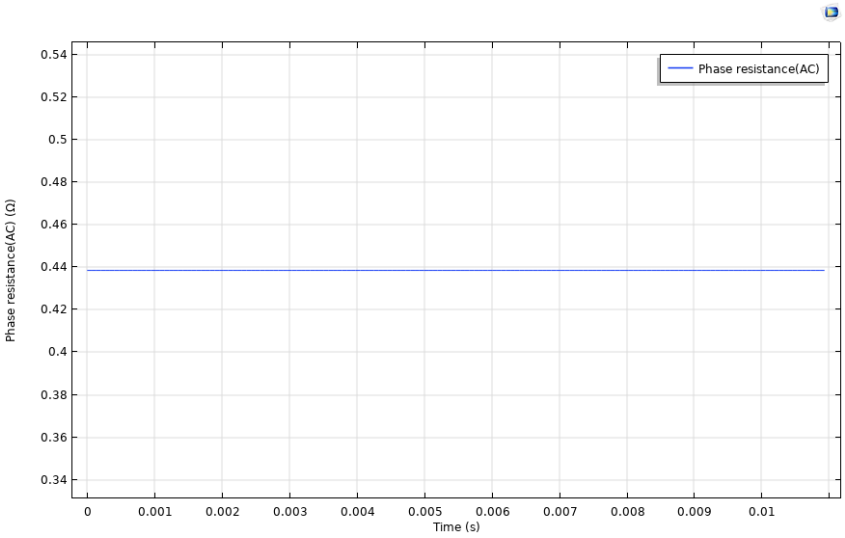

Figure B.2.7: Total Slot Resistance for Non-Modular Machine per Phase, Gear

B.2.3 Torque

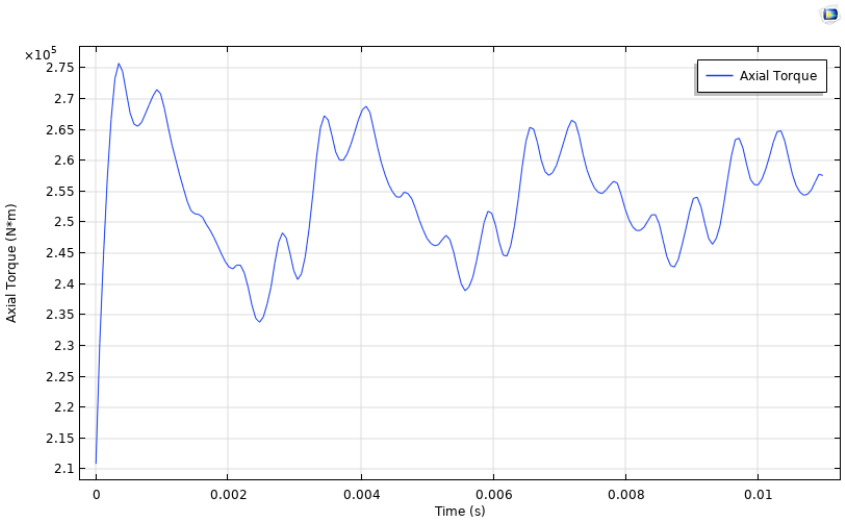

Figure B.2.8: Nominal Torque for Non-Modular Machine, Gear

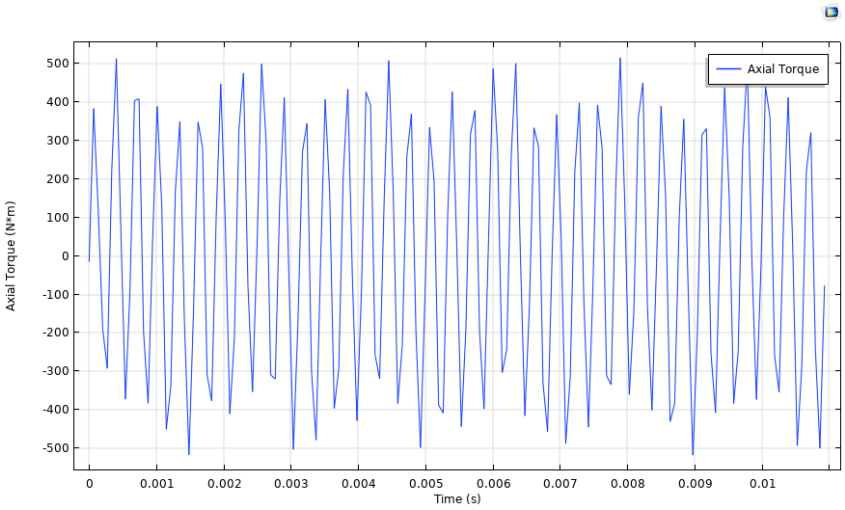

Figure B.2.9: Cogging Torque for Non-Modular Machine, Gear

B.2.4 Loss

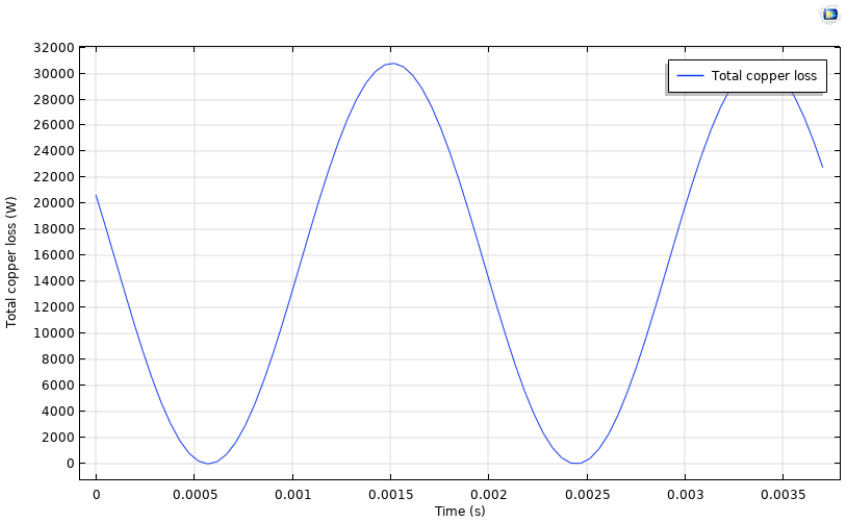

Figure B.2.10: Phase Copper Loss for Non-Modular Machine, Gear

Appendix C

Modular Machine with Increased Flux Gap Width

C.1 FEM-simulation with β=1.5 cm

C.1.1 Direct Drive

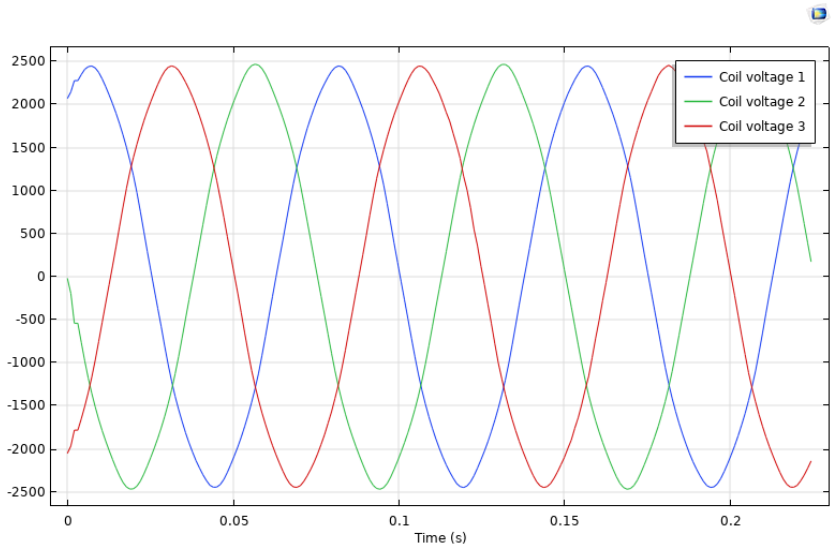

Figure C.1.1: No-load Phase Back-EMF for Modular Machine, Direct Drive

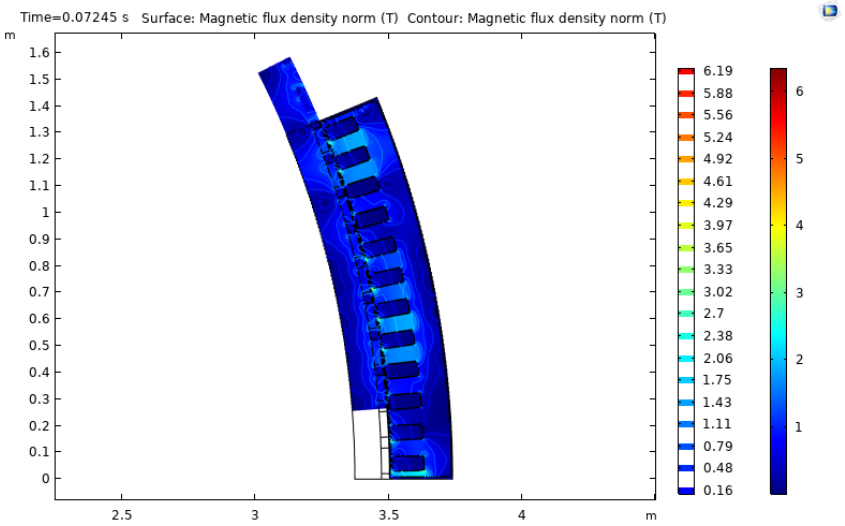

Figure C.1.2: Full Load Flux Density for Modular Machine, Direct Drive

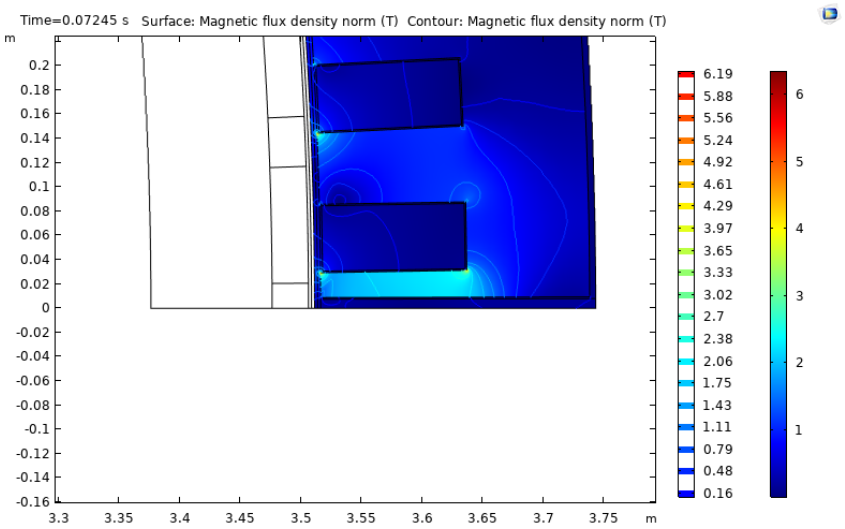

Figure C.1.3: Full Load Flux Density Close Up for Modular Machine, Direct Drive

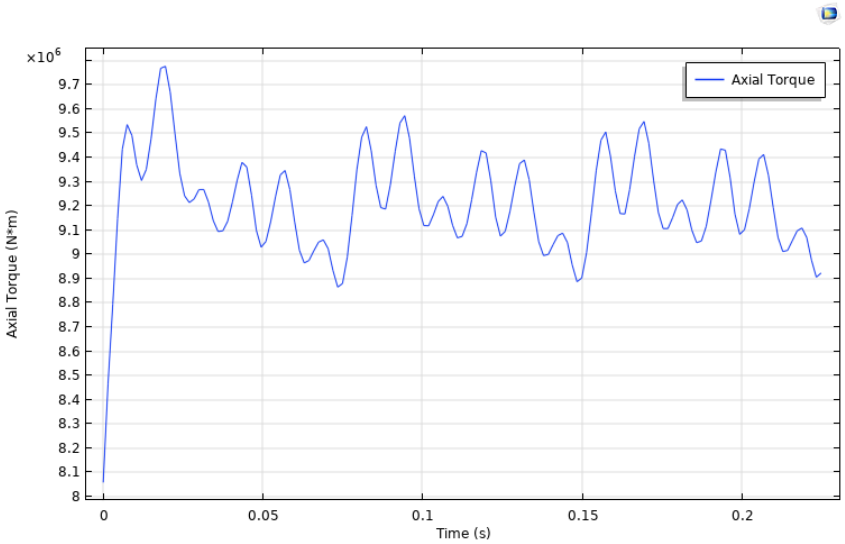

Figure C.1.4: Full Load Torque for Modular Machine, Direct Drive

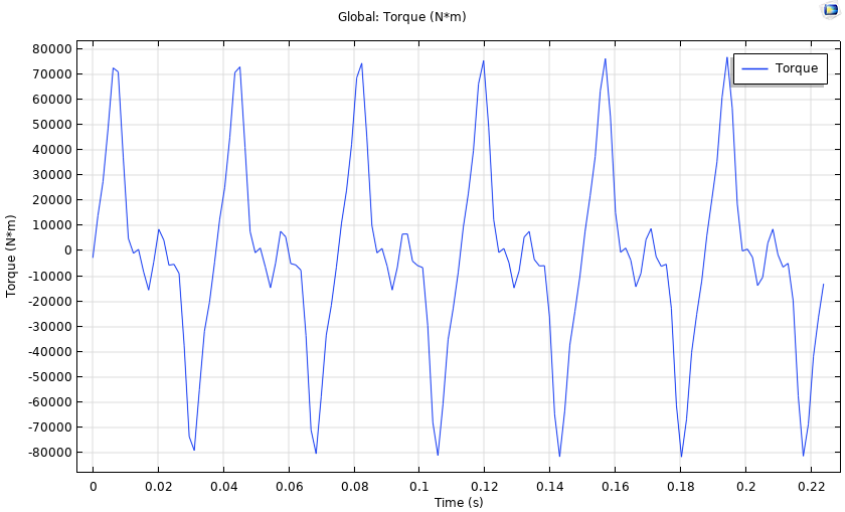

Figure C.1.5: Cogging Torque for Modular Machine, Direct Drive

C.1.2 Gear

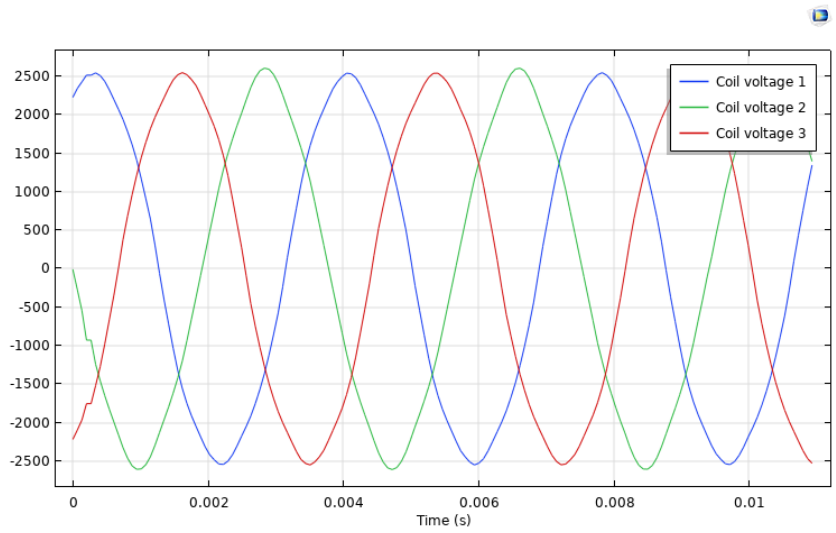

Figure C.1.6: No-Load Phase back-EMF for Modular Machine, Gear

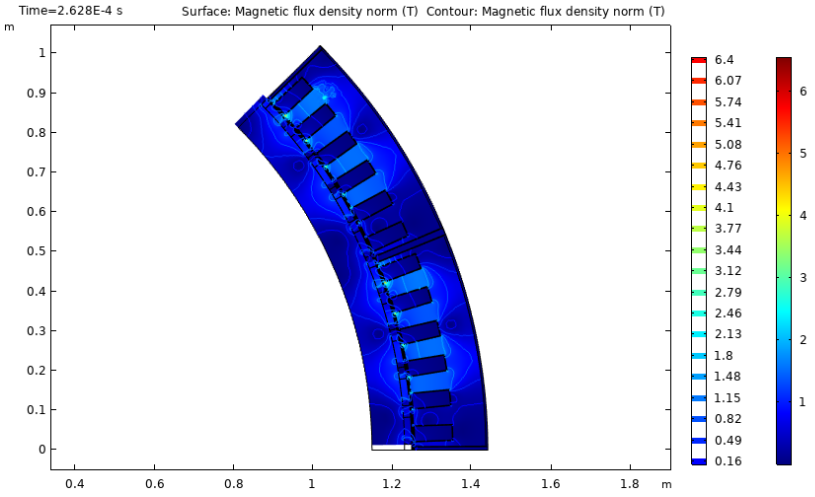

Figure C.1.7: Full Load Flux Density for Modular Machine, Gear

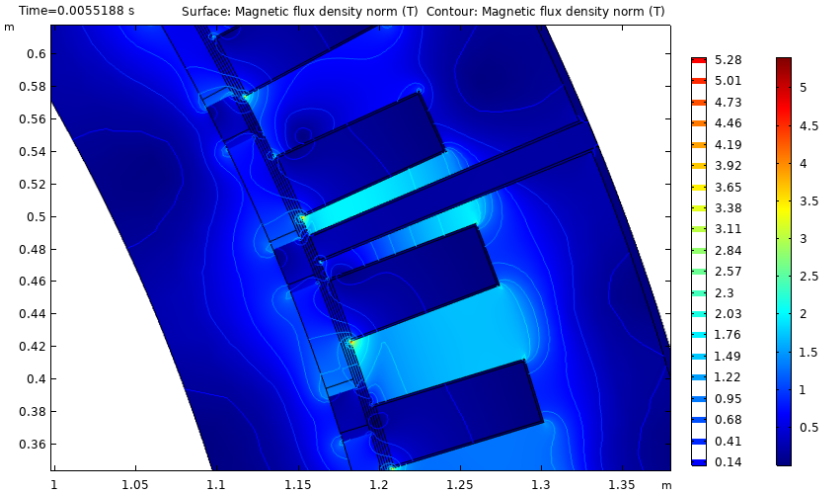

Figure C.1.8: Full Load Flux density Close Up for Modular Machine, Gear

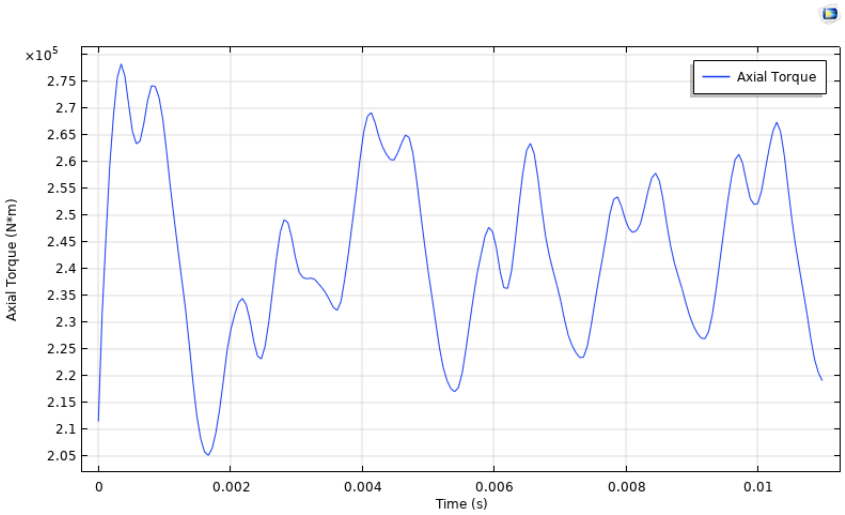

Figure C.1.9: Full Load Torque for Modular Machine, Gear

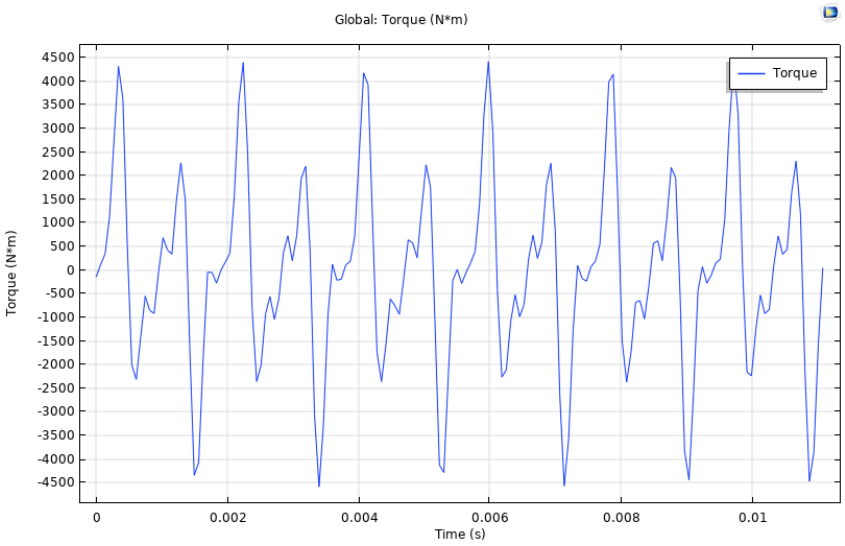

Figure C.1.10: Cogging Torque for Modular Machine, Gear

C.2 FEM-simulation with $\beta = 2$ cm

C.2.1 Direct Drive

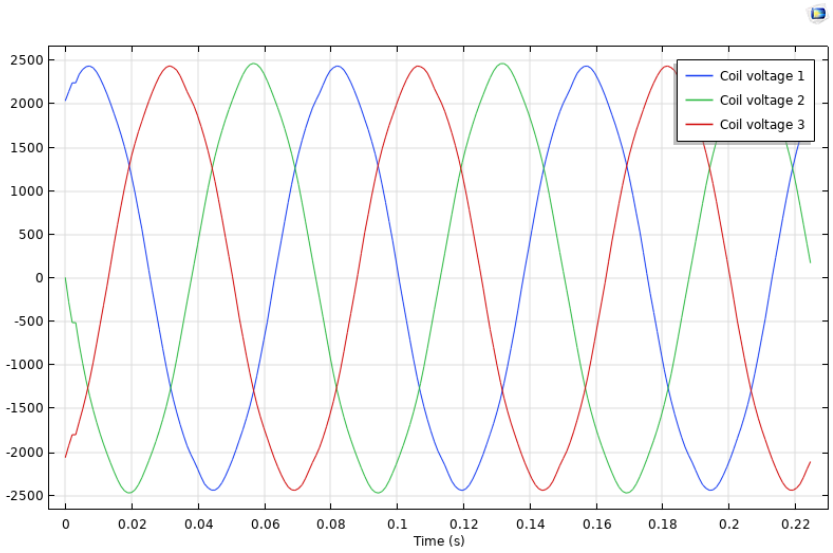

Figure C.2.1: No-load Phase Back-EMF for Modular Machine, Direct Drive

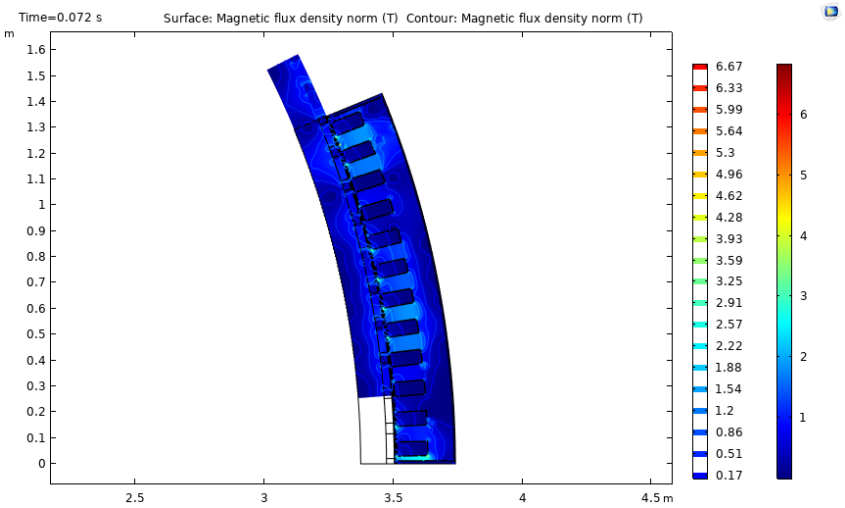

Figure C.2.2: Full Load Flux Density for Modular Machine, Direct Drive

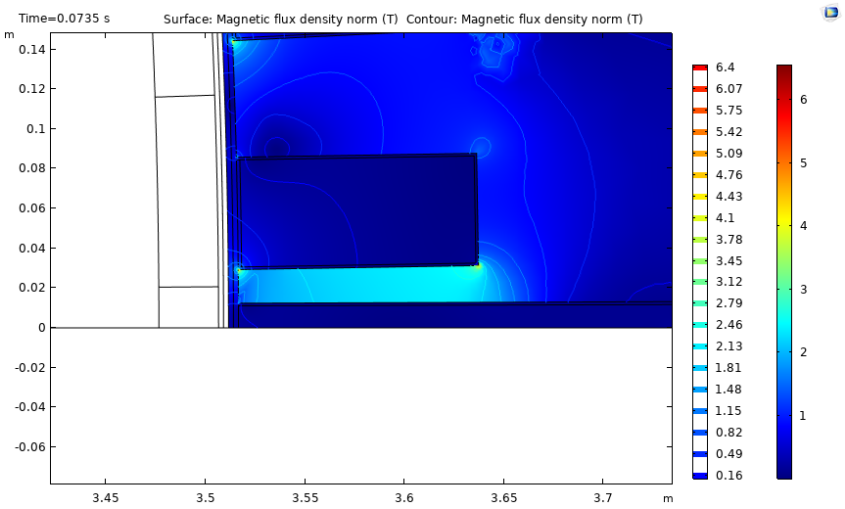

Figure C.2.3: Full Load Flux Density Close Up for Modular Machine, Direct Drive

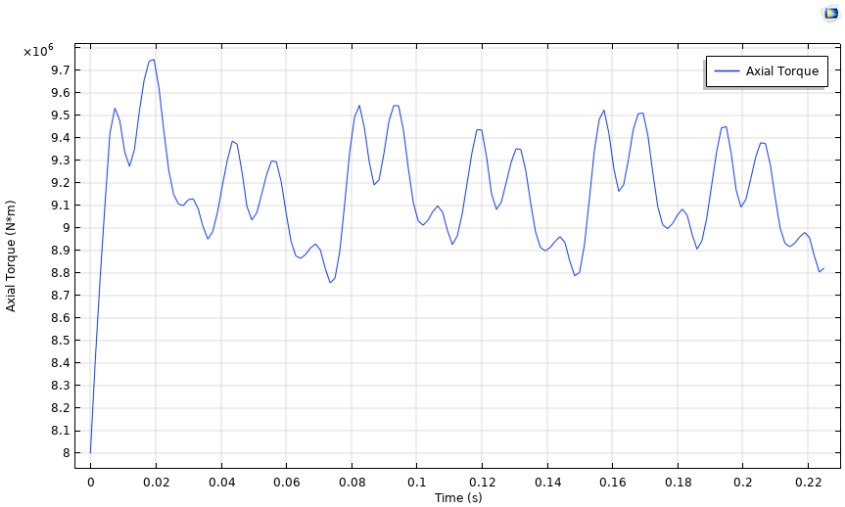

Figure C.2.4: Full Load Torque for Modular Machine, Direct Drive

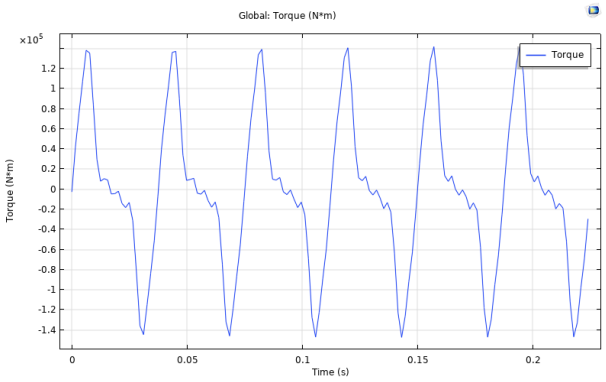

Figure C.2.5: Cogging Torque for Modular Machine, Direct Drive

C.2.2 Gear

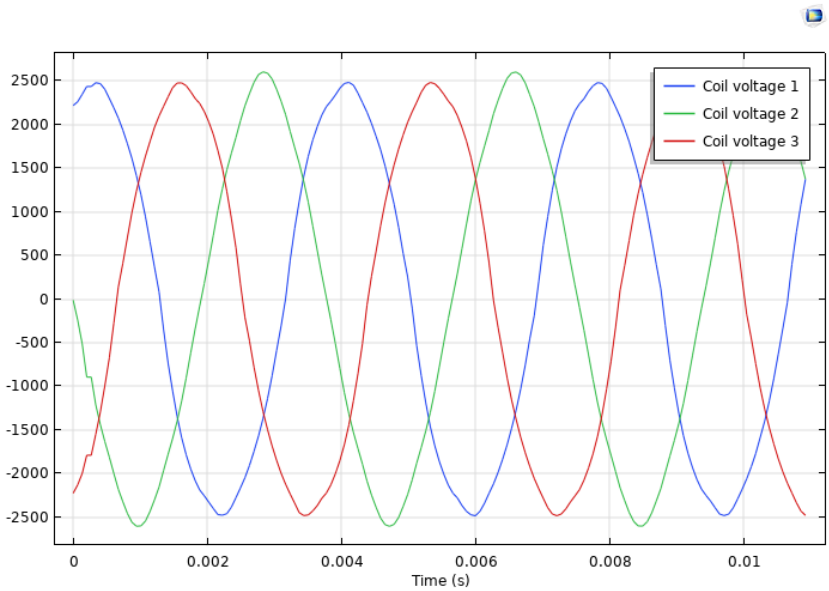

Figure C.2.6: No-load Phase Back-EMF for Modular Machine, Gear

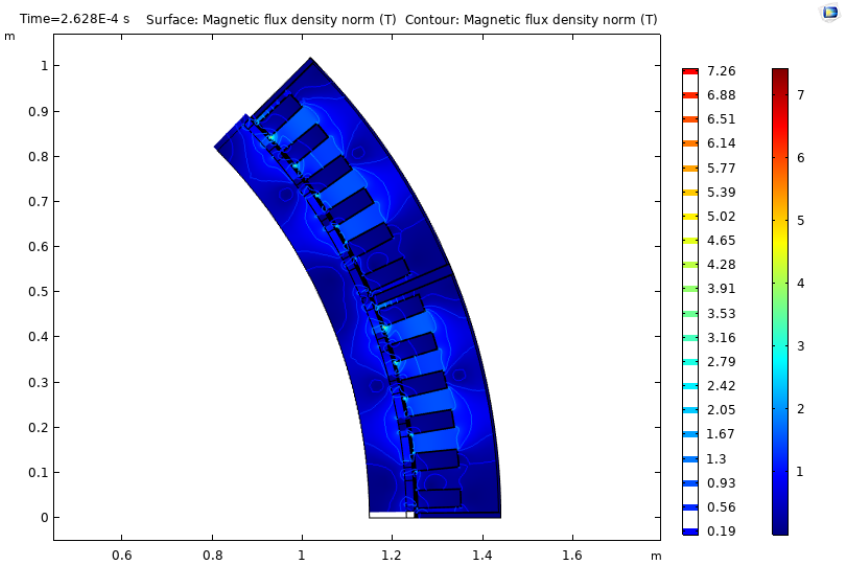

Figure C.2.7: Full Load Flux Density for Modular Machine, Gear

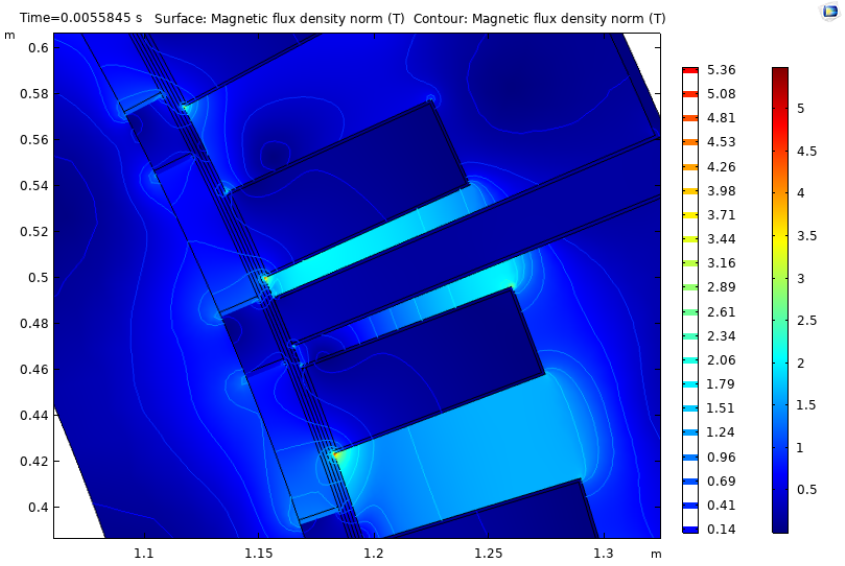

Figure C.2.8: Full Load Flux Density Close Up for Modular Machine, Gear

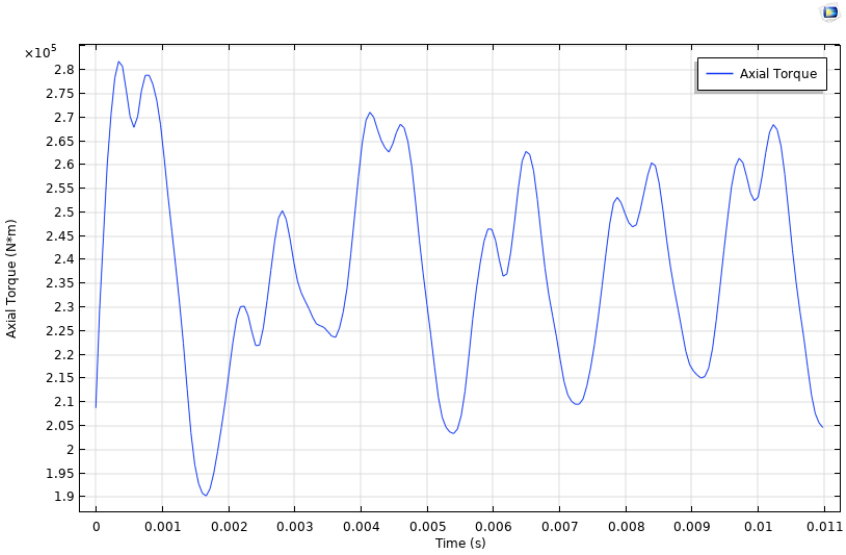

Figure C.2.9: Full Load Torque for Modular Machine, Gear

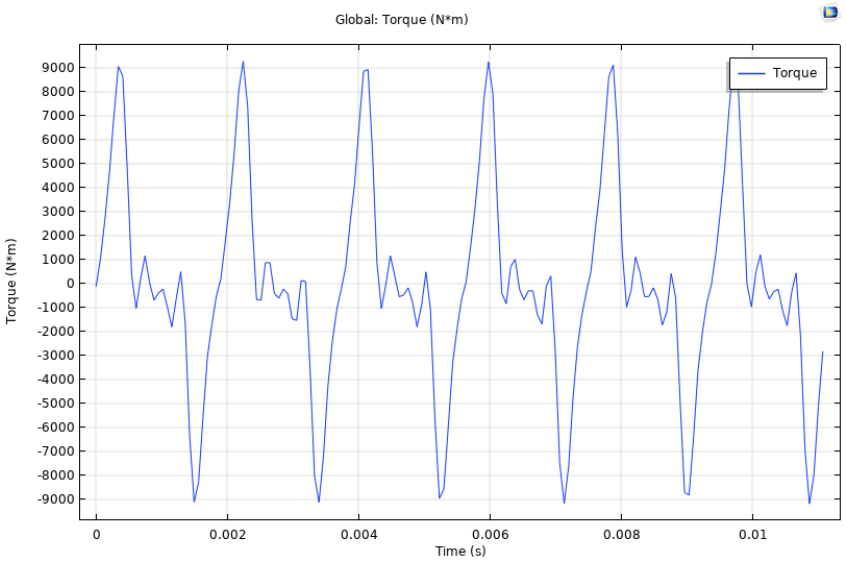

Figure C.2.10: Cogging Torque for Modular Machine, Gear

Appendix D

Relevant Design Features

D.1 Material Properties

Table D.1.1: Relevant Material Properties for Permanent Magnets (NdFeB) [16]

Parameter	Value
Conductivity	$6.25{\cdot}10^5 S/m$
Relative permeability	1.05 T
Temperature dependency	0.1%/C
Temperature maximum	80°C
Remanence flux density	1.2 T

Table D.1.2: Relevant Material Properties for Steel (M250-50A) [16]

Parameter	Value
Conductivity	$6.7{\cdot}10^6 S/m$
Density	7600 kg/m^3
Lamination conductivity	0 S/m
Lamination thickness	0.5 mm

Table D.1.3: Relevant Material Properties for Copper (Cu) [16]

Parameter	Value
Conductivity	$58{\cdot}10^6 S/m$
Maximum temperature	$150°C$

Table D.1.4: Relevant Material Properties for Chosen Insulation [24]

Parameter	Value
E_{DC}	10 kV/mm^2
E_{AC}	3 kV/mm^2
Safety factor (K)	1.5

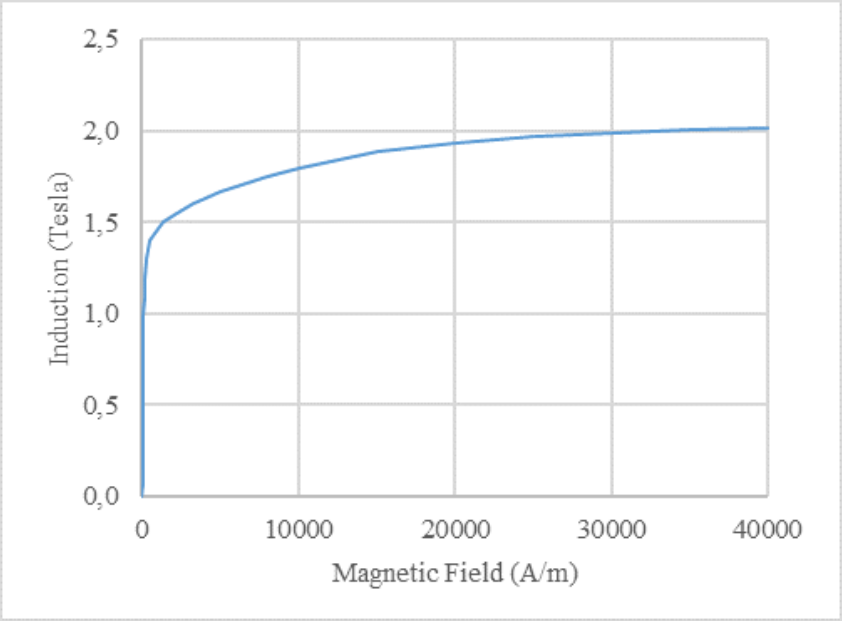

Figure D.1.1: H-B Curve for Steel (M250-50A) [2]

Loss [W/kg]		Frequency [Hz			
		50	100	200	400
Flux density [T]	0.5	0.31	0.78	2.11	6.0
	0.6	0.42	1.08	2.99	8.5
	0.7	0.54	1.40	3.86	11.3
	0.8	0.68	1.77	4.91	14.7
	0.9	0.83	2.18	6.12	18.7
	1.0	0.99	2.63	7.50	23.4
	1.1	1.18	3.13	9.02	28.8
	1.2	1.39	3.70	10.77	35.2
	1.3	1.64	4.28	12.75	42.4
	1.4	1.96	5.22	15.42	50.9
	1.5	2.34	6.24	18.31	60.7
	2*	4.68	13.28	36.62	121.4

Figure D.1.2: Power Loss Matrix for Steel (M250-50A) [16]

D.2 Curve Fitting

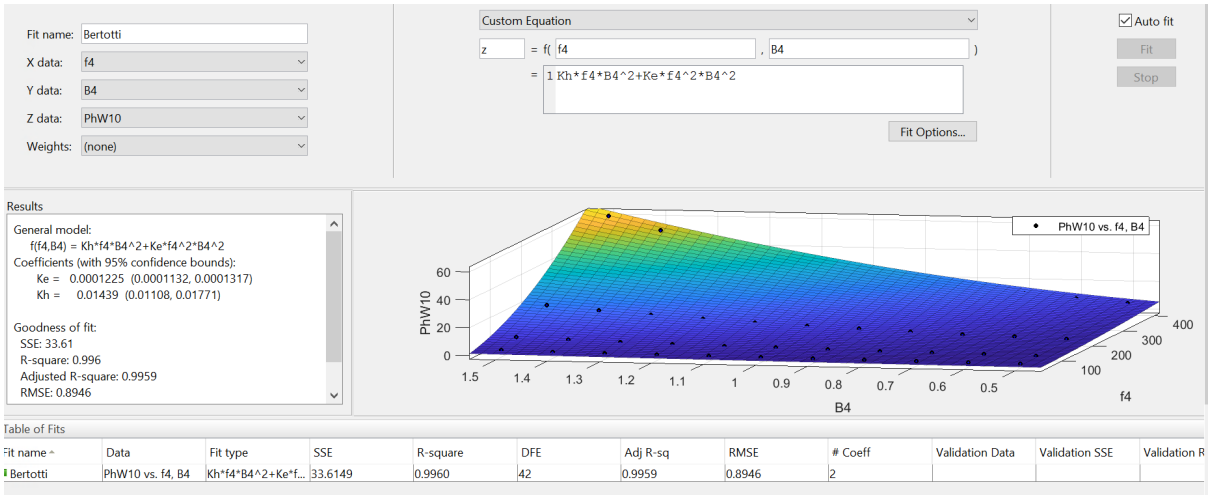

Figure D.2.1: Curve Fitting Simulation in Matlab

D.3 Analytical Calculations

D.3.1 Fundamental Design

D.3.1.1 Direct drive

```
1
2  %Rated data
3  T = 10*10^6/(10*2*pi/60);
4  wm = 1.0472; %speed in rad/s
5
6  %Material specification
7
8  kst =1;  % laminatipn stack coeficient due to 2D model
9  br = 1.2; %magnet remanence
10 mur = 1.05; %magnet relative recoil permability
11 muo = 4*pi*10^(-7); %zero permability
12
13 density= 1.68e-8; %copper density
14
15 a1 = 0.001; %magnet temperature dependency
16 T1 = 80; %maximum magnet temperature
17 T0=20; %Temperature Br0
18 Br= (1.2*(1-a1*(T1-T0))); %Remance temperature when
      acocunting for temperature increase
19
20 % Permissible material stress loading
21 Btsmax = 1.5; %max stator tooth flux density
22 Jmax =3000000; %maximum currenty density A/m^2
23 J = 3000000; %current density
24 Jmax1 = 3; %current density in A/mm2
25
```

```
%Geometrical and winding specifications
%lambda = L/Rro;
Nm = 160; %number of poles
Ns = 192; %number stator slots
Nph = 3; %phases
Nsp = Ns/3; %number of stator slots per phase
Nspp = Nsp/Nm; %number of slots per pole per phase
Nsm = Nspp*Nph;  %number of slots per pole


hag =0.01; %airgap length
g = 0.01; %airgap length
lm = 0.03; %magneth height
alphaM = 0.7; %stator length in percentage compared to pole
   pitch
L = 1.5; %Machine length

we = Nm*wm/2; %electrical speed
fe = we/(2*pi); %frequency

%Geometric dimensions

Dag = (3.507)*2; %airgap diameter
Rro = Dag/2; %airgap radius
Rsi= Rro+g; %inner stator radius


ThetaP = 2*pi/Nm; %angular pole pitch
ThetaS = 2*pi/Ns; %angular slot pitch
ThetaSE = pi/Nsm; %slot picth electrical radians
TauP = Rsi*ThetaP; %Pole picth
TauS = Rsi*ThetaS; %coil pitch

ks = 1-ThetaSE/(2*pi); %skew factor
kdn = (sin(Nspp*(ThetaSE./2)))/(Nspp*sin(ThetaSE./(2))); %
   distribution factor for nth harmonic

%coil span factor
ys =(pi*Nm)./(Ns);
E = (pi-ys);
TauC = (E/pi);
ThetaCe = pi*TauC/TauP;
kp = sin(ThetaCe/2); %picthfactor
q1 = Nsp/(Nm*3);

ke1 = cos(E/2); %coil/chording picth factor for 1st harmonic
kd1 = (sin(pi/(3*2)))/(sin(pi/(2*3))); %distribution for 1st
   harmonic
```

```
71 kw1 = kd1*ke1; %winding factor for 1st harmonic
72 a=16; %number of fluxgaps
73 delta = a*sin(0.001344/2*Rsi);
74 kes = sin((TauS*pi-delta)/(TauP*2)); %Fundamental factor when
       accounting for flux gaps
75
76
77 gc = g+lm/mur; %effective air gap for carter coefficient
78 ws = 0.0567; %stator slot width, program run untill ws and
     wst given later in the program converge
79 kc = (1-1./(TauS./ws*(5*gc./ws+1))).^(-1); % Carter
     coefficient
80 h_ag = hag*kc;
81 l_m = lm./mur;
82
83 Bg = Br*l_m./(l_m+h_ag); %airgap flux density
84 Bg1 = 4*Bg*sin(alphaM*pi./2)./pi; %maximum flux density in
     the airgap
85
86 Mm = alphaM*TauP; %magnet circumference length
87 Op = Bg*Mm*L; %flux per pole
88 Op1 = 2*Bg1*TauP*L./pi; %fundamentale space component of flux
       per pole
89
90
91 Ks =T./((sqrt(2)*pi/4)*Bg1*(Dag).^2*L*kst); %linear current
     density required form the torque
92 Tr = sqrt(2)*pi*Bg1*Ks*Dag.^2*L./4;
93
94 %om = T./(pi/2*L*Dag^2);
95 %om = Bg1/sqrt(2)*Ks/(pi*Dag);
96 %Ksf = (om*pi*Dag)/(Bg1/sqrt(2));
97
98 %Os = Op*0.5/(0.12*0.97*L);
99 %Or = Op*0.5/(0.12*0.97*L);
100 %Ott1 = Btsmax*L*wtt*0.97;
101
102 Jl= J*Ks;
103
104 kwdg = kw1; %winding faktor
105 kfill = 0.7516; %fill faktor given by coil script
106 kcp = kfill; %fill factor
107 wtt = Bg*alphaM*TauP./(Btsmax)-(Bg*(TauS-TauP))./(2*Btsmax);
     %stator teeth width at the smallest point
108 wst = Rsi*2*pi/Ns-wtt; % stator slots width
109 Aus = (Ks*pi*Rsi*2)./(J*Ns*kwdg*kfill); %Stator slot area
110 hus= Aus/wst; %stator slot height
111 q = Ns/(Nm*3); %stator slot per pole per phase
```

```
112
113
114
115 %determining the rotor depth
116 %Oyr = Op/2;
117 %hyr = [0.01:0.001:0.15];
118 %Byr = Oyr./(hyr*L*kst);
119 %plot(hyr,Byr)
120 %xlabel('Rotor yoke height[m]')
121 %ylabel('Open circuit flux density in rotor yoke[T]')
122 %title('Flux density')
123
124
125 %determining the stator depth
126 Oys = Op/2;
127 hys = [0.01:0.001:0.15];
128 Bys = Oys./(hys*L *kst);
129 plot(hys,Bys)
130 xlabel('Stator yoke height[m]')
131 ylabel('Open circuit flux density in stator yoke[T]')
132 %title('Flux density [T]')
133
134
135 Rsb =Rro+g+hus; %radius at stator slot height
136 Rso1 = Rsb+0.10; %machine outer radius
137 Rri = Rro-0.10-lm; % Rotor inner radius
138
139 %ELECTRICAL
140
141 AwireN = Aus*kfill*Ns/(3); %equivalent coil in series per
      phase to carru the winding
142 Tw= (1-(kp*Nm)/Ns)*pi*(Rsi*2+hus)./Nm; %diameter of
      endwinding
143 kew = pi/2; %often close to this values so assumed equal to
      pi/2 since the model is in 2D
144 Lew = kew*Tw; %endwinding length
145 Lturn = 2*(L+Lew); %complete length of coil
146
147
148 %K12 = (density*L)./(kcp*Aus)+(density*pi*TauC)/(2*kcp*Aus);
      %motstand
149 K1 = (density*Lturn)./(AwireN*2)+(density*pi*TauC)/(2*kcp*Aus
      ); %motstand ;
150 K3 = 4.444*fe*kwdg*Op1./(2); %Emf
151 K4 = Jmax*Aus*kfill*Ns./(3); % current
152 K2 = 2*pi*fe*((muo*mur*TauS*L)./(2*(lm+kc*mur*g))+(muo*L*hus)
      ./(3*wst)+(muo*TauC./4*log(TauC*sqrt(pi/(hus*wst))./2)));
153 %inductance
```

```
154
155 Vdc = 100000; %DC voltage
156 Vdcseg = 100000/16; %DC voltage per section
157 VllAc = Vdcseg/1.35; %line to line voltage, ac
158 VphaseSrms = VllAc/sqrt(3); %Phase voltage rms
159 Vphaserms = VphaseSrms*16; %Phase voltage for alle segments
    for one phase
160 VphasepeakS =VphaseSrms*sqrt(2); %Peak phase per segments
161 Vphasepeak = Vphaserms*sqrt(2); %peak phase per segments
162 Vr = Vphaserms;
163
164 %ncoil = Vr./sqrt((K3+K1*K4).^(2)+(K2*K4).^(2)): %number of
    coils required
165 ncoil = 130; % integer of the number of coils obtained from
    the equation above
166
167 Jmax1 =3;
168 Aus1 = Aus*1000000;
169 Ir = Jmax1*Aus1*kfill*Ns./(3*ncoil);
170 Iph = Jmax1*Aus1*kfill/ncoil; %rms current per coil
171 Ipp = Iph*sqrt(2); %peak phase current
172
173 Lg = (ncoil^2*muo*mur*TauS*L)./(2*(lm+kc*mur*g)); %gap
    inductance
174 Ls = ncoil^(2)*((muo*L*hus)./(3*wst)); %slot inductance
175 Le = ncoil^2*(muo*TauC./4*log(TauC*sqrt(pi/(hus*wst))./2)); %
    end winding inductance
176 Lph1 = (Lg+Ls+Le);
177 Lph = Nsp*(Ls+Lg);
178 LphS = Lph/16; %phase inductance per segment
179
180 Rss = density*ncoil^(2)*L/(kcp*Aus); %slot inductance
181 Re = density*ncoil^(2)*pi*TauC/(2*kcp*Aus); %end winding
    inductance
182 Rph1 = Rss+Re;
183 Rph = Nsp*(Rss+Re); %total phase resistance
184 Rphs = Rph/16; %phase resistance per segment
185 Rph2D = Nsp*Rss; %given for 2d simulation
186
187
188 Eo = 4.44*fe*kwdg*Op1*ncoil/2;
189 Eph = Eo*4; % Emf in each segment
190 Eoh=16*Eph; %total EMF per phase
191 Epeak = Eoh*sqrt(2);
192
193 Awire = Aus*kfill/(ncoil);
194 AwireN = Aus*kfill*Ns/(ncoil*3);
```

D.3.2 Gear

```
%Rated data
T = 10*10^6/(400*2*pi/60);
wm = 41.8879; %speed in rad/s

%Material specification
kst =1; % lamination stack coeficient  given as 1 due to 2d
   model
br = 1.2; %magnet remanence
mur = 1.05; %magnet relative recoil permability
muo = 4*pi*10^(-7); %zero permability

density = 1.68e-8; %copper density

a1 = 0.001;
T1 = 80;
T0=20;
Br= (1.2*(1-a1*(T1-T0))) %magnet remanence when corrected for
    max temperature

% Permissible material stress loading
Btsmax = 1.5; %max stator tooth flux density
Bysmax= 1.5; %max stator yoke flux density
Byrmax = 1.5; %max rotor yoke flux density
Jmax =3000000; %maximum currenty density A/m^2
J = 3000000; %current density
Jmax1 = 3; %current density in A/mm2

%Geometrical and winding specifications
Nm = 80; %number of poles
Ns = 96; %number stator slots
Nph = 3; %phases
Nsp = Ns/3; %number of stator slots per phase
Nspp = Nsp/Nm; %number of slots per pole per phase
Nsm = Nspp*Nph;  %number of slots per pole


hag =0.006; %airgap length
g = 0.006; %airgap length
lm = 0.018; %magneth height
alphaM = 0.7; %stator length in percentage compared to pole
   pitch
L = 0.38; %Machine length

we = Nm*wm/2; %electrical speed
fe = we/(2*pi); %frequency

%geomtric sizes
```

```
45
46 Dag = 2.5; %airgap diameter
47 Rro = Dag/2; %airgap radius
48 Rsi= Rro+g; %inner stator radius
49
50
51 ThetaP = 2*pi/Nm; %angular pole pitch
52 ThetaS = 2*pi/Ns; %angular slot pitch
53 ThetaSE = pi/Nsm; %slot picth electrical radians
54 TauP = Rsi*ThetaP; %Pole picth
55 TauS = Rsi*ThetaS; %coil pitch
56
57 ks = 1-ThetaSE/(2*pi); %skew factor
58 kdn = (sin(Nspp*(ThetaSE./2)))/(Nspp*sin(ThetaSE./(2))); %
   distribution factor for nth harmonic
59
60 %coil span factor
61
62 ys =(pi*Nm)./(Ns); %slot pitch of 150
63 E = (pi-ys);
64 TauC = (E/pi);
65 ThetaCe = pi*TauC/TauP;
66 kp = sin(ThetaCe/2); %picthfactor
67
68
69 q1 = Nsp/(Nm*3);
70 ke1 = cos(E/2); %coil/chording picth factor for 1st harmonic
71 kd1 = (sin(pi/(3*2)))/(sin(pi/(2*3))); %distribution for 1st
   harmonic
72 kw1 = kd1*ke1; %winding factor for 1st harmonic
73 a=16; %number of flux gaps
74 b = 10;
75 delta = a*sin(b/2*Rsi);
76 kps = sin((TauS*pi-delta)/(TauP*2));  %Fundamental factor
   when accounting for flux gaps
77
78
79 gc = g+lm/mur; %effective air gap for carter coefficient
80 ws = 0.0408;  %stator slot width, program run untill ws and
   wst given later in the program converge
81 kc = (1-1./(TauS./ws*(5*gc./ws+1))).^(-1); % Carter
   coefficient
82 h_ag = hag*kc;
83 l_m = lm./mur;
84
85 Bg = Br*l_m./(l_m+h_ag); %airgap flux density
86 Bg1 = 4*Bg*sin(alphaM*pi./2)./pi; %maximum flux density in
   the airgap
```

```
87
88  Mm = alphaM*TauP; %magnet circumference length
89  %Der = (Rro-lm)*2;
90  Op = Bg*Mm*L; %flux per pole
91  Op1 = 2*Bg1*TauP*L./pi; %fundamentale space component of flux
        per pole
92
93
94  Ks =T./((sqrt(2)*pi/4)*Bg1*(Dag).^2*L); %linear current
       density required form the torque
95  Tr = sqrt(2)*pi*Bg1*Ks*Dag.^2*L./4;
96
97  %om = T./(pi/2*L*Dag^2);
98  %om = Bg1/sqrt(2)*Ks/(pi*Dag);
99  %Ksf = (om*pi*Dag)/(Bg1/sqrt(2));
100
101 %Os = Op*0.5/(0.12*0.97*L);
102 %Or = Op*0.5/(0.12*0.97*L);
103 %Ott1 = Btsmax*L*wtt*0.97;
104
105 Jl= J*Ks;
106
107 kwdg = kw1; %winding faktor
108 kfill = 0.7448; %fill faktor
109 kcp = kfill; %fill factor
110 wtt = Bg*alphaM*TauP./(Btsmax)-(Bg*(TauS-TauP))./(2*Btsmax);
       %stator teeth width at shortest point
111 wst = Rsi*2*pi/Ns-wtt; % stator slots width
112 Aus = (Ks*pi*Rsi*2)./(J*Ns*kwdg*kfill); %Stator slot area
113 hus= Aus/wst; %stator slot height
114 q = Ns/(Nm*3); %stator slot per pole per phase
115
116
117 %determining the rotor thickness
118 %Oyr = Op/2;
119 %hyr = [0.01:0.001:0.15];
120 %Byr = Oyr./(hyr*L*kst);
121 %plot(hyr,Byr)
122 %xlabel('Rotor yoke height[m]')
123 %ylabel('Open circuit flux density in rotor yoke[T]')
124 %title('Flux density')
125
126
127 %determining the stator thickness
128 Oys = Op/2;
129 hys = [0.01:0.001:0.15];
130 Bys = Oys./(hys*L*kst);
131 plot(hys,Bys)
```

```
132 xlabel('Stator yoke thickness[m]')
133 ylabel('Open circuit flux density in stator yoke[T]')
134 %title('Flux density [T]')
135
136
137 Rsb =Rro+g+hus; %radius at stator slot height
138 Rso1 = Rsb+0.12; %machine outer radius
139 Rri = Rro-0.12-lm; % Rotot inner radius
140
141 %ELECTRICAL
142
143 AwireN = Aus*kfill*Ns/(3); %equivalent coil in series per
       phase to carru the winding
144 Tw= (1-(kp*Nm)/Ns)*pi*(Rsi*2+hus)./Nm; %diameter of
       endwinding
145 kew = pi/2; %often close to this values so assumed equal to
       pi/2 since the model is in 2D
146 Lew = kew*Tw; %endwinding length
147 Lturn = 2*(L+Lew); %complete length of coil
148
149
150 %K12 = (density*L)./(kcp*Aus)+(density*pi*TauC)/(2*kcp*Aus);
       %motstand
151 K1 = (density*Lturn)./(AwireN*2)+(density*pi*TauC)/(2*kcp*Aus
       ); %motstand ;
152 K3 = 4.444*fe*kwdg*Op1./(2); %Emf
153 K4 = Jmax*Aus*kfill*Ns./(3); % Str m
154 K2 = 2*pi*fe*((muo*mur*TauS*L)./(2*(lm+kc*mur*g))+(muo*L*hus)
       ./(3*wst)+(muo*TauC./4*log(TauC*sqrt(pi/(hus*wst))./2)));
155 %inductance
156
157 Vdc = 100000; %DC voltage
158 Vdcseg = 100000/16; %DC voltage per section
159 VllAc = Vdcseg/1.35; %line to line voltage, ac
160 VphaseSrms = VllAc/sqrt(3); %Phase voltage rms
161 Vphaserms = VphaseSrms*16; %Phase voltage for alle segments
       for one phase
162 VphasepeakS =VphaseSrms*sqrt(2); %Peak phase per segments
163 Vphasepeak = Vphaserms*sqrt(2); %peak phase per segments
164 Vr = Vphaserms;
165
166 %ncoil = Vr./sqrt((K3+K1*K4).^(2)+(K2*K4).^(2)) %number of
       coils required
167 ncoil = 78; %integer of equation given over
168
169 Jmax1 =3;
170 Aus1 = Aus*1000000; %*1.4;
171 Ir = Jmax1*Aus1*kfill*Ns./(3*ncoil);
```

```
Iph = Jmax1*Aus1*kfill/ncoil; %rms current per coil
Ipp = Iph*sqrt(2); %peak phase current

Lg = (ncoil^2*muo*mur*TauS*L)./(2*(lm+kc*mur*g));  %gap
   inductance
Ls = ncoil^(2)*((muo*L*hus)./(3*wst)); %slot inductance
Le = ncoil^2*(muo*TauC./4*log(TauC*sqrt(pi/(hus*wst))./2)); %
   end winding inductance
Lph1 = (Lg+Ls+Le); %total inductance per slot
Lph = Nsp*(Ls+Lg); %total phase inductance
LphS = Lph/16;   %phase inductance per segment

Rss = density*ncoil^(2)*L/(kcp*Aus); %slot inductance
Re = density*ncoil^(2)*pi*TauC/(2*kcp*Aus); %end winding
   inductance
Rph1 = Rss+Re;
Rph = Nsp*(Rss+Re); %total phase resistance
Rphs = Rph/16; %phase resistance per segment
Rph2D = Nsp*Rss;



Eo = 4.44*fe*kwdg*Op1*ncoil/2;
Eph = Eo*4; % Emf in each segment
Eoh=8*Eph; %per phase for whole machin
Epeak = Eoh*sqrt(2);

Awire = Aus*kfill/(ncoil);
AwireN = Aus*kfill*Ns/(ncoil*3);
```

D.3.3 Modular Insulation Design

D.3.3.1 Direct drive Modular Insulation Calculations

```
%Isolasjonsberegninger for segmentert maskin
%directe drvet

Udc=100; %DC voltage required
Vdcseg = 100/16;%DC voltage per segment
Vphase = 2.66; %kV phase rms per segment
Nsegm= 16; %number of segments
Ns = 192; %number of slots
Nm = 160; %number of poles

Uphph = Udc./Nsegm; %voltage phase to phase
Uphscr = 0.5*(Udc./Nsegm); %voltage phase to screen
Uscrgr = (Udc-Udc./Nsegm)./2; %voltage screen to ground
Uscrscr =2*Udc./Nsegm; %voltage screen to screen

Eac =3; %voltage in kV/mm^2 before insulation breaks doem
```

```
Edc = 10; %voltage in kV/mm^2 before screen insulation breaks dowm
wslot = 56.7; %stator slot width in cm
Hslot = 118.2; %stator slot height in cm


Kt = (1-(Uphph./Eac+Uscrscr./(Nsegm*Edc))./(wslot)); %
Kr = (1-2*(Uphscr./Eac+Uscrgr./Edc)./(Hslot));
%Ke = (1-(3*Nsegm)/(Nslot));  empty slots not utilised

Ka = Kt*Kr; %*Ke %ekvivalent circuit

Tspor = 1.5*Vphase/(Eac); %thickness ofstator slot , 1.5 is given as safety factor

Afill = (1-2*Tspor/wslot)*(1-2*Tspor/Hslot) %stator slot fill factor when the insulation of coils and air are neglected

Tsegm = 2*Vdcseg/Edc;  %mm %Segmentation insulation around a segments


Tearth = 0.5*Udc/Edc; %mm %insulation thickness at the outer radius of the machine
```

D.3.3.2 Gear Modular Insulation Calculations

```
%Isolasjonsberegninger for segmentert maskin
%gear

Udc=100; %DC voltage required
Vdcseg = 100/16;%DC voltage per segment
Vphase = 2.66; %kV phase rms per segment
Nsegm= 16; %number of segments
Nslot = 96; %number of slots
Nm = 80; %number of poles

Uphph = Udc./Nsegm; %voltage phase to phase
Uphscr = 0.5*(Udc./Nsegm); %voltage phase to screen
Uscrgr = (Udc-Udc./Nsegm)./2; %voltage screen to ground
Uscrscr =2*Udc./Nsegm; %voltage screen to screen

Eac =3; %voltage in kV/mm^2 before insulation breaks doem
Edc = 10; %voltage in kV/mm^2 before screen insulation breaks dowm
wslot = 40.7; %stator slot width in cm
Hslot =  92.7; %stator slot height in cm


Kt = (1-(Uphph./Eac+Uscrscr./(Nsegm*Edc))./(wslot)); %
```

```
23 Kr = (1-2*(Uphscr./Eac+Uscrgr./Edc)./(Hslot));
24 %Ke = (1-(3*Nsegm)/(Nslot));  empty slots not utilised
25
26 Ka = Kt*Kr; %*Ke %ekvivalent circuit
27
28 Tspor = 1.5*Vphase/(Eac); %thickness ofstator slot , 1.5 is
      given as safety factor
29 Afill = (1-2*Tspor/wslot)*(1-2*Tspor/Hslot) %stator slot fill
       factor when the insulation of coils and air are neglected
30 Tsegm = 2*Vdcseg/Edc;  %mm %Segmentation insulation around a
      segments
31 Tjord = 0.5*Udc/Edc; %mm %insulation thickness at the outer
      radius of the machine
```

Solveig Samseth Strand

Electromagnetic Design of Modular Generators for Offshore Wind Power Applications

NTNU
Norwegian University of
Science and Technology